Forschungszentrum Jülich
in der Helmholtz-Gemeinschaft

Institut für Kernphysik

Pion Production and Absorption in πN and 3N Systems

Sonja Schneider

Jül-4134

Pion Production and Absorption in πN and 3N Systems

Sonja Schneider

Berichte des Forschungszentrums Jülich ; 4134
ISSN 0944-2952
Institut für Kernphysik Jül-4134
D 5 (Diss., Bonn, Univ., 2004)

Zu beziehen durch: Forschungszentrum Jülich GmbH · Zentralbibliothek
D-52425 Jülich · Bundesrepublik Deutschland
☎ 02461 61-5220 · Telefax: 02461 61-6103 · e-mail: zb-publikation@fz-juelich.de

Pion Production and Absorption in πN and $3N$ Systems

We study pion-induced two-pion production on the nucleon in the framework of a relativistic meson-exchange model constrained by Chiral Perturbation Theory in the low-energy limit. Unitarisation effects are included for the resonance pole diagrams. This leads to a significant improvement over a simple tree-level model in the description of the angular distributions for the $\pi^+ p \to \pi^+\pi^+ n$ reaction. In the reaction channels $\pi^- p \to \pi^+\pi^- n$ and $\pi^- p \to \pi^0\pi^0 n$ we find a contribution of the two-pion decay of the Roper resonance. This contribution does however not manifest itself in a qualitative change in the description of the differential distributions.

In the second part of this thesis we use the pion as a probe to study the short range part of the three-nucleon wave function in π^+ absorption on ^{3}He. We employ a parametrisation of the three-nucleon wave function based on modern NN models. The use of this parametrisation leads to a significant improvement over previous calculations in the description of cross section and polarisation data. However, the polarisation data hint at the need of other mechanisms beyond a two-nucleon absorption mechanism for the description of positive pion absorption on ^{3}He even in quasifree kinematics.

Pion Produktion und Absorption in πN und $3N$ Systemen

Wir untersuchen die pioninduzierte Zwei-Pion-Produktion am Nukleon im Rahmen eines relativistischen Mesonenaustauschmodells, das sich im Niederenergiebereich auf die Chirale Störungstheorie zurückführen läßt. Für die Poldiagramme der Resonanzen werden Unitarisierungseffekte berücksichtigt. Dies führt zu einer signifikanten Verbesserung der Beschreibung der Winkelverteilungen für die Reaktion $\pi^+ p \to \pi^+\pi^+ n$ im Vergleich mit einem Modell auf dem Niveau einfacher Baumgraphen. In den Reaktionskanälen $\pi^- p \to \pi^+\pi^- n$ und $\pi^- p \to \pi^0\pi^0 n$ finden wir einen Beitrag des Zwei-Pion Zerfalls der Roper-Resonanz . Dieser Beitrag führt jedoch nicht zu einer qualitativen Veränderung in der Beschreibung der differentiellen Wirkungsquerschnitte.

Im zweiten Teil dieser Arbeit nutzen wir das Pion als Sonde für die Untersuchung des kurzreichweitigen Anteils der Drei-Nukleon-Wellenfunktion in der π^+ Absorption am ^{3}He. Wir verwenden eine Parametrisierung der Drei-Nukleon-Wellenfunktion, die auf modernen NN-Modellen basiert. Die Verwendung dieser Parametrisierung führt zu signifikanten Verbesserungen in der Beschreibung der Wirkungsquerschnitte und der Polarisationsdaten im Vergleich zu früheren Berechnungen. Die Polarisationsdaten deuten jedoch darauf hin, dass sogar in quasifreier Kinematik Mechanismen, die über eine Zwei-Nukleon Absorption hinausgehen, zur Beschreibung der Absorption positiver Pionen am ^{3}He notwendig sind.

Contents

Chapter 1

Introduction

Today we believe that the theory of the strong interactions is Quantum Chromo Dynamics (QCD). This non-abelian theory describes the interactions of quarks and gluons both carrying a quantum number called colour. One consequence of the non-abelian structure of the theory is asymptotic freedom: the forces between quarks and gluons become small at short distances (corresponding to large energies), and the interaction can be treated perturbatively. With decreasing energy, the strong coupling constant becomes larger, and the perturbative approach becomes useless. At energies corresponding to the mass of the nucleon, no exact solution of QCD is known.

Furthermore, free quarks have never been observed. This led to the postulate of confinement: all observable particles have to be colour singlet states. The relevant degrees of freedom at low and intermediate energies are these colourless states, the mesons and baryons. The spectroscopy of the baryons has in the past contributed two main ideas to the development of QCD: the notion of "quark" as a building block of hadrons and the hidden degree of freedom called colour.

At present, a detailed experimental investigation of the baryon spectrum is being performed at both electron and hadron facilities. One hope is to find states that have been predicted by quark models but have not yet been observed.

In the naive quark model, baryons can be described qualitatively as bound states of three constituent quarks. The question comes up whether all baryon resonances can be described as three-quark states. There has been much discussion on the nature of the $\Lambda(1405)$ [1–3] and the Roper resonance. The low-lying Roper resonance poses a problem to constituent quark models based on one-gluon exchange [4]. In these models, the Roper resonance as a positive parity excited state corresponds to a $2\hbar\omega$ radial excitation in a harmonic oscillator potential and is always heavier than the first excitation of negative parity. The consideration of other interaction mechanisms like

flavour-dependent instanton forces [5] or Goldstone boson exchange [6] is needed to change the level ordering of the low-lying positive and negative parity excited states. Also on the lattice, it is controversial whether the low-lying Roper resonance can be obtained as a qqq state. One group finds the lightest positive parity excited state above the negative parity state [7], another group observes a level crossing between positive and negative parity states which would reproduce the experimentally observed spectra [8]. Another possibility is the interpretation of the Roper resonance as a dynamical resonance [9–11]. In these cases it is difficult to make a clear and model-independent claim that these states are not consistent with the qqq hypothesis. The recent observation of a manifestly exotic resonance, the Θ^+ [12–15] clearly cannot be reconciled with the naive three-quark picture. This resonance has strangeness $S = 1$, and the simplest quark content would consist of at least five quarks, $uudd\bar{s}$. The evidence for the existence of the Θ^+ illustrates the importance to look for exotic resonances. In the present work, we are however mainly interested in the Roper resonance.

Experimentally, baryons and their decay properties have been most extensively studied in pion-nucleon scattering. However, to obtain a complete picture of the properties of resonances, different excitation channels and different decay channels have to be considered. Precise data on two-pion photoproduction have also become available from the MAMI facility at Mainz [16–18]. The γN reactions are however largely dominated by the excitation of the Δ isobar and the $D_{13}(1520)$ [19]. Therefore these reactions offer no ideal situation to search for an effect of the Roper resonance. This may change when polarised photons [20] or electro-production reactions are used. So the $N^\star$ program at Jefferson Lab [21] is dedicated to the experimental study of resonance excitation in electroproduction.
Detailed differential distributions have recently been measured for the $\pi^- p \to \pi^0\pi^0 n$ reaction over a wide energy range from threshold up to 1.53 GeV [22]. In the present thesis we investigate these data for information on the two-pion decay of the Roper resonance.

In the study of resonances one is faced with the problem of how to separate their properties from the background contributions of non-resonant meson-baryon interactions and from final state interactions. To describe such complicated processes over a wide energy range one has to rely on models.

The Jülich πN [9–11] model allows for a good qualitative description of the pion-nucleon phase shifts and inelasticities in an energy range from threshold up to 1.9 GeV [11]. It takes into account the inelastic channels $\pi\Delta$, σN, ρN (as effective parameterisations of $\pi\pi N$ intermediate states) and the ηN channel. The interaction is iterated in a Lippmann-Schwinger equation. This unitarisation method allows for

the dynamical generation of resonances from the meson-baryon dynamics. Indeed, one has found that the Roper resonance $N^\star(1440)$ can be interpreted as such a dynamical state. In the Jülich model, this resonance is generated from the coupling of the πN channel to the effective $\pi\pi N$ channel σN. For the investigation of the decay properties of this resonance a closer look at its two-pion decay suggests itself. But the investigation of also the $\pi N \to \pi\pi N$ total cross sections within the Jülich πN model poses problems because of the complicated analytical structure of the model.

On the other hand, the reaction $\pi N \to \pi\pi N$ has been successfully described in the framework of Chiral Perturbation Theory already at next-to-leading order, with contributions only from tree-level diagrams [23]. Chiral Perturbation Theory is the effective theory of strong interactions at low energies, but resonances are not included as dynamical degrees of freedom. Our long term aim is however the investigation of the decay properties of resonances. So we develop a resonance exchange model that is constrained by Chiral Perturbation Theory in the low-energy regime.

The ingredients of our model are similar to the isobar model of Oset and Vicente-Vacas that was later extended by Fazel et al. [24, 25]. Their model was designed to describe pion interaction in nuclei and for this application was formulated in the nonrelativistic approximation. It could describe the total cross sections of the $\pi N \to \pi\pi N$ reaction quite successfully and was also used for an interpretation of the $M_{\pi\pi}$ distributions in [26]. It was found, that the $M_{\pi\pi}$ distributions in the $\pi^+ p \to \pi^+\pi^+ n$ and $\pi^- p \to \pi^+\pi^- n$ channels could not simultaneously be described.

We formulate a resonance exchange model in a relativistic framework, taking into account contributions from σ and ρ exchange and the excitation of the baryonic resonances $\Delta(1232)$, $N^\star(1440)$, $N^\star(1520)$ and $N^\star(1535)$. In our model we go beyond a "pure" tree-level ansatz by including some unitarisation effects for the pole contributions.

One aim of this investigation is to find out to what degree of accuracy the various differential cross sections in the $\pi N \to \pi\pi N$ reaction can be described by a simple tree-level ansatz and where the inclusion of initial and final state interactions has an effect on the description of the data.

A second motivation for our investigation lies in the study of the resonance contributions to the pion production reaction and whether the reaction allows to disentangle the information on the two-pion decay of the resonances from the background.

This thesis is organised as follows. In Chapter 2 we introduce the effective Lagrangian for the meson-baryon interactions and present our model for the pion induced pion production. The parameters of this model, the coupling constants and the masses of the resonances, are fitted to pion-pion and pion-nucleon scattering in Chapter 3. Our

results for the reaction $\pi N \to \pi\pi N$ are shown in Chapter 4. The investigation of pion-induced pion production ends with a few concluding remarks in Chapter 5.

The work of the Jülich group does not only concentrate on the investigation of the pion-nucleon interaction. In fact, also the pion-pion and the nucleon-nucleon interactions are investigated with the aim of finding a consistent description of strong interaction processes at low and intermediate energies. Chapter 6 is dedicated to the investigation of positive pion absorption on ^{3}He. In such a reaction, the nucleon-nucleon interaction can be probed at short distances and medium effects can be studied in a theoretically tractable system.

Chapter 2

Introduction to the Model for $\pi N \longrightarrow \pi\pi N$

In this chapter we introduce our model for pion-induced pion production on the nucleon, the reaction $\pi N \to \pi\pi N$. We work in the framework of a resonance-exchange model considering processes with intermediate mesonic (σ, ρ) and baryonic $(\Delta, N^\star)$ resonances. The interactions of the pions, the nucleons and these resonances are described by effective Lagrangians. The coupling constants in these Lagrangians are parameters that have to be determined from the data. The interaction Lagrangians are given in section 2.1. In section 2.2 we discuss the ingredients of our model for $\pi N \to \pi\pi N$.

2.1 Symmetries of QCD and Effective Lagrangian

To describe the interaction of mesons and baryons, we make use of phenomenological Lagrangians that respect the symmetries of QCD. These symmetries are Lorentz invariance, the invariance under time reversal, charge conjugation and parity transformations, and in particular the (approximate) invariance under chiral $SU(2) \times SU(2)$ transformations.

Invariance under chiral transformations means that the QCD Lagrangian is invariant under rotations which act independently on the lefthanded and righthanded quark fields. The group of these rotations is $SU(2)_L \times SU(2)_R$. Alternatively, the rotation group can be written as $SU(2)_V \times SU(2)_A$ with vector and axial-vector transformations

acting on the quark fields,

$$q \to e^{-i\frac{\vec{\tau}}{2}\vec{\alpha}}q \tag{2.1}$$

$$q \to e^{-i\gamma_5\frac{\vec{\tau}}{2}\vec{\alpha}}q\,, \tag{2.2}$$

where the τ_i, $i = 1, 2, 3$, are the Pauli matrices in isospin space and

$$q = \begin{pmatrix} u \\ d \end{pmatrix} \tag{2.3}$$

is an iso-spinor collecting the up and the down quark fields. The symmetry of the QCD Lagrangian under the vector transformations eq. (2.1) is also called isospin symmetry.

These symmetries are only approximate symmetries: isospin symmetry is explicitely broken by the mass difference of the u- and d-quark. The invariance under axial-vector transformations is explicitely broken by the non-vanishing quark mass. However, the u- and d-quark masses (and their difference) are small compared to the typical hadronic scale of 1 GeV, so the effect of this explicit symmetry breaking should be small.

In nature, isospin symmetry is realised to a high level of accuracy. This is evident from the existence of isospin multiplets in the hadronic mass spectrum. The mass splitting in these multiplets is of the order of a few percent only.
So isospin symmetry is certainly a good symmetry to work with.

Chiral symmetry[1], on the other hand, is not realised in nature in the same way (the so-called Wigner-Weyl mode). This would lead to the observation of parity doublets in the mass spectrum. For example, the ρ and the a_1 should then have the same mass. But the mass difference is of the order of the ρ mass. Such a huge difference cannot be accounted for by the explicit breaking of chiral symmetry through the small quark masses. So the Wigner-Weyl mode drops out as a possible realisation of chiral symmetry.
Instead, chiral symmetry is spontaneously broken. This means that the vacuum does not exhibit the symmetry of the Lagrangian. According to the Goldstone theorem, there should be a massless excitation of the vacuum for each spontaneously broken generator of a symmetry. In the case of broken $SU(2)_A$ symmetry, we expect the existence of three massless pseudoscalars in the spectrum. These can be identified with the pions. Of course, the pions are not exactly massless, but they are (by far) the lightest hadrons. Their non-vanishing mass is attributed to the explicit breaking of chiral symmetry by the non-vanishing quark masses. The observation of the Goldstone bosons in the mass spectrum lends support to the theory of the spontaneous

[1] Here the expression 'chiral symmetry' is used for the axial-vector symmetry alone.

breaking of chiral symmetry. So chiral symmetry is a good symmetry for the QCD Lagrangian and thus it should also be respected in any effective Lagrangian for the strong interaction.

The Goldstone bosons — being the lightest particles of the theory — dominate the physics at low energies. Up to the mass of the lightest non-Goldstone particle, the pions should thus be the appropriate degrees of freedom to work with. Furthermore, the interaction of the Goldstone bosons becomes weak at low energies. This allows for a perturbative treatment of the interaction in terms of small pion momenta. Guided by the symmetry constraints, Chiral Perturbation Theory, the effective field theory for QCD at low energies has been constructed for the interactions of pions [27]. Chiral Perturbation Theory is a systematic expansion of the interaction in terms of pion mass and energy over a scale Λ, below which the effective theory is applicable. This scale is set by the mass of the ρ meson.
The leading order in the chiral expansion contains only known parameters, so that the leading order is fixed. The coupling constants of the higher order interactions, the so called low-energy constants, are free parameters. In principle they are calculable from the underlying theory, but such a calculation is beyond the possibilities of lattice QCD at present. So the low-energy constants have to be determined from experiment.

Also the interaction of pions with the nucleon can be described in Chiral Perturbation Theory. This makes Chiral Perturbation Theory a powerful tool for the investigation of hadronic interactions at low energies. But the further one goes away from the threshold, the larger becomes the expansion parameter E/Λ, and one has to include higher and higher orders in order to describe the interaction. The expansion will finally break down at energies of the order of the masses of the lightest resonances. In the pion sector, this happens at the mass of the ρ meson, in the pion-nucleon sector the mass difference $M_\Delta - M_N$ limits the radius of convergence of the chiral expansion.

Our focus lies on the investigation of the resonance region. That is why we do not work in the framework of Chiral Perturbation Theory. We have to take resonances explicitely into account as dynamical degrees of freedom. In the threshold region, however, our model should be constrained by Chiral Perturbation Theory. The contributions of resonances should manifest themselves in the values of the low-energy constants. It has been shown by Ecker et al. [28] for the mesonic sector that the low-energy constants of the next-to-leading order can be saturated by resonance exchange. For the pion-nucleon sector, such a study has been performed by Bernard et al. [29] who also find nice agreement between the phenomenological values of the low-energy constants and their values from resonance saturation.

A chirally symmetric Lagrangian for the interaction of vector and axial-vector mesons with pions and nucleons was formulated by Wess and Zumino [30]. This Lagrangian

is based on the (chirally symmetric) nonlinear σ-model that describes the interaction of pions and nucleons. Vector and axial-vector mesons are then introduced as gauge fields of a local chiral $SU(2) \times SU(2)$ symmetry. From this Lagrangian we take the πNN, $3\pi N$ and 4π interaction as well as the ρNN and $\pi\pi\rho$ interaction. Note that we use a different sign convention. We fixed the overall phase by the choice $\mathcal{L}_{\pi NN} = -(f_{\pi NN}/m_\pi)\bar{\Psi}\gamma_5\gamma_\mu\vec{\tau}\,\partial^\mu\vec{\pi}\Psi$, which is the sign convention typically used in photoproduction. Then also our $3\pi N$ vertex gets this relative sign with respect to the Wess-Zumino Lagrangian.
In addition we need Lagrangians for the coupling of the scalar σ meson, which parametrises a correlated pion pair in the scalar-isoscalar partial wave, and for the coupling of the Δ and the $N^\star$ resonances. These terms of the interaction Lagrangian are taken from [10] with the following exceptions:

- The $\sigma\pi\pi$ coupling of [10] is supplemented by a scalar coupling proportional to the square of the pion mass $g_1 m_\pi^2 \vec{\pi}\vec{\pi}\sigma$.

- For the coupling of the Roper resonance to the πN, σN and $\pi\Delta$ channel we use the same interaction Lagrangian as for the Nucleon. The Lagrangian of [10] does not contain any coupling for the Roper resonance, because in that work, the Roper resonance is not a genuine resonance but generated from the meson-baryon dynamics.

- For the D_{13} we choose a coupling that is similar to the coupling of the Δ isobar with an additional γ_5 matrix to account for the different parity of the Δ and the D_{13}. Of course, we use also the isospin-1/2 operator for the D_{13}. As in [10] the D-wave character of the $\pi N D_{13}$ interaction is put directly into the vertex by using an additional derivative on the pion field $i\gamma_\mu\partial^\mu$ with respect to the $\pi N\Delta$ Lagrangian.

- The S_{11} resonances are coupled to the πN and ηN channel via gradient coupling. In [10] a scalar coupling for these vertices is assumed, which leads to an unreasonably high contribution of the $S_{11}(1650)$ resonance already at the πN threshold.
  In our model, the contribution of the $S_{11}(1650)$ at the πN threshold is compensated for by σ exchange with a scalar $\sigma\pi\pi$ coupling.
  In an improved version of the Jülich πN model [11] the high contribution of the $S_{11}(1650)$ at threshold has been removed by replacing the scalar coupling with gradient coupling.

The Lagrangian for each vertex is given in Table 2.1.

vertex	$\mathcal{L}$
πNN	$-\frac{f_{\pi NN}}{m_\pi}\bar{\Psi}\gamma_5\gamma_\mu\vec{\tau}\partial^\mu\vec{\pi}\Psi$
$\pi\pi\pi NN$	$-\frac{g_A}{16F_\pi^3}\bar{\Psi}\gamma_5\gamma_\mu\vec{\tau}\left(\partial^\mu\pi^2\vec{\pi}+\vec{\pi}\partial^\mu\pi^2\right)$
$\pi\pi\pi\pi(1)$	$\frac{1}{8F_\pi^2}\left(\partial_\mu\vec{\pi}^2\partial^\mu\vec{\pi}^2-m_\pi^2\vec{\pi}^4\right)$
$\pi\pi\pi\pi(2)$	$\frac{g_{\rho\pi\pi}^2}{2m_\rho^2}\left(\vec{\pi}\times\partial_\mu\vec{\pi}\right)^2$
$\pi N\Delta$	$\frac{f_{\pi N\Delta}}{m_\pi}\bar{\Delta}^\mu\vec{T}^\dagger\partial_\mu\vec{\pi}\Psi+\text{h.c.}$
$\rho\pi\pi$	$-g_{\rho\pi\pi}\left(\vec{\pi}\times\partial_\mu\vec{\pi}\right)\vec{\rho}^\mu$
ρNN	$-g_{\rho NN}\bar{\Psi}\left(\gamma^\mu-\frac{\kappa}{2M_N}\sigma^{\mu\nu}\partial_\nu\right)\vec{\tau}\vec{\rho}_\mu\Psi$
$\sigma\pi\pi$	$-g_1m_\pi^2\vec{\pi}\vec{\pi}\sigma+\frac{g_2}{2}\partial_\mu\vec{\pi}\partial^\mu\vec{\pi}\,\sigma$
σNN	$-g_{\sigma NN}\bar{\Psi}\Psi\sigma$
$\sigma\sigma\sigma$	$-g_{\sigma\sigma\sigma}m_\sigma\sigma\sigma\sigma$
$\pi\Delta\Delta$	$\frac{f_{\pi\Delta\Delta}}{m_\pi}\bar{\Delta}_\mu\gamma_5\gamma_\nu\vec{T}\partial^\nu\vec{\pi}\Delta^\mu$
$\rho N\Delta$	$-i\frac{f_{\rho N\Delta}}{m_\rho}\bar{\Delta}^\mu\gamma_5\gamma^\nu\vec{T}^\dagger\vec{\rho}_{\mu\nu}\Psi+\text{h.c.}$
$\rho\Delta\Delta$	$-g_{\rho\Delta\Delta}\bar{\Delta}_\sigma\left(\gamma^\mu-\frac{\kappa_{\rho\Delta\Delta}}{2M_\Delta}\sigma^{\mu\nu}\partial_\nu\right)\vec{T}\vec{\rho}_\mu\Delta^\sigma$
$P_{11}\pi N$	$-\frac{f_{P_{11}\pi N}}{m_\pi}\bar{\Psi}_{N^\star}\gamma_5\gamma_\mu\vec{\tau}\partial^\mu\vec{\pi}\Psi+\text{h.c.}$
$P_{11}\pi\Delta$	$\frac{f_{P_{11}\pi\Delta}}{m_\pi}\bar{\Delta}^\mu\vec{T}^\dagger\partial_\mu\vec{\pi}\Psi_{N^\star}+\text{h.c.}$
$P_{11}\sigma N$	$-g_{P_{11}\sigma N}\bar{\Psi}_{N^\star}\Psi\sigma+\text{h.c.}$
$D_{13}\pi N$	$i\frac{f_{D_{13}\pi N}}{m_\pi^2}\bar{\Psi}^\mu_{N^\star}\gamma_5\gamma^\nu\vec{\tau}\Psi\partial_\nu\partial_\mu\vec{\pi}+\text{h.c.}$
$D_{13}\pi\Delta$	$\frac{f_{D_{13}\pi\Delta}}{m_\pi}\bar{\Psi}^\mu_{N^\star}\gamma_\nu\vec{T}\partial^\nu\vec{\pi}\Delta_\mu+\text{h.c.}$
$S_{11}\pi N$	$\frac{f_{S_{11}\pi N}}{m_\pi}\bar{\Psi}_{N^\star}\gamma_\mu\vec{\tau}\partial^\mu\vec{\pi}\Psi+\text{h.c.}$
$S_{11}\eta N$	$\frac{f_{S_{11}\eta N}}{m_\eta}\bar{\Psi}_{N^\star}\gamma_\mu\partial^\mu\eta\Psi+\text{h.c.}$

Table 2.1: The interaction Lagrangian of our model.

2.2 Contributions to the Pion Production Reaction $\pi N \to \pi\pi N$

The contributions to the pion-induced pion production reaction are displayed in Figs. 2.1–2.3. The corresponding expressions for the invariant matrix elements are listed in Appendix D.

The diagrams (A.1)–(C.1) contain only pion-nucleon and pion-pion interaction vertices. They constitute the contributions of Chiral Perturbation Theory at leading order together with a $\pi\pi NN$ contact term with a third pion line attached to the nucleon. This $\pi\pi NN$ contact term, the Weinberg–Tomazawa term, is in our model saturated completely by the ρ-exchange in (D.1)–(D.6) and therefore must not appear explicitely.

In addition to the leading order 4π interaction vertex, we use σ and ρ exchange in order to parametrise the scalar-isoscalar and vector-isovector partial waves in $\pi\pi$ scattering. The second 4π vertex in diagram (C.4) is needed to cancel the contribution of the s-channel rho exchange to $\pi\pi$ scattering at leading order in the chiral expansion.

In diagrams (D.1)–(E.6) we take into account the exchange of a σ or a ρ meson. ρ exchange in the t channel is responsible for the isovector part of the pion-nucleon s-wave scattering, while t-channel σ exchange describes the isoscalar part.

The next group of diagrams involves the excitation of a Δ isobar in the intermediate state. The mass of the Δ, $M_\Delta = 1232$ MeV, lies only a few MeV above the $\pi\pi N$ threshold at $\sqrt{s}_{\text{thr.}} = 1215$ MeV. Thus we expect a large contribution from Δ excitation, in particular from diagrams (F.1) and (F.2) already at the pion production threshold.

Finally, we consider the contributions from $N^\star$ excitation and the subsequent decay of the $N^\star$ resonances into the $\pi\pi N$ final state. We take into account contributions from the $N^\star$ resonances with a mass below 1600 MeV, which are the $P_{11}(1440)$, the so-called Roper resonance, the $D_{13}(1520)$ and the $S_{11}(1535)$.
From a look at the baryon summary tables of the Particle Data Group [31] we expect only a small $\pi\pi N$ decay of the $S_{11}(1535)$. However, one needs a $\pi\pi N$ decay of the $S_{11}(1535)$ in order to describe the πN inelasticities and the $\pi N \to \eta N$ cross sections simultaneously. Assuming that the πN inelasticities in the S_{11} partial wave at the resonance energy are completely saturated by the coupling to the ηN channel leads to an overestimation of the $\pi N \to \eta N$ cross sections. This can be mended if one allows for a $\pi\pi N$ decay of the resonance [11]. We have included the possibility of a $\pi\pi N$ decay of the $S_{11}(1535)$ via the decay to a πN intermediate state and the subsequent decay of the nucleon to πN.

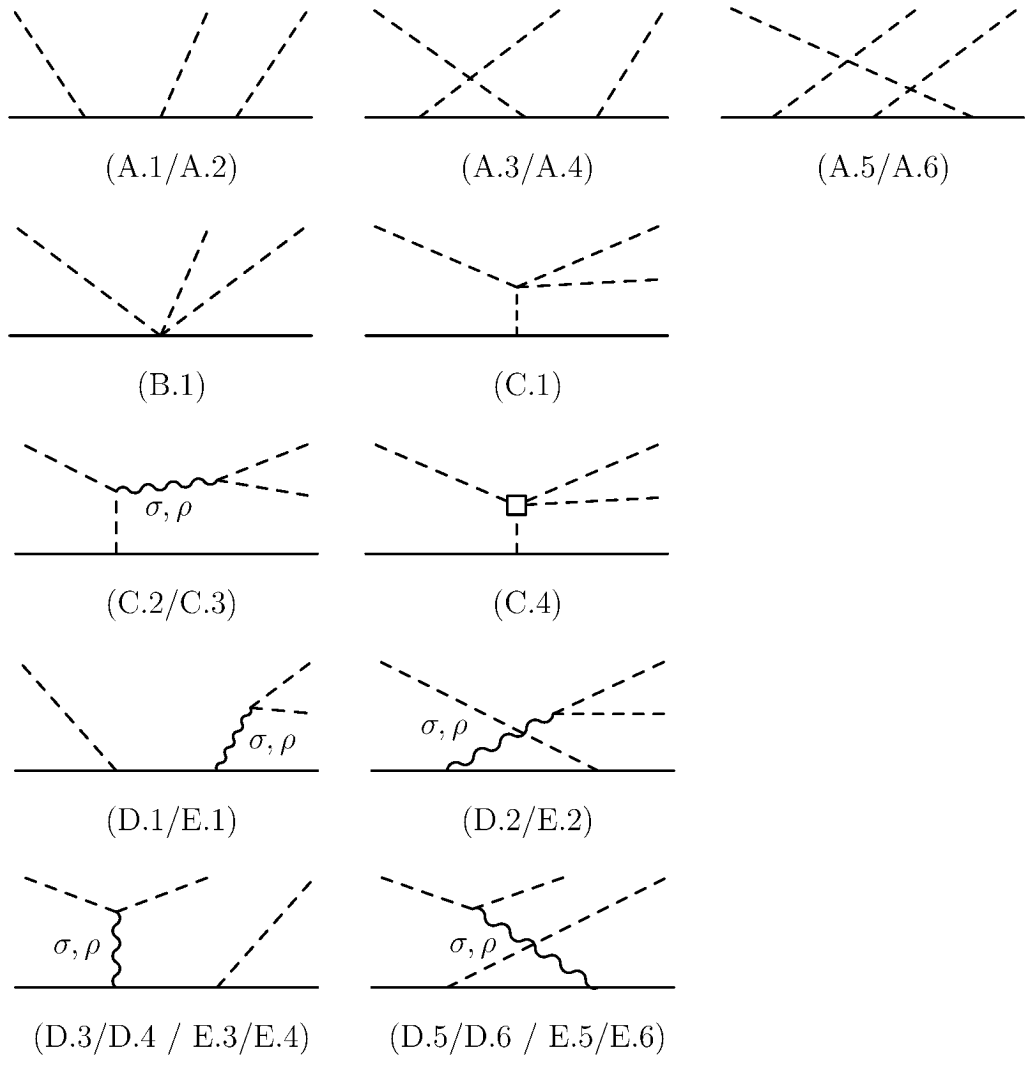

Figure 2.1: Contributions to the $\pi N \to \pi\pi N$ reaction in our model. The labels below the diagrams refer to the labelling of the expressions for the amplitudes listed in Appendix D.

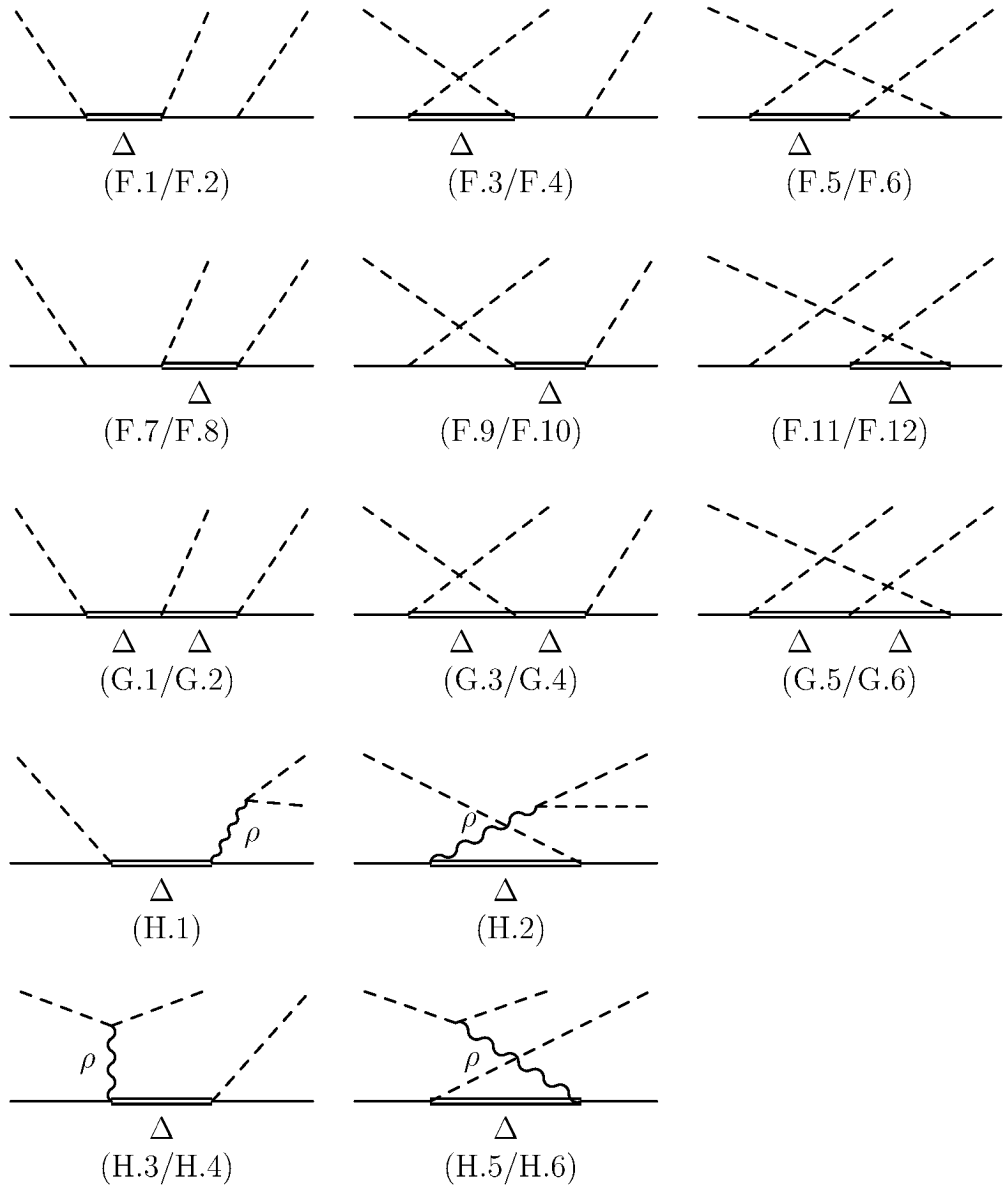

Figure 2.2: Contributions to our model involving Δ excitation.

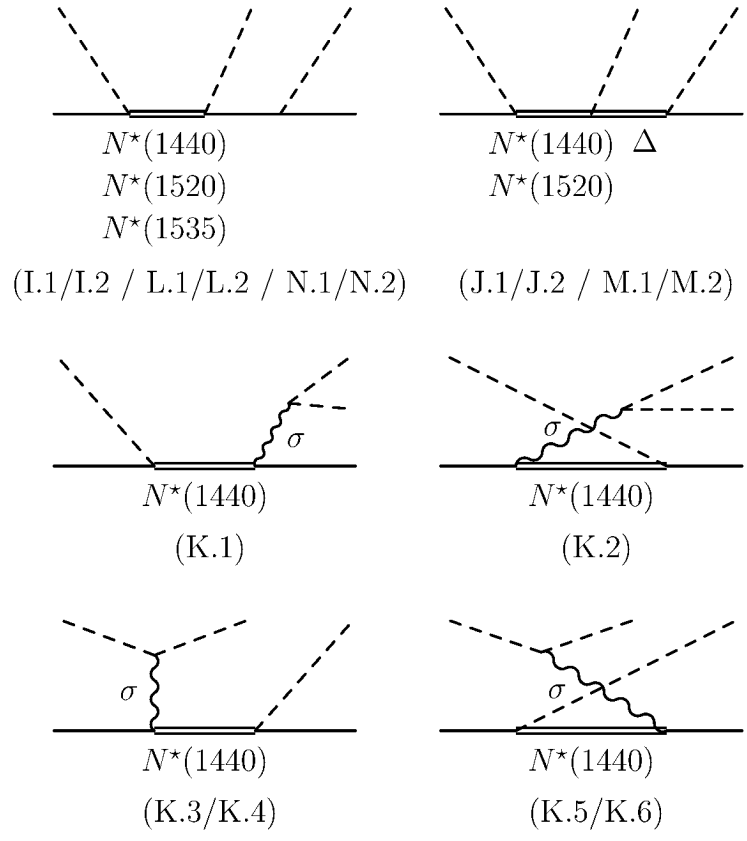

Figure 2.3: Contributions to $\pi N \to \pi\pi N$ from $N^\star$ excitation.

According to [31], the $D_{13}(1520)$ should decay with a fraction of $40-50\%$ to the $\pi\pi N$ channel. Of these $15-25\%$ should go into the $\pi\Delta$ channel and the same fraction to the ρN channel. We have only included the decay to the $\pi\Delta$ channel. We expect the effect of the ρN channel to be small in the energy range up to 1.5 GeV, because the $\pi\pi$ interaction in the ρ partial wave is still small for the corresponding maximal energy of the $\pi\pi$ system of ~ 0.6 GeV.
The important $\pi\pi N$ decay channels of the Roper resonance are the $\pi\Delta$ and the σN decay. Although the σN decay is quoted with a fraction of $5-10\%$ only, it should still make important contributions to the two-pion decay of the Roper resonance. The presence of a large contribution of the $(\pi\pi)_s$ decay of the Roper resonance at the $\pi\pi N$ threshold has already been observed in the Oset–Vicente-Vacas model [24].

With the exception of diagram (B.1), the contributions to $\pi N \to \pi\pi N$ can be grouped in the following way:

- diagrams describing $\pi\pi$ scattering with a nucleon attached to a pion leg ((C.1)–(C.4)),
- diagrams describing πN scattering with an additional pion attached to the nucleon line ((A.1)–(A.6), (D.3)–(D.6), (E.3)–(E.6), (F.1)–(F.4), (F.9)-(F.12) and (I/L/N.1/2)),
- and diagrams contributing to the transition of the πN channel to an inelastic channel (C.2/3), (D/E.1/2), (F.3)–(F.6), (G.1)–(H.6), (J/M.1/2) and (K.1)–(K.6).

Of course, our model should also be able to describe these sub-processes. We can make use of these sub-processes to fix the parameters of our model, the masses of the resonances and the coupling constants.

The fitting of the parameters to the $\pi\pi$ and πN phase shifts and inelasticities is described in the following chapter. The results obtained with our model for the reaction $\pi N \to \pi\pi N$ are presented in Chapter 4.

Chapter 3

Pion-Pion and Pion-Nucleon Scattering

In this chapter we describe how the parameters for the $\pi N \to \pi\pi N$ model are determined from pion-pion and pion-nucleon scattering. Detailed phase shift analyses are available for both reactions. In order to compare with those analyses, it is necessary to demand that the model employed fulfils unitarity. This can be achieved by iterating the interaction in a scattering equation.

At the same time we intend to keep the scattering equation as simple as possible. For this reason, we choose to work with the K-matrix approximation, which will be described in the following section.

3.1 The K-Matrix Formalism

The relativistic scattering of two particles is described by the Bethe-Salpeter Equation

$$\begin{aligned}\langle\, k'\lambda_3\lambda_4\, f\,|T|\, k\,\lambda_1\lambda_2\, i\,\rangle &= \langle\, k'\lambda_3\lambda_4\, f\,|U|\, k\,\lambda_1\lambda_2\, i\,\rangle \\ &+ \sum_{\kappa_1\kappa_2\, n}\int \frac{d^4q}{(2\pi)^4}\,\langle\, k'\lambda_3\lambda_4\, f\,|U|\, q\,\kappa_1\kappa_2\, n\,\rangle G(P,q)\langle\, q\,\kappa_1\kappa_2\, n\,|T|\, k\,\lambda_1\lambda_2\, i\,\rangle\,. \quad (3.1)\end{aligned}$$

In this equation, $G(q)$ denotes the two-particle propagator, which is the product of the Feynman propagators of the particles in the intermediate state,

$$G(P,q) = (-i)\,\frac{i}{(\frac{P}{2}+q)^2 - M_1^2 + i\epsilon}\,\frac{i}{(\frac{P}{2}-q)^2 - M_2^2 + i\epsilon}\,, \quad (3.2)$$

for a two-particle intermediate state with M_1 and M_2 the masses of the two particles. P is the sum of the two particles' four-momenta. We work in the centre-of-momentum

frame, where $P = (\sqrt{s}, \vec{0})$. q is the relative momentum in the two-particle intermediate state. k and k' are the relative momenta in the initial and final state, respectively. The λ_i and κ_i are the helicities of the particles, and f, i, n label the different two-particle channels. For $\pi\pi$ scattering we take only the $\pi\pi$ channel into account, for πN scattering we include the coupled channels πN, σN, $\pi\Delta$ and ηN. The channel indices will be suppressed in the following.

The integral kernel U consists of all connected two-particle irreducible interactions. Irreducible are those two-to-two particle interactions that do not contain intermediate states with *only* two particles.
An infinite number of reducible interactions is generated by the scattering equation. In principle also the number of two-particle irreducible interactions is infinite, so for any application, the kernel has to be approximated.

Another approximation is connected with the fact, that the Bethe-Salpeter Equation (3.1) is a four-dimensional integral equation. The solution of an integral equation in four dimensions is technically very involved. With the coupled channels, such a calculation is hardly feasible. In practice, one works with a three-dimensional reduction of the Bethe-Salpeter Equation. A reduction can be achieved by writing the Bethe-Salpeter Equation as a set of coupled equations,

$$T = V + VgT \tag{3.3}$$
$$V = U + U(G - g)V \tag{3.4}$$

with an arbitrary two-particle propagator g [32]. g is often chosen to contain a one-dimensional δ-distribution that puts a constraint on the zeroth component of the relative momentum. A possible choice for g is [33]

$$g(P,q) = 2\pi \frac{\delta(q^0)}{s - s_q + i\epsilon} \frac{\sqrt{s_q}}{2E_1(s_q)E_2(s_q)} f(s, s_q)\,, \tag{3.5}$$

with $s_q = (E_1(s_q) + E_2(s_q))^2$ and $E_i = \sqrt{M_i^2 + \vec{q}^2}$. $f(s, s_q)$ is any function that fulfils $f(s,s) = 1$. This condition for $f(s, s_q)$ comes from the requirement that $g(P,q)$ has the same discontinuity along the real axis as the full two-particle propagator $G(P,q)$. So the imaginary part of g is fixed. The real part of $g(P,q)$ is completely arbitrary. With $g(P,q)$ as in Equation (3.5), one gets a three-dimensional equation for T,

$$\begin{aligned}\langle\, k'\lambda_3\lambda_4\,|T|\,k\,\lambda_1\lambda_2\,\rangle &= \langle\, k'\lambda_3\lambda_4\,|V|\,k\,\lambda_1\lambda_2\,\rangle \\ &+ \sum_{\kappa_1\kappa_2} \int \frac{d^3q}{(2\pi)^3} \langle\, k'\lambda_3\lambda_4\,|V|\,q\,\kappa_1\kappa_2\,\rangle \tilde{g}(P,q) \langle\, q\,\kappa_1\kappa_2\,|T|\,k\,\lambda_1\lambda_2\,\rangle\,,\end{aligned} \tag{3.6}$$

with

$$\tilde{g}(P,q) = \frac{1}{s - s_q + i\epsilon} \frac{\sqrt{s_q}}{2E_1(s_q)E_2(s_q)} f(s, s_q)\,. \tag{3.7}$$

The driving term of this scattering equation, the quantity V is in principle determined by equation (3.4). In view of (a) the difficulty of solving a four-dimensional integral equation and (b) the fact that the integral kernel U is not precisely known anyway, one chooses V to be given by a subset of irreducible interactions. Usually, one takes into account the interaction up to second order in the coupling constant. This approximated V is often referred to as the pseudopotential.

The three-dimensional scattering equation (3.6) can be further simplified by working in the K-matrix approximation.
The K-matrix is defined by the equation [34, 35]

$$\langle \vec{k}'\lambda_3\lambda_4 |K| \vec{k}\,\lambda_1\lambda_2 \rangle = \langle \vec{k}'\lambda_3\lambda_4 |V| \vec{k}\,\lambda_1\lambda_2 \rangle + \sum_{\kappa_1\kappa_2} \int \frac{d^3q}{(2\pi)^3} \langle \vec{k}'\lambda_3\lambda_4 |V| \vec{q}\,\kappa_1\kappa_2 \rangle \mathrm{Re}\,[\tilde{g}(P,q)] \langle \vec{q}\,\kappa_1\kappa_2 |K| \vec{k}\,\lambda_1\lambda_2 \rangle . \tag{3.8}$$

The T-matrix can be expressed in terms of the K-matrix as

$$\langle \vec{k}'\lambda_3\lambda_4 |T| \vec{k}\,\lambda_1\lambda_2 \rangle = \langle \vec{k}'\lambda_3\lambda_4 |K| \vec{k}\,\lambda_1\lambda_2 \rangle + \sum_{\kappa_1\kappa_2} \int \frac{d^3q}{(2\pi)^3} \langle \vec{k}'\lambda_3\lambda_4 |K| \vec{q}\,\kappa_1\kappa_2 \rangle\, i\mathrm{Im}\,[\tilde{g}(P,q)] \langle \vec{q}\,\kappa_1\kappa_2 |T| \vec{k}\,\lambda_1\lambda_2 \rangle . \tag{3.9}$$

Given an expression for the K-matrix, this equation for the T-matrix can be easily solved, because the imaginary part of the two-particle propagator is proportional to a δ-function that puts both particles in the intermediate state on their mass shell,

$$\mathrm{Im}\,[\tilde{g}(P,q)] = -\frac{\pi}{4q_{\mathrm{on}}\sqrt{s}}\delta(q - q_{\mathrm{on}}) , \tag{3.10}$$

with the on-shell momentum

$$q_{\mathrm{on}} = \frac{1}{2\sqrt{s}}\sqrt{s - (M_1 + M_2)^2}\sqrt{s - (M_1 - M_2)^2} . \tag{3.11}$$

As already mentioned, the imaginary part of the propagator is unambiguous.

The K-matrix approximation consists of setting $K = V$, thus neglecting the principal value integral in Equation (3.8). The unitarity cut is taken into account properly in equation (3.9), so the resulting transition matrix T is unitary. Neglecting the principal value integral leads to a reduction of strength for the multiple scattering contributions as only on-shell intermediate states (coming from equation (3.9)) are allowed in the K-matrix approximation. Taking into account only the on-shell intermediate states means in particular that the different channels can only contribute above their production threshold. So analyticity is violated in this approach. However, Pearce and Jennings [36] compared the quality of the K-matrix approximation to other choices of

the propagator for *elastic* πN scattering. They found that the effect from the principle value integral is small in this particular reaction, so that the parameters extracted for the different approximations do not differ much.

Our aim is not to formulate a unitary, analytic model for $\pi\pi$ and πN scattering. Instead, we aim at a fit of the coupling constants and resonance masses for the tree-level $\pi N \to \pi\pi N$ model. This model contains *tree-level* contributions corresponding to $\pi\pi$ and πN scattering. In order to fit the parameters of these contributions to the results of the phase shift analyses for $\pi\pi$ and πN scattering, we have to unitarise these tree-level contributions, and we want to unitarise them in a most simple way. For this purpose, the K-matrix appears to be most convenient.

Finally, we want to point out that as a consequence of neglecting the principal value integral (3.8) the K-matrix approximation cannot generate poles in the T-matrix dynamically. Such a dynamical pole is generated if the series

$$K = V + V\,\mathcal{P}G\,V + V\,\mathcal{P}G\,V\,\mathcal{P}G\,V + \ldots \tag{3.12}$$

is divergent. For πN scattering the Jülich model [10] predicts the dynamical generation of the Roper resonance from the coupling of the πN to the σN channel. However, in the framework of the K-matrix approximation, this pole can be introduced 'by hand' by including it as a genuine pole in the potential.

Because of the rotational invariance of the strong interactions, the matrix elements of the potential and the transition matrix can be decomposed into submatrices of definite angular momentum. This partial wave decomposition is shown in detail in appendix B. The three-dimensional integral equation (3.6) is reduced by the K-matrix approximation together with the partial wave decomposition to a set of algebraic equations of definite angular momentum J,

$$\begin{aligned}\langle\, k'\lambda_3\lambda_4\,|T^J|\,k\,\lambda_1\lambda_2\,\rangle = \langle\, k'\lambda_3\lambda_4\,|V^J|\,k\,\lambda_1\lambda_2\,\rangle - \frac{i\pi}{(2\pi)^3}\frac{q_{\text{on}}}{4\sqrt{s}} \\ \cdot \sum_{\kappa_1\kappa_2} \langle\, k'\lambda_3\lambda_4\,|V^J|\,q_{\text{on}}\,\kappa_1\kappa_2\,\rangle \langle\, q_{\text{on}}\,\kappa_1\kappa_2\,|T^J|\,k\,\lambda_1\lambda_2\,\rangle\,. \end{aligned} \tag{3.13}$$

It is convenient to write the matrix elements in terms of the JLS basis for several reasons. A state in JLS basis has definite parity. Thus, the parity of a resonance can be determined directly from the partial wave to which it contributes in the JLS representation. Some of the transition matrix elements $\langle\, k'L'S'\,|V^J|\,k\,LS\,\rangle$ vanish because of parity conservation and angular momentum conservation. And finally, the results from partial wave analyses of experimental data are usually given in the JLS basis for the abovementioned reasons. The transformation from helicity basis to JLS basis is given in appendix B.

Since the strong interactions approximately conserve isospin, the states are in addition characterised by their total isospin I. The scattering equations for different isospin decouple. The coupled-channels two-body scattering equation in JLS basis is given by

$$\langle\, k'L'S' \,|T^{IJ}|\, k\,LS\,\rangle = \langle\, k'L'S' \,|V^{IJ}|\, k\,LS\,\rangle - \frac{i\pi}{(2\pi)^3}\frac{q_{\text{on}}}{4\sqrt{s}} \cdot \sum_{L''S''} \langle\, k'L'S' \,|V^{IJ}|\, q_{\text{on}}\,L''S''\,\rangle \langle\, q_{\text{on}}\,L''S'' \,|T^{IJ}|\, k\,LS\,\rangle\,. \quad (3.14)$$

3.1.1 The σN and $\pi\Delta$ Propagators

The σ is a parameterisation of a correlated pion pair in the scalar-isoscalar channel. So in the σN channel we effectively deal with a three particle channel of two pions and a nucleon. In the K-matrix approximation we want to account for those three-particle states with the nucleon and two pions on their mass shell.

In our parameterisation the σ consists of a 'bare' σ which is dressed by pion loops.

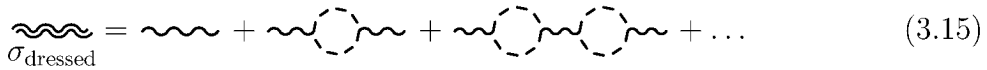

(3.15)

In order to get the contribution with two pions on-shell, we have to take the imaginary part of the σ propagator, since the expression (3.15) can only acquire an imaginary part if the two pions in a loop are on their mass shell. The imaginary part of the propagator is related to the imaginary part of the self-energy by

$$\text{Im}\left[\frac{1}{P^2 - m_\sigma^2 - \Sigma_\sigma(P^2)}\right] = \text{Im}\left[\Sigma_\sigma(P^2)\right]\left|\frac{1}{P^2 - m_\sigma^2 - \Sigma_\sigma(P^2)}\right|^2 . \quad (3.16)$$

The self-energy can be calculated from $\pi\pi$ scattering. It is given by

$$\Sigma_\sigma(P^2) = f_0^\dagger G f_0 \quad (3.17)$$

with f_0 the bare vertex function of the $\sigma\pi\pi$ vertex and G the pion-pion propagator,

$$\begin{aligned} f_0 &= -\sqrt{12\pi}\left(2g_1 m_\pi^2 + \frac{g_2}{2}(P^2 - 2m_\pi^2)\right) \\ G &= -\frac{1}{2}\frac{i\pi}{(2\pi)^3}\frac{1}{4\sqrt{P^2}}\sqrt{\frac{P^2}{4} - m_\pi^2} \end{aligned}$$

with the $\sigma\pi\pi$ scalar and gradient coupling constant g_1 and g_2 as defined in Table 2.1.

In a similar manner, the $\Delta(1232)$ acquires a self-energy by the dressing with πN loops. For the Δ self-energy, we take into account only the part of the width coming from πN loops and neglect any non-pole πN interaction. We get

$$\Sigma_\Delta(s) = f_0^\dagger G_{\pi N} f_0 \quad (3.18)$$

with f_0 the vertex function of the $\pi N\Delta$ vertex in the Δ pole potential in the P_{33} partial wave of πN scattering. Expressing the vertex function explicitely with the help of our $\pi N\Delta$ Lagrangian, we get

$$\Sigma_\Delta(s) = -i\,\frac{q_{\rm on}^3}{6m_\pi^2\sqrt{s}}\,(E_N+M_N)(\sqrt{s}+M_\Delta)\,\frac{f_{\pi N\Delta}^2}{4\pi}\,. \tag{3.19}$$

$f_{\pi N\Delta}$ denotes the $\pi N\Delta$ coupling constant, $q_{\rm on}$ is the on-shell momentum of the πN state in the loop and $E_N = \sqrt{M_N^2+q_{\rm on}^2}$.
This should actually be a very good description of the Δ self-energy, because the P_{33} partial wave in pion-nucleon scattering can already be nicely described by a Δ pole diagram alone for energies up to ≈ 1.3 GeV.

With the help of the relation (3.16) we can write down the propagator for the σN and $\pi\Delta$ intermediate state — more generally for an intermediate state with one stable particle (we choose particle 1) and one unstable particle. For such a state, the scattering equation (3.1) contains the expression with the two-particle propagator,

$$i\int\frac{d^4q}{(2\pi)^4}V(k',q)\,\frac{1}{q^2-M_1^2+i\epsilon}\,\frac{1}{(P-q)^2-m_2^2-\Sigma_2((P-q)^2)}\,T(q,k)\,. \tag{3.20}$$

We put particle 1 on its mass shell by exploiting the Cutkosky rules [37], $\frac{1}{q^2-M_1^2+i\epsilon}\to-\frac{2\pi i}{2E_1}\,\delta(q^0-E_1)$. Of the unstable particle's propagator we keep only the imaginary part which is related to the two-particle cut. After a partial wave decomposition we get

$$\begin{aligned} i\int_0^{q_{\rm max}}\frac{dq}{(2\pi)^3}V^J(k',q)\,\frac{q^2}{2E_1}\,&{\rm Im}\left(\Sigma_2((\sqrt{s}-E_1)^2-q^2)\right)\\ &\cdot\left|\frac{1}{(\sqrt{s}-E_1)^2-q^2-m_2^2-\Sigma_2((\sqrt{s}-E_1)^2-q^2)}\right|^2\,T^J(q,k)\,. \end{aligned} \tag{3.21}$$

For the σN propagator, the maximal momentum $q_{\rm max}$ is reached for the minimal invariant mass of the two pions,

$$q_{\rm max} = \frac{1}{2\sqrt{s}}\,\sqrt{(s-(M_N+2m_\pi)^2)\,(s-(M_N-2m_\pi)^2)}\,. \tag{3.22}$$

In the case of the $\pi\Delta$ propagator, the maximal momentum is given by

$$q_{\rm max} = \frac{1}{2\sqrt{s}}\,\sqrt{(s-(M_N+2m_\pi)^2)\,(s-(M_N)^2)}\,. \tag{3.23}$$

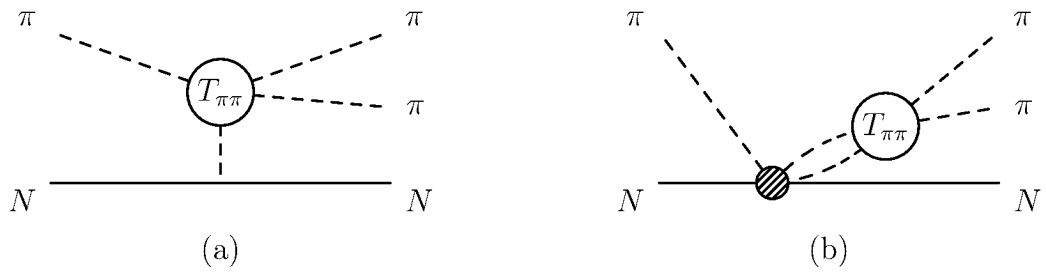

Figure 3.1: Contribution of the $\pi\pi$ T-matrix to $\pi N \to \pi\pi N$. (a) The pion exchange diagram. (b) Pion-Pion rescattering. The 'blob' in (b) includes all tree-level diagrams that lead to a $\pi\pi N$ final state. Note, that the decomposition into (a) and (b) is arbitrary and just for illustrative purpose.

3.2 Pion-Pion scattering

Pion-Pion scattering contributes to $\pi N \to \pi\pi N$ as final state interaction (Fig. 3.1). At pion momenta of tens of GeV, pion induced pion production on the nucleon is dominated by the pion-exchange diagram Fig. 3.1(a) and a_1- and a_2-exchange. This allows the extraction of information on the $\pi\pi$ interaction. So beside $\pi N \to \pi\pi\Delta$ [38] and K_{e4} decays[1] [39], pion induced pion production is a source of information on pion-pion scattering.
Then, there is also a contribution of $\pi\pi$ scattering in the rescattering of the final state pions (Fig. 3.1(b)). This rescattering contribution is partly accounted for in our tree-level model through the inclusion of σ and ρ exchange as a parameterisation of a correlated pion pair. In this section we describe a model for $\pi\pi$ scattering, from which we also determine the parameters for σ and ρ exchange.

In order to get a reasonable description of pion-induced two-pion production up to $\sqrt{s} = 1.5$ GeV we need a model that can describe $\pi\pi$ scattering up to ≈ 0.6 GeV. The lowest-lying two-particle channel that couples strongly to the $\pi\pi$-channel, the $K\bar{K}$-channel, opens only at 990 MeV. For our purpose it is hence entirely adequate to deal with the $\pi\pi$-channel only.

We now write down the potential for $\pi\pi$ scattering. This potential is then iterated in the scattering equation (3.14) to obtain the T-matrix from which the observables are calculated.

We start from the chiral Lagrangian at leading order,

$$\mathcal{L}_2 = \frac{F^2}{4}\langle D_\mu U^\dagger D^\mu U + \chi^\dagger U + \chi U^\dagger \rangle \,. \tag{3.24}$$

[1] K_{e4} decays are the semileptonic four-body decays $K \to \pi\pi l \nu_l$.

The pion fields are contained in the unitary matrix U. The representation of U in terms of the pion fields is not unique. Observables must, however, be invariant under a redefinition of the pion fields. We work with the so-called σ-model gauge,

$$U = \sqrt{1 - \frac{\vec{\pi}^2}{F_\pi^2}} + i\,\frac{\vec{\tau}\vec{\pi}}{F_\pi}\,. \tag{3.25}$$

D_μ is the covariant derivative, which in our case is just the derivative of the pion fields as we are not concerned with external vector and axial-vector fields. The brackets $\langle \ldots \rangle$ denote the trace in flavour space. χ contains the quark masses,

$$\chi = 2B\mathcal{M} = 2B \begin{pmatrix} m_u & 0 \\ 0 & m_d \end{pmatrix}\,, \tag{3.26}$$

and is related to the pion mass via the relation

$$m_\pi^2 = B(m_u + m_d)\left\{1 + \mathcal{O}(\mathcal{M})\right\} = \frac{1}{2}\left\langle\chi\right\rangle\left\{1 + \mathcal{O}(\mathcal{M})\right\}\,. \tag{3.27}$$

So at leading order, $\frac{1}{2}\left\langle\chi\right\rangle$ is just the square of pion mass.
F is the pion decay constant in the chiral limit, $F_\pi = F\left\{1 + \mathcal{O}(\mathcal{M})\right\}$. We use the value $F_\pi = 92.4$ MeV.
The first term in $\mathcal{L}_2$ is invariant under a chiral transformation, the second term describes the explicit breaking of chiral symmetry by the small quark masses.

Expanding the Lagrangian $\mathcal{L}_4$ up to four pion fields, we get the interaction Lagrangian of the nonlinear sigma model plus a mass term,

$$\mathcal{L}_{4\pi} = \frac{1}{8F_\pi^2}\left(\partial_\mu\vec{\pi}^2\partial^\mu\vec{\pi}^2 - m_\pi^2\vec{\pi}^4\right)\,. \tag{3.28}$$

The Lagrangian $\mathcal{L}_{4\pi}$ leads to a potential in the s and p waves of pion-pion scattering. After a partial wave decomposition we get the following expressions[2]:

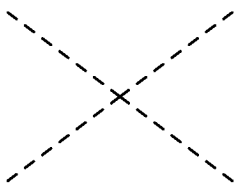

$$\begin{aligned} V^{00} &= -\frac{4\pi}{F_\pi^2}\left(2s - m_\pi^2\right)\,, \\ V^{11} &= -\frac{16\pi}{3F_\pi^2}\left(\frac{s}{4} - m_\pi^2\right)\,, \\ V^{20} &= -\frac{4\pi}{F_\pi^2}\left(-s + 2m_\pi^2\right)\,. \end{aligned} \tag{3.29}$$

[2]We use the notation V^{IJ} with total isospin I and angular momentum J.

Iterating the leading order Chiral Perturbation Theory potential in the K-matrix approximation is not enough to describe the $\pi\pi$ phases in the scalar-isoscalar and vector-isovector partial wave up to $\sqrt{s} \simeq 600$ MeV (see Fig 3.2).

In order to parametrise the strong $\pi\pi$ correlation in the scalar-isoscalar partial wave, we introduce the s-channel exchange of a scalar-isoscalar resonance, the σ. This is coupled to the pions via gradient and scalar coupling,

$$\mathcal{L}_{\sigma\pi\pi} = -g_1 m_\pi^2 \vec{\pi}\vec{\pi}\sigma + \frac{g_2}{2}\,\partial_\mu\vec{\pi}\,\partial^\mu\vec{\pi}\sigma\,. \tag{3.30}$$

The σ s-channel exchange leads to a separable potential in the $I = J = 0$ partial wave.

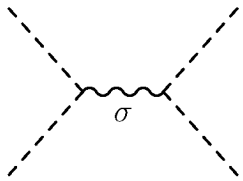

$$V_\sigma^{00} = \frac{f_0 f_0^\dagger}{s - m_\sigma^2} \tag{3.31}$$

$$f_0 = 2\pi\sqrt{3}\left[2g_1 m_\pi^2 + \frac{g_2}{2}(s - 2m_\pi^2)\right] \tag{3.32}$$

In the $I = J = 1$ partial wave we include the s-channel exchange of the ρ meson in addition to the leading order chiral perturbation theory (3.28). The interaction Lagrangian reads

$$\mathcal{L}_{\rho\pi\pi} = -g_{\rho\pi\pi}\,(\vec{\pi}\times\partial_\mu\vec{\pi})\,\rho^\mu + \frac{g_{\rho\pi\pi}^2}{2m_\rho^2}\,(\vec{\pi}\times\partial_\mu\vec{\pi})^2\,. \tag{3.33}$$

The first term of (3.33) alone would lead to a contribution of the ρ-exchange in $\pi\pi$-scattering at leading order in the chiral expansion in addition to the contribution from $\mathcal{L}_{4\pi}$. But $\mathcal{L}_{4\pi}$ already gives the complete interaction at $\mathcal{O}(p^2)$, so that the leading order contribution from ρ exchange has to vanish. For this purpose, the second term in $\mathcal{L}_{\rho\pi\pi}$, a $\pi\pi$ contact interaction, is needed. The $\pi\pi$ contact interaction in $\mathcal{L}_{\rho\pi\pi}$ appears quite naturally if one introduces the ρ meson as a massive gauge boson [40]. Another possibility to avoid a contribution of the ρ-meson at leading order would be to introduce the ρ-meson not as a vector field but as an antisymmetric tensor field [27, 28, 41].

The potential from ρ-exchange in the s-channel is given by

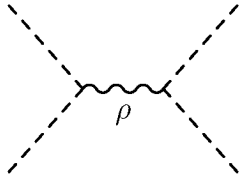

$$V_\rho^{11} = \frac{f_0 f_0^\dagger}{s - m_\rho^2} \tag{3.34}$$

$$f_0 = g_{\rho\pi\pi}\sqrt{\frac{32\pi}{3}\left(\frac{s}{4} - m_\pi^2\right)} \tag{3.35}$$

From the $\pi\pi$ contact interaction in (3.33) we keep only the part that cancels the ρ exchange in the s-channel at $\mathcal{O}(p^2)$.

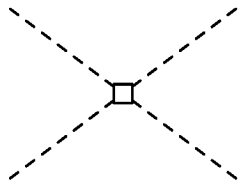

$$V^{11}_{\rho\mathrm{ct}} = \frac{32\pi}{3}\frac{g^2_{\rho\pi\pi}}{m^2_\rho}\left(\frac{s}{4}-m^2_\pi\right) \qquad (3.36)$$

With this potential, a good description of the pion-pion phase shifts up to the $K\bar{K}$ threshold and up to $J = 1$ is possible. We fit the coupling constants and masses of the σ and the ρ to the $\pi\pi$ phase shifts δ_{00} and δ_{11}, respectively. The resulting fits are shown in Fig. 3.2. The fitted parameters are given in Table 3.1.

3.2.1 Comparison with Chiral Perturbation Theory

Now let us check whether the low-energy limit of our meson exchange contributions agrees with Chiral Perturbation Theory. As has been shown by Ecker et al., the next-to-leading order Chiral Lagrangian can be expressed in terms of resonance exchange and the low-energy constants can be saturated to good accuracy by this resonance exchange [28].

The Chiral Lagrangian at $\mathcal{O}(p^4)$ reads:

$$\begin{aligned}\mathcal{L}_4 &= L_1\langle D_\mu U^\dagger D^\mu U\rangle^2 + L_2\langle D_\mu U^\dagger D_\nu U\rangle\langle D^\mu U^\dagger D^\nu U\rangle \\ &+ L_3\langle D_\mu U^\dagger D^\mu U D_\nu U^\dagger D^\nu U\rangle + L_4\langle D_\mu U^\dagger D^\mu U\rangle\langle\chi^\dagger U+\chi U^\dagger\rangle \\ &+ L_5\langle D_\mu U^\dagger D^\mu U\left(\chi^\dagger U+\chi U^\dagger\right)\rangle + L_6\langle\chi^\dagger U+\chi U^\dagger\rangle^2 \\ &+ L_8\langle\chi^\dagger U\chi^\dagger U+\chi U^\dagger\chi U^\dagger\rangle + \ldots \end{aligned} \qquad (3.37)$$

The ellipsis stands for those terms in $\mathcal{L}_4$ that do not contribute to pion-pion scattering.

The low-energy constants L_i contain finite and divergent pieces. The divergent pieces are needed to cancel the divergences of the pion loops at $\mathcal{O}(p^4)$. The renormalised values of the finite pieces will thus depend on some renormalisation scale λ. For the purpose of resonance saturation this scale should not be too far away from the resonance region, so is chosen to be equal to the mass of the ρ [28]. At present, it is not possible to calculate their values from QCD directly. Instead, they have been determined phenomenologically from experiment and by invoking large-N_C arguments [46]. Their values are listed in Table 3.2.

The contribution of resonance excitation to the low-energy constants can be determined by replacing the resonance degrees of freedom with an effective interaction.

m_σ	0.8346 GeV
$\frac{g_1^2}{4\pi}$	98.94 GeV^{-2}
$\frac{g_2^2}{4\pi}$	7.322 GeV^{-2}
m_ρ	0.772 GeV
$\frac{g_{\rho\pi\pi}^2}{4\pi}$	2.905

Table 3.1: Parameters for the σ and ρ exchange.

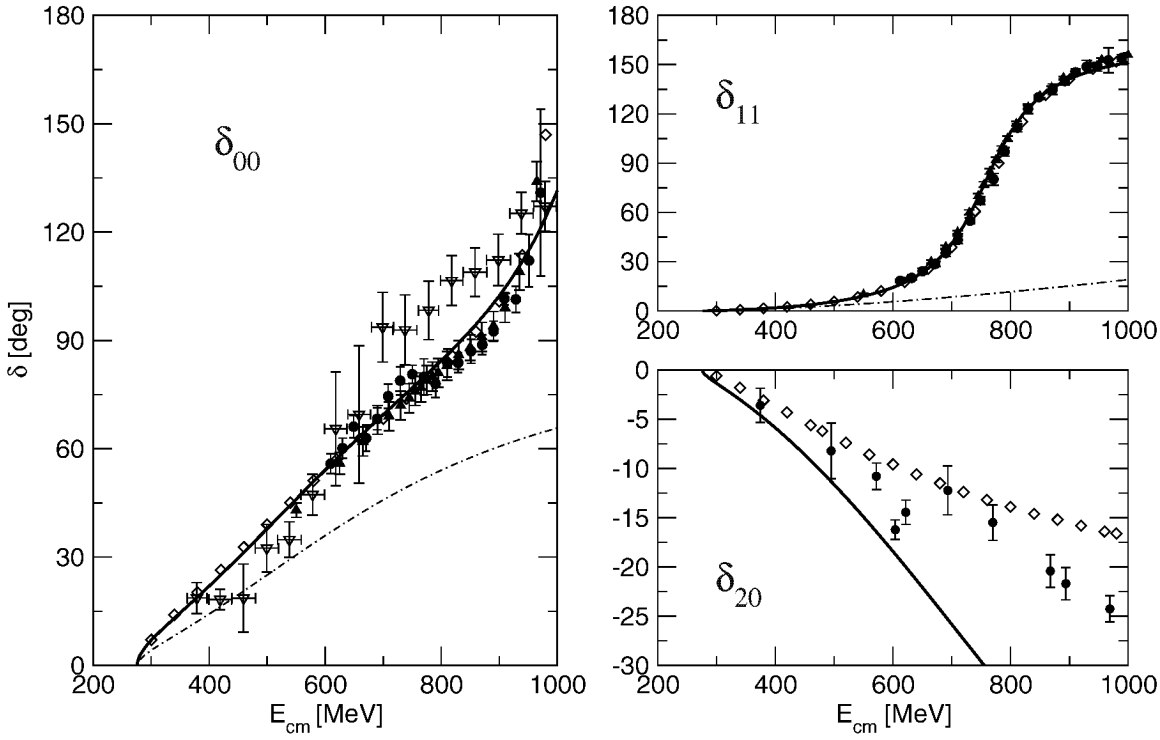

Figure 3.2: The pion-pion phase shifts up to $J = 1$. The solid lines show the results of our K-matrix model. For comparison we also show the results with the potential from leading order Chiral Perturbation Theory alone (dot-dashed lines). The data stem from the analyses of Protopopescu [38] (filled triangle-up), Hyams [42] (filled circles), Froggatt [43] (open diamonds), Takamatsu [44] (open triangle-down) and from a compilation by Martin [45] (filled diamonds).

For momentum transfers much smaller than the resonance mass m_x, the propagator of the resonance can be expanded in a Taylor series,

$$\frac{1}{q^2 - m_x^2} = -\frac{1}{m_x^2}\left(1 + \frac{q^2}{m_x^2} + \mathcal{O}\left(\frac{q^4}{m_x^4}\right)\right) . \tag{3.38}$$

For the ρ exchange, the $\pi\pi$ contact interaction arising from the first term in the expansion is cancelled by the contact interaction in the Lagrangian (3.33). The contact term from the second term in the expansion of the propagator contributes as desired at $\mathcal{O}(p^4)$.

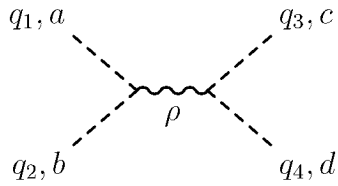

$$\Rightarrow \quad V = \frac{4g_{\rho\pi\pi}^2}{m_\rho^4}\left[(q_1 \cdot q_2)^2 - (q_1 \cdot q_3)^2\right]\left[\delta_{ab}\delta_{cd} - \delta_{ac}\delta_{bd}\right]$$

By comparing this to the Lagrangian $\mathcal{L}_4$, one finds that the contribution of ρ exchange comes in the combination $\frac{1}{2}\langle D_\mu U^\dagger D^\mu U\rangle^2 + \langle D_\mu U^\dagger D_\nu U\rangle\langle D^\mu U^\dagger D^\nu U\rangle - 3\langle D_\mu U^\dagger D^\mu U D_\nu U^\dagger D^\nu U\rangle$. The low-energy constants L_1, L_2 and L_3 are given in terms of the ρ mass and the $\rho\pi\pi$ coupling constant,

$$\begin{aligned} L_1^\rho &= \frac{g_{\rho\pi\pi}^2 F_\pi^4}{8m_\rho^4} \\ L_2^\rho &= 2L_1^\rho \\ L_3^\rho &= -6L_1^\rho . \end{aligned}$$

σ exchange contributes to the low-energy constants L_1, L_4 and L_6,

$$\begin{aligned} L_1^\sigma &= \frac{g_2^2 F_\pi^4}{32m_\sigma^2} \\ L_4^\sigma &= \frac{g_1 g_2 F_\pi^4}{8m_\sigma^2} \\ L_6^\sigma &= \frac{g_1^2 F_\pi^4}{8m_\sigma^2} . \end{aligned}$$

These expressions agree with the expressions derived in [28]. To see this more clearly for the ρ meson, one can reformulate the interaction Lagrangian for the ρ meson represented by an asymmetric tensor field given in [28] in terms of an interaction Lagrangian for the vector field representation [41]. Then the coupling constant G_V is identified with the expression $g_{\rho\pi\pi}F_\pi^2/m_\rho$ and we retrieve the expressions for the L_i^ρ given by Ecker et al..

i	L_i^ρ	L_i^σ	$L_i^{\rho+\sigma}$	$L_i^r(m_\rho)$
1	0.9	0.3	1.2	0.7 ± 0.3
2	1.8	—	1.8	1.3 ± 0.7
3	–5.6	—	–5.6	-4.4 ± 2.5
4	—	14.0	14.0	-0.3 ± 0.5
5	—	—	—	1.4 ± 0.5
6	—	16.3	16.3	-0.2 ± 0.3
8	—	—	—	0.9 ± 0.3

Table 3.2: The values of the low-energy constants determined from ρ and σ exchange compared to the empirical values from [46]. The entries are given in units of 10^{-3}.

The numerical values of the resonance contributions to the low-energy constants are compared to the empirical values in Table 3.2. The meson exchange contributions for L_1, L_2 and L_3 are in rather good agreement with the phenomenologically determined values. Also the agreement with the values for resonance saturation obtained by Ecker et al. is reasonable. For L_1^ρ, for example, they get $0.6 \cdot 13^{-3}$ while we get $0.9 \cdot 10^{-3}$. The difference can be traced back completely to the use of different values for the coupling constants. Also our $L_1^\sigma = 0.3 \cdot 10^{-3}$ agrees nicely with their large N_C estimate of $0.2 \cdot 10^{-3}$.
The values we obtain for L_4 and L_6 are two orders of magnitude too large and of the wrong sign. The reason for this is twofold. Firstly, we do not consider the exchange of a scalar isotriplet. This would contribute to L_1, L_4 and L_6 with the opposite sign as compared to the isosinglet. The scalar isotriplet would also contribute to L_5 and L_8. Secondly, the contribution of the scalar isoscalar within our model is by itself two orders of magnitude above the estimate of Ecker et al. [28]. At this point one should note that the structures in the Chiral Lagrangian $\mathcal{L}_4$ to which we compare the resonance exchange contributions also comprise t- and u-channel meson exchanges. We assume that neglecting such contributions in our model does hardly have an effect on the parameters of the ρ exchange, so that the low-energy constants from ρ-exchange are in good agreement with the phenomenological ones. But the effect of the t- and u-channel meson exchanges should be important in the scalar-isoscalar partial wave. In the Jülich model for $\pi\pi$ scattering it is actually the iteration of ρ exchange in the t channel that causes the strong attraction in the $I = J = 0$ partial wave at low

energies [47]. The strength that would come from such contributions is absorbed in the scalar coupling g_1 of the σ in our simple parameterisation. The σ contribution to the low-energy constants is thus overestimated because we parametrise other physical effects into the σ exchange. The numbers given for the resonance saturation from σ exchange should thus not be taken too seriously.
We are thus convinced that we could improve the mapping of our model to Chiral Perturbation Theory by considering the exchange of a scalar isotriplet and the inclusion of t- and u-channel meson exchanges. However, this will most probably not lead to an improvement in the quality of the parameterisation as compared to the data. So at this point we refrain from including more contributions into our model.

3.2.2 The $\pi\pi$ Final State Interaction in $\pi N \to \pi\pi N$

In this section we discuss how to include the pion-pion-T-matrix into a model for the pion production reaction $\pi N \to \pi\pi N$.
It is technically highly involved to include the full two-body T-matrix in a three-body final state such as $\pi\pi N$. In order to perform partial wave decompositions, one would have to boost between three two-body systems in the final state. One can also not simply neglect the πN versus the $\pi\pi$ final state interaction or vice versa, because these two-body final state interactions are approximately of the same size. In the simplest scenario one would neglect all of the two-body final state interactions. Such a procedure would work at the threshold, but for higher energies the unitarity bounds $0 \leq \eta \leq 1$ would be violated.
In order to take some of the final state interaction into account and at the same time avoid the technical complications mentioned above, we cast a part of the two-body T-matrix into a compact expression that we can use in the description of the final state-interaction.

We have already noted that s-channel meson exchanges lead to separable potentials of the form $V = \frac{f_0 f_0^\dagger}{s-m_x^2}$. In the presence of such separable potentials, also the T-matrix can be decomposed into a separable (pole) and a non-separable (non-pole) part,

$$T = \frac{f f^\dagger}{s - m_x^2 - \Sigma} + T^{NP} \,. \tag{3.39}$$

This decomposition is shown in detail in Appendix C. The pole part of the T-matrix is just a meson exchange interaction with the propagator modified through the self-energy $\Sigma = f_0^\dagger G f$ of the meson and with 'dressed' vertex functions $f = (1 + T^{NP} G) f_0$. T^P can be further approximated by neglecting the effect of the non-pole interaction,

$$T^P \simeq \frac{f_0 f_0^\dagger}{s - m_x^2 - \Sigma_0} \,. \tag{3.40}$$

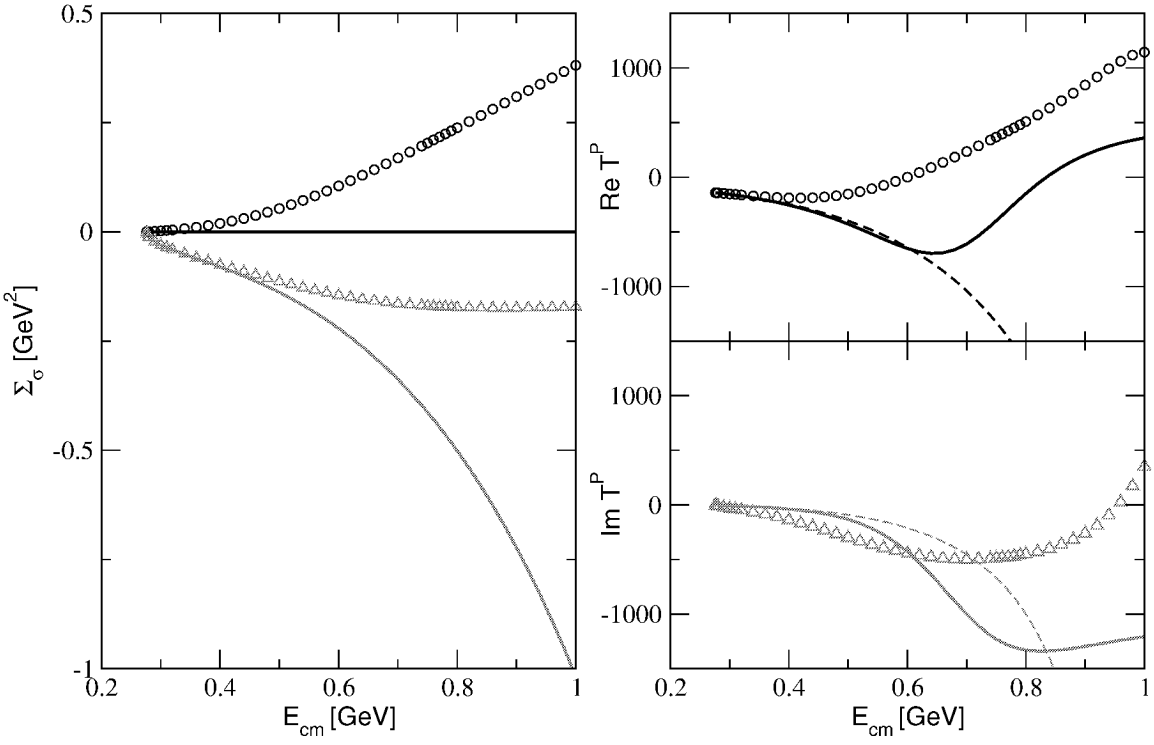

Figure 3.3: On the left side we show the self energy of the sigma. The real part of the 'full' self-energy (including the effect of T^{NP}) is shown as circles, the imaginary part as triangles. The solid lines show the self energy without an effect from T^{NP}. The figure on the right side shows the pole part of the T-matrix in the scalar isoscalar partial wave. The real and imaginary parts of the 'full' T^P are shown as circles and triangles, respectively. Upon neglecting the effect of T^{NP} completely, one arrives at the solid lines. The dashed lines show an approximation for T^P that takes the effect of T^{NP} into account only for the self-energy.

This leads to a simpler expression for the self-energy, which is then only given by the pion loop and the bare vertex functions of the pole potential, $\Sigma_0 = f_0^\dagger G f_0$.

The quality of this approximation is shown for the pole potential and the self-energy in the scalar-isoscalar partial wave in Fig. 3.3.
In the K-matrix approximation, the real part of the self-energy Σ_0 has to vanish, because the vertex functions are real and we take only the imaginary part of the pion loop. The imaginary part of the self energy is however nicely approximated up to 500 MeV if the effect of the non-pole T-matrix is neglected. The situation for the pole T-matrix looks a little different. The approximation gives reasonable results for the real part of T^P up to 400 MeV, but the imaginary part can not be reproduced as soon as one goes away from the threshold.

A different approximation would be to take into account the effect of T^{NP} for the self energy, but working with the bare vertex functions in the nominator of T^P,

$$T^P \simeq \frac{f_0 f_0^\dagger}{s - m_x^2 - \Sigma} \,. \tag{3.41}$$

This leads to similar results in the energy region up to 500 MeV. For higher energies, approximation (3.41) deviates more strongly from the 'full' T^P than approximation (3.40). So the better (and also more consistent) approximation is to neglect the effect of the non-pole T-matrix completely.

As already noted, T^P and the abovementioned approximations have the form of a meson exchange contribution. So the pole part of the $\pi\pi$ final state interaction in the $\pi\pi N$ final state is already described by taking into account the correlation of the final state pions through a σ and a ρ exchange as for example in diagrams (D.1/E.1) in Fig. 2.1 on page 11. For the final state interaction, the non-pole T-matrix will be neglected.
For the pion-exchange contribution, Fig. 3.1(a), we will approximate the pion-pion-T-matrix with

$$T \simeq \frac{f_0 f_0^\dagger}{s - m_x^2 - \Sigma_0} + V^{NP} \,. \tag{3.42}$$

In Fig. 3.4 we show how the different approximations $T = T^P + V^{NP}$ and equation (3.42) influence the description of the elastic $\pi^+\pi^-$ cross sections.
The unitary K-matrix model $T = T^P + T^{NP}$ describes the cross sections reasonably well even above the ρ peak. Above $\sqrt{s} = 800$ MeV, it starts to overestimate the data. The reason for this is that our model gives a too high partial wave cross section for the $I = 2$, $J = 0$ partial wave cross section, as can be seen from the overestimation of the magnitude of the phase shifts in Fig. 3.2.

The approximation of the non-pole T-matrix with the non-pole potential, $T \approx T^P + V^{NP}$ also gives reasonable results in comparison to the data as well as to the calculation with the full T-matrix.

Up to 600 MeV, the data hardly allow to decide between the approximation with the full pole T matrix and equation (3.42). However, the latter approximation deviates more from the calculation with the full T-matrix. At higher energies one sees that the usage of equation (3.42) leads to an overestimation of the data in the region of the ρ peak and above.

For the $\pi N \to \pi\pi N$ model we will work mainly with the approximation (3.42). The approximation with the bare vertex functions is typical of a usual tree-level model. However, we will also investigate the effect of taking into account the full pole T-matrix for $\pi N \to \pi\pi N$.

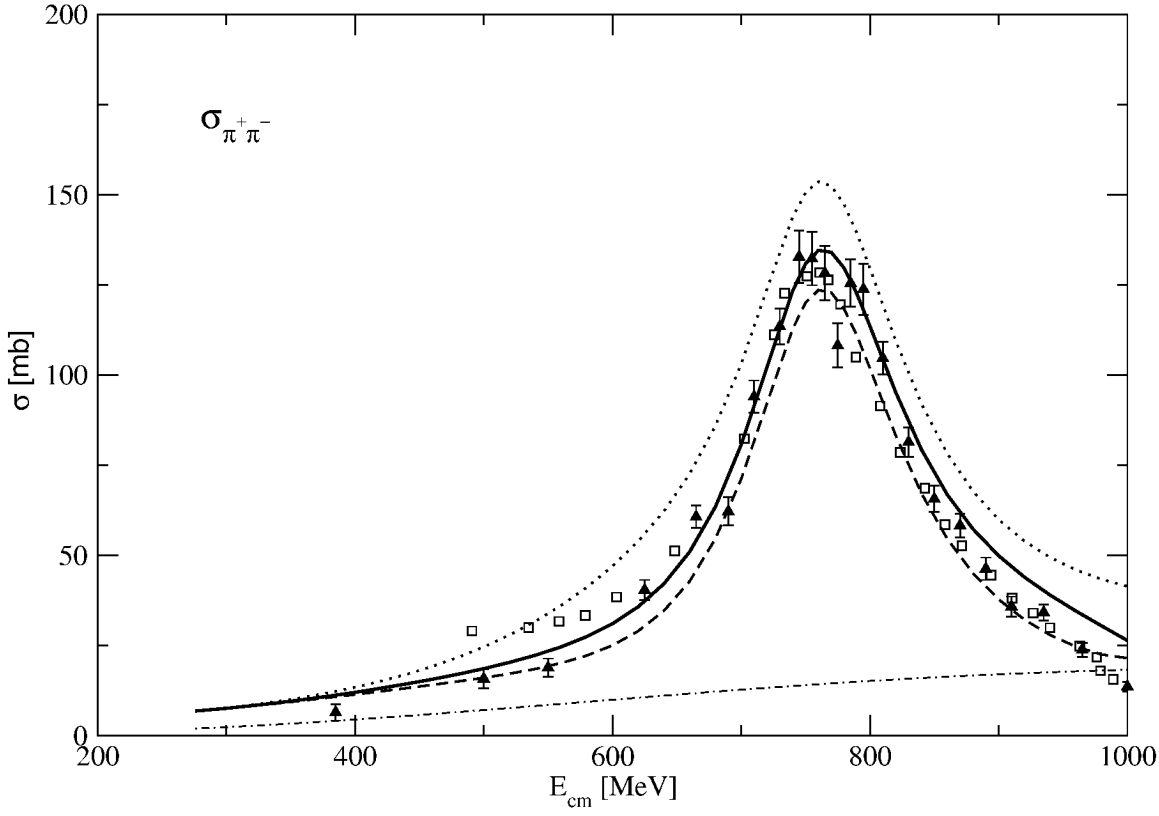

Figure 3.4: The total cross section for $\pi^+\pi^-$ scattering. The solid line gives the result of the K-matrix model, the dashed line was calculated for the approximation $T = T^P + V^{NP}$ and for the dotted line we in addition omit the effect of T^{NP} in T^P. The dot-dashed curve is the result obtained with the potential from leading order Chiral Perturbation Theory alone. The data are from [42] and [38].

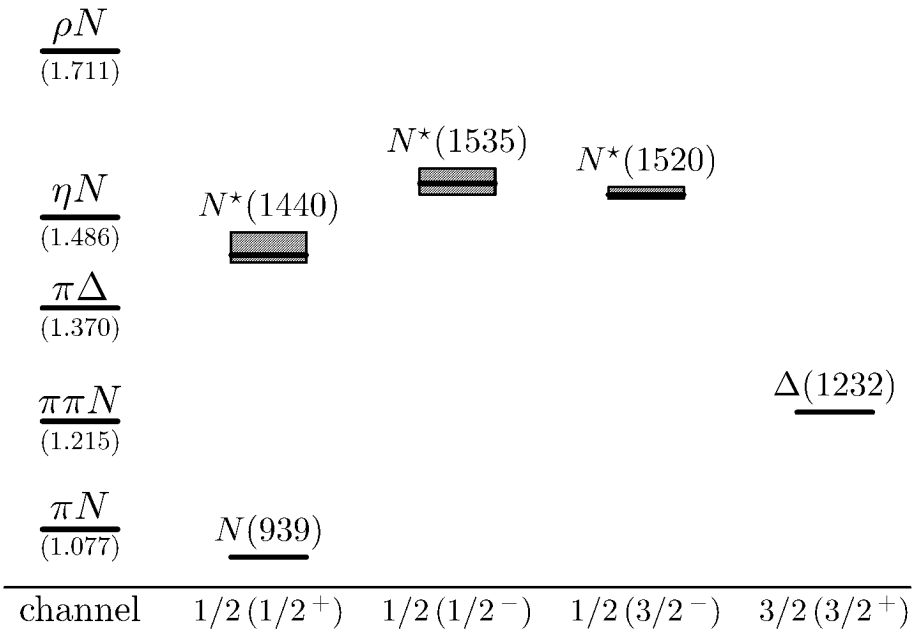

Figure 3.5: The coupled channels with their threshold energies (in GeV) and the N and Δ resonances below 1.6 GeV with their quantum numbers $I(J^P)$. The shaded boxes indicate the mass range of the resonances as given by the particle data group [31].

3.3 Pion-Nucleon scattering

In order to describe πN scattering up to a centre-of-mass energy of 1.5 GeV, we take into account the coupled channels πN, σN, $\pi\Delta$ and ηN. The σN and $\pi\Delta$ channels serve as effective parameterisations of $\pi\pi N$ channels. They open at the $\pi\pi N$ threshold at 1.21 GeV.

Also the ρN channel parametrises a $\pi\pi N$ channel. But as can be seen from the $\pi\pi$ phase shifts in Fig. 3.2, the $\pi\pi$ interaction is weak in the $I = J = 1$ channel below the ρ resonance. Based on this observation we assume that the contribution of the ρN channel should be irrelevant in the energy region up to 1.5 GeV that we here concentrate on.

The ηN channel is taken into account because of its large coupling to the $S_{11}(1535)$ resonance. We need this coupling to the ηN channel to get a reasonable description of the S_{11} partial wave around the $S_{11}(1535)$ resonance. We only take into account the $S_{11}(1535)$ pole contribution for the ηN interaction. This should dominate the ηN interaction in the energy regime considered.

The only direct coupling between two non-πN channels occurs for $\sigma N \to \pi\Delta$ in the

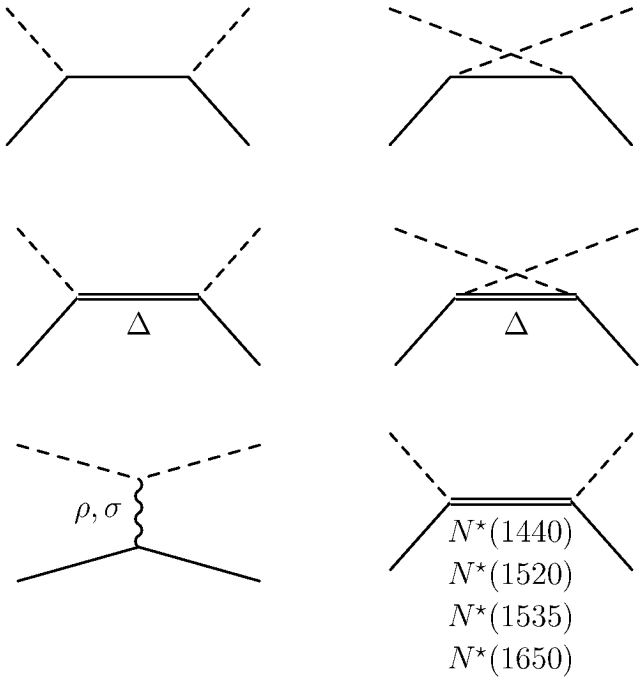

Figure 3.6: Diagrams contributing to the πN potential.

P_{11} partial wave via the Nucleon pole diagram and the pole diagram of the Roper Resonance. Because these particles couple to both channels, it is mandatory that these direct potentials are present. In all other cases, the inelastic channels are only coupled directly to the πN channel. The coupling between all channels contributing to a particular partial wave is generated by the iteration of the potential in the scattering equation.

The contributions to the potentials are shown diagrammatically in Figs. 3.6 – 3.12.

We take into account all the non-strange resonances below 1600 MeV. They are plotted together with the thresholds of the coupled channels in Fig. 3.5. For the description of the S_{11} partial wave we in addition include a contribution from the $S_{11}(1650)$, which gives some background below the $S_{11}(1535)$. On top of that background we can fit the parameters of the $S_{11}(1535)$ to the phase shifts.

The resonance pole diagrams are supplemented by t-channel meson exchanges and u-channel N and Δ exchange. We do not consider the u-channel exchange of heavier resonances because the contribution of the Δ u-channel exchange is already small, and the contribution of heavier resonances should be even smaller.

In the $\pi\Delta$ potential we do not take into account the nucleon and the Δ u-channel exchange diagrams. In the nucleon exchange diagram, the $\pi\pi N$ intermediate state

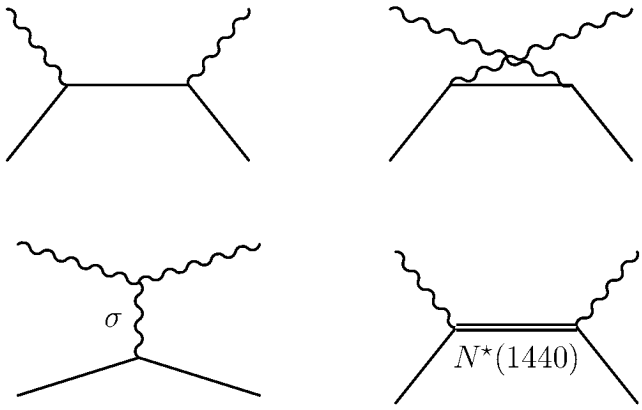

Figure 3.7: The σN potential.

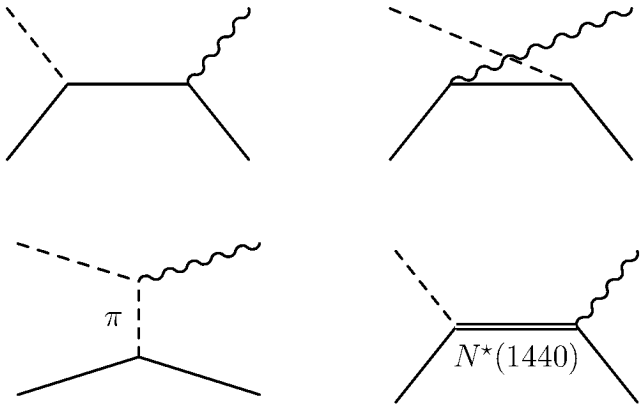

Figure 3.8: The $\pi N \to \sigma N$ potential.

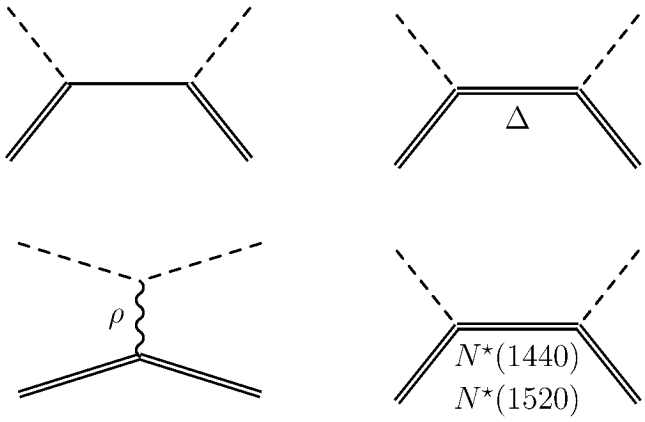

Figure 3.9: The $\pi\Delta$ potential.

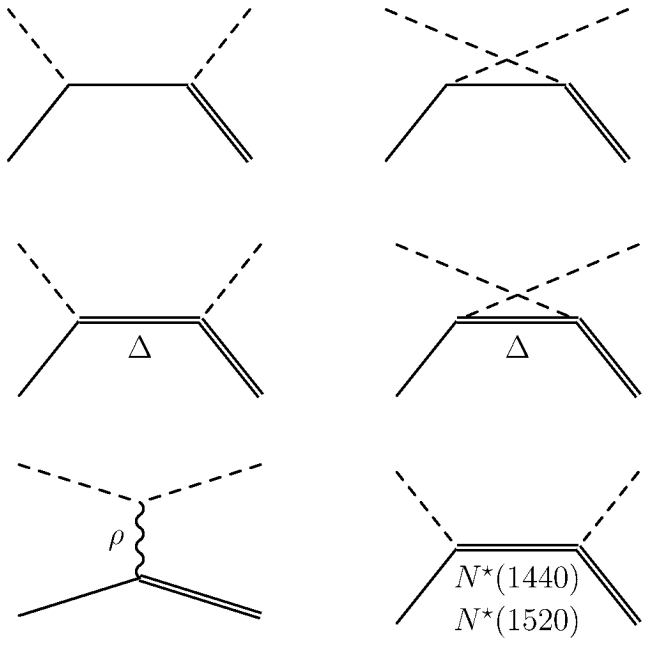

Figure 3.10: The $\pi N \rightarrow \pi\Delta$ potential.

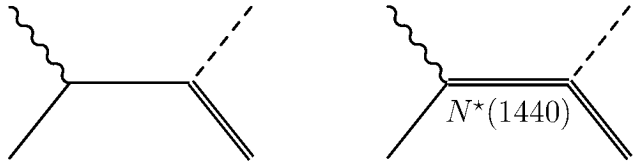

Figure 3.11: The $\sigma N \to \pi\Delta$ potential.

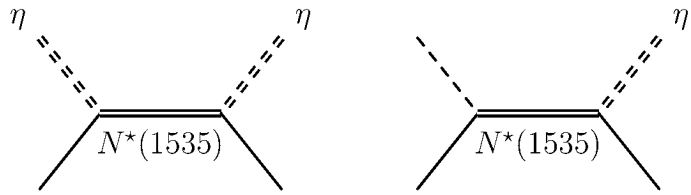

Figure 3.12: The ηN and the $\pi N \to \eta N$ potential.

can go on-shell already at the $\pi\pi N$ threshold, and the potential becomes singular. To avoid a complicated renormalisation procedure, we neglect the contribution of the nucleon exchange diagram in the $\pi\Delta$ potential. We are convinced that the nucleon exchange diagram in the $\pi\Delta$ potential would anyhow only make a small contribution. We can make an estimate of the size of this contribution if we work with a stable $\pi\Delta$ channel. If the invariant mass of the Δ is fixed to M_Δ, the singularities in the potential occur only for energies between 1.48 GeV and 1.6 GeV. Outside this region, the contribution from nucleon exchange on the πN phase shifts and inelasticities is indeed negligible.
For the Δ u-channel exchange in the $\pi\Delta$ potential, such singularities can occur when the heavier $\pi\pi\Delta$ intermediate state can go on-shell, which can happen only at energies above 1.5 GeV. We have checked that disregarding the Δ u-channel has no effect on the observables below 1.5 GeV.

The potentials are calculated from the Lagrangian given in Table 2.1. The expressions for the amplitudes can be found in Appendix D.

For the nucleon and the pion we use the isospin-averaged masses $M_N = 938.926$ MeV and $m_\pi = 138.03$ MeV. The value of the η mass is given by the 2002 Particle Listing of the Particle Data Group [31] to be $m_\eta = 547.3$ MeV. We take the value of the πNN coupling constant, $f^2_{\pi NN}/(4\pi) = 0.0778$, from the Bonn potential [35]. This is the value also used in the Jülich πN model. Note, however, that the presently accepted value is somewhat smaller (~ 0.074). The ρ and σ masses and their couplings to $\pi\pi$ are determined from our fit to $\pi\pi$ scattering. The remainder of the coupling constants

M_N	*0.938926 GeV*
m_π	*0.13803 GeV*
m_η	*0.5473 GeV*
m_ρ	*0.772 GeV*
m_σ	*0.8346 GeV*
M_Δ	1.232 GeV
$M_{P_{11}(1440)}$	1.491 GeV
$M_{D_{13}(1520)}$	1.515 GeV
$M_{S_{11}(1535)}$	1.535 GeV
$M_{S_{11}(1650)}$	1.701 GeV

Table 3.3: The masses of the particles. The values in italics are input quantities, the remainder of the parameters are fitted to the πN phase shifts and inelasticities.

and masses are fitted to the πN phase shifts and inelasticities. We start by fitting the parameters of the πN potential without the $N^\star$ pole diagrams to the scattering lengths and volumes and to the phase shifts below 1.2 GeV. Then the $\pi\Delta\Delta$, $\rho N\Delta$ and the $\rho\Delta\Delta$ coupling are fitted to the inelasticities in the $I = 3/2$ partial waves. The σN channel only makes significant contributions in the P_{11} partial wave. The σ-exchange diagram in the σN potential has no impact on the results. We take the $\sigma\sigma\sigma$ coupling to be $g^2_{\sigma\sigma\sigma}/(4\pi) = 0.625$ as in the Jülich πN model [10]. Varying this parameter by an order of magnitude has no effect on the phase shifts and inelasticities. Finally we fix the parameters of the $N^\star$ resonances.

The parameters resulting from the fit to the πN phase shifts and inelasticities are listed in Tables 3.3 and 3.4. For the tensor coupling at the ρNN vertex we find $\kappa = 1.94$, while the value obtained from the analysis of the process $\bar{N}N \to \pi\pi$ and the dispersion theoretical analysis of the nucleon electromagnetic form factor is $\kappa \simeq 6$ [48, 49]. A description of the πN threshold data is not possible with the latter value for κ. It has already been noted by Pearce and Jennings in their investigation of πN scattering [36] that κ obviously has some t-dependence. The value of $\kappa \simeq 6$ is determined for $t = m_\rho$, while they find smaller values between 1.4 and 3.2 for κ in their fit to elastic πN scattering, where κ is needed for negative values of t.

A comment on the size of the ρNN and $\rho\pi\pi$ coupling is in order. Hadron universality

$\frac{f^2_{\pi NN}}{4\pi}$	*0.0778*
$\frac{f^2_{\pi N\Delta}}{4\pi}$	0.36
$\frac{g^2_{\rho\pi\pi}}{4\pi}$	*2.905*
$\frac{g^2_{\rho NN}}{4\pi}$	0.80
κ	1.94
$\frac{g_1^2}{4\pi}$	*98.94 GeV*$^{-2}$
$\frac{g_2^2}{4\pi}$	*7.32 GeV*$^{-2}$
$\frac{g^2_{\sigma NN}}{4\pi}$	1.03
$\frac{f^2_{\pi\Delta\Delta}}{4\pi}$	0.04
$\frac{f^2_{\rho N\Delta}}{4\pi}$	4.5
$\frac{g^2_{\rho\Delta\Delta}}{4\pi}$	16.0
$\kappa_{\rho\Delta\Delta}$	15.0
$\frac{g^2_{\sigma\sigma\sigma}}{4\pi}$	*0.625*

$\frac{f^2_{P_{11}(1440)\pi N}}{4\pi}$	0.011
$\frac{f^2_{P_{11}(1440)\pi\Delta}}{4\pi}$	0.04
$\frac{f^2_{P_{11}(1440)\sigma N}}{4\pi}$	13.0
$\frac{f^2_{D_{13}(1520)\pi N}}{4\pi}$	0.0009
$\frac{f^2_{D_{13}(1520)\pi\Delta}}{4\pi}$	0.03
$\frac{f^2_{S_{11}(1535)\pi N}}{4\pi}$	0.003
$\frac{f^2_{S_{11}(1535)\eta N}}{4\pi}$	0.47
$\frac{f^2_{S_{11}(1650)\pi N}}{4\pi}$	0.009

Table 3.4: Values of the coupling constants (as defined in Table 2.1) from the fit to the πN scattering lenghts and the phase shifts and inelasticities. The values in italics are input quantities, the remainder of the parameters are fitted to the πN phase shifts and inelasticities.

	our fit	Koch and Pietarinen [50]	SM95 [51]
S_{11}	0.175	0.173 ± 0.003	0.175
S_{31}	-0.096	-0.101 ± 0.004	-0.087
P_{11}	-0.088	-0.081 ± 0.002	-0.068
P_{31}	-0.051	-0.045 ± 0.002	-0.039
P_{13}	-0.038	-0.030 ± 0.002	-0.022
P_{33}	0.216	0.214 ± 0.002	0.209
a_+	-0.006	-0.01 ± 0.01	-0.003

Table 3.5: The pion-nucleon scattering lengths and volumes. The numbers are given in units of $m_{\pi^+}^{-(2L+1)}$.

demands that $g_{\rho NN} = g_{\rho\pi\pi} = g_\rho$ with the Lagrangians $\mathcal{L}_{\rho\pi\pi} = -g_{\rho\pi\pi}(\vec{\pi} \times \partial_\mu \vec{\pi})\vec{\rho}^\mu$ and $\mathcal{L}_{\rho NN} = -1/2 g_{\rho NN} \bar{\Psi} \left(\gamma^\mu - \kappa/(2M_N)\sigma^{\mu\nu}\partial_\nu\right) \vec{\tau}\vec{\rho}\Psi$. Note that we have absorbed the prefactor 1/2 into the coupling constant in our definition of the ρNN Lagrangian in Table 2.1 on page 9. So hadron universality of the ρ couplings is fulfilled approximately in our model with $4g_{\rho NN}^2/(4\pi) = 3.2 \simeq g_{\rho\pi\pi}^2/(4\pi)$.

The scattering lengths obtained from our model are compared to the analysis of Koch and Pietarinen [50] and the SM95 analysis [51] in Table 3.5. We find that the scattering volumes in the P_{11}, P_{13} and P_{31} are a bit too small compared to the values of [50], and compared to the SM95 scattering volumes [51] the difference becomes even more obvious. But in general there is reasonable agreement.

The phase shifts and inelasticities for the πN partial waves up to $J = 3/2$ are displayed in Figs. 3.13 and 3.14.

We find reasonable agreement between our model and the results from the phase shift analyses up to 1.5 GeV. In particular, the threshold behaviour in each partial wave is nicely described already by the non-resonant background.
The S_{11} partial wave is described with the help of the two S_{11} resonances and the coupling to the ηN channel. If we switch off the contribution from the $S_{11}(1650)$, the phase shifts start to deviate from the data above 1.2 GeV. The difference is not large below 1.5 GeV but would make it difficult to fit the parameters of the $S_{11}(1535)$ to the phase shifts.

In the S_{31} partial wave, our model results start to deviate from the phase shifts already

at 1.2 GeV. This is due to the missing contribution from the $S_{31}(1620)$ resonance which we have not included in our model. Also the inelasticities are not reproduced correctly above 1.5 GeV because of the missing of this resonance.

Also the description of the P_{13}, the P_{31} and the D_{33} can certainly be improved by including additional resonances in our model. However, up to 1.5 GeV, the deviations of our results from the data are only small in these partial waves.

In the D_{13} we miss some of the strength of the resonance above 1.5 GeV. Maybe this is due to the missing of coupling to the ρN channel. Below 1.5 GeV this partial wave is however well described by our model.

The Roper Resonance $P_{11}(1440)$ is described reasonably well up to 1.6 GeV. Above this energy, the calculated phase shifts start to go down while the data keep rising. For the inelasticities we find reasonable agreement, although the opening of the inelasticities in our model takes place not quite as early as in the data.

3.3.1 Resonance Saturation of the Low-Energy Constants

In the low-energy limit we compare our model to Heavy Baryon Chiral Perturbation Theory. The πN Lagrangian at next-to-leading order is given by [53]

$$\mathcal{L}^{(2)}_{\pi N} = \bar{N}\left(c_1\langle\chi_+\rangle + c_2(v\cdot u)^2 + c_3 u\cdot u + c_4[S_\mu, S_\nu]u^\mu u^\nu + \ldots\right)N\,, \tag{3.43}$$

where we have omitted terms coming from the $1/M_N$ expansion of the Heavy Baryon Lagrangian and terms not contributing to πN scattering in the limit of isospin symmetry. χ_+ and u_μ are given in terms of χ and the pion fields $U = u^2$ defined in equations (3.25) and (3.26):

$$\chi_+ = u^\dagger\chi u^\dagger + u\chi^\dagger u\,, \tag{3.44}$$

$$u_\mu = iu^\dagger D_\mu U u^\dagger\,. \tag{3.45}$$

v_μ denotes the four-velocity of the nucleon and S_μ its spin operator. To reduce our model to the non-relativistic limit of Heavy Baryon Chiral Perturbation Theory, we make use of the following relations (see, for example, the review [53]):

$$\begin{aligned}\bar{N}\gamma_\mu N &= v_\mu \bar{N}N\\ \bar{N}\gamma_5\gamma_\mu N &= -2\bar{N}S_\mu N\\ \bar{N}\sigma_{\mu\nu}N &= 2\epsilon_{\mu\nu\alpha\beta}v^\alpha\bar{N}S^\beta N = -2i\bar{N}[S^\mu, S^\nu]N\,.\end{aligned} \tag{3.46}$$

The low-energy constants at next-to-leading order are finite, because loops appear only at $\mathcal{O}(p^3)$. The resonance saturation of the low-energy constants was investigated

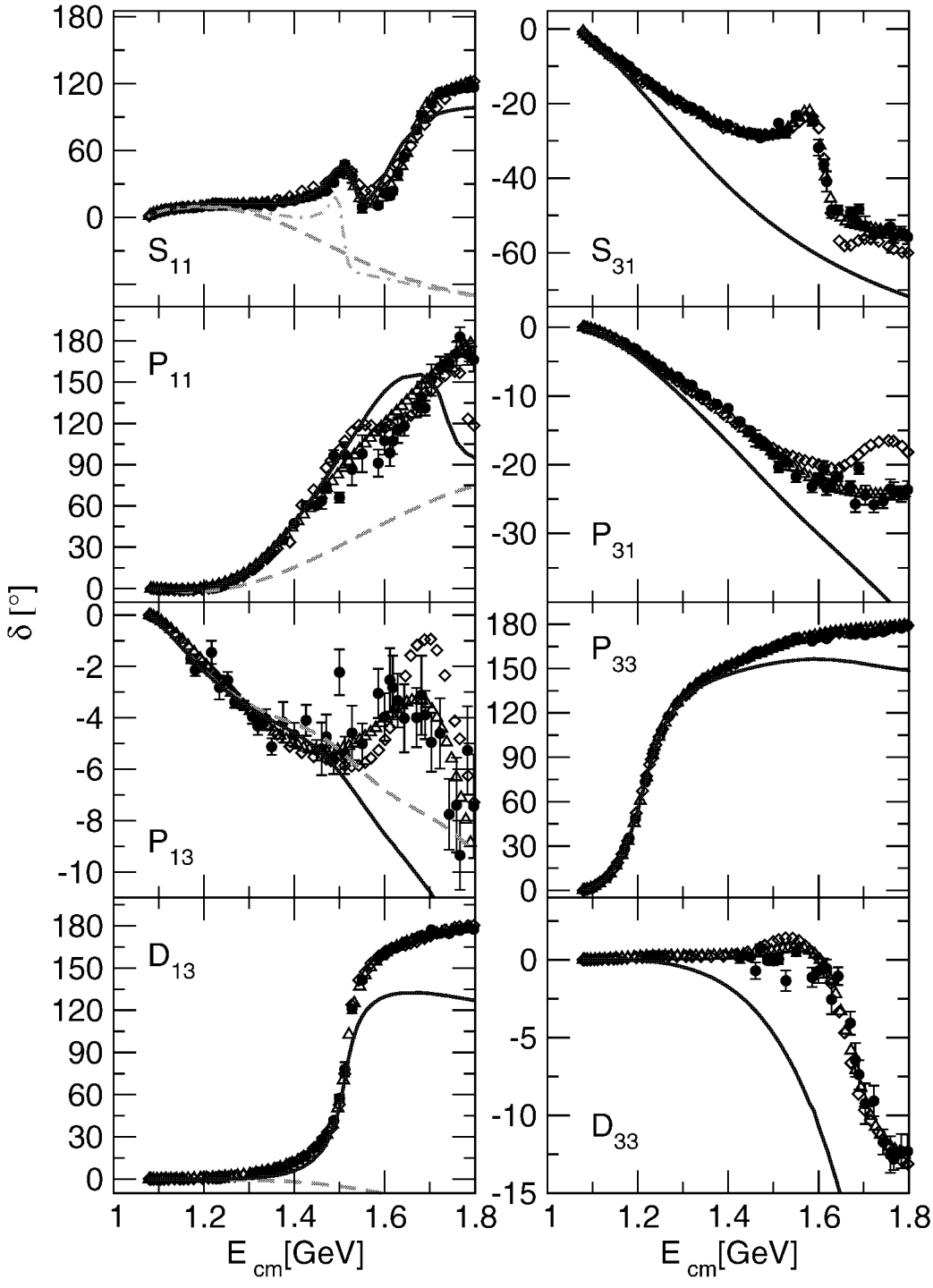

Figure 3.13: πN phase shifts. The solid lines show the results of our model. The dashed lines are calculated without the $N^\star$ resonances. The dot-dashed line is without the $S_{11}(1650)$. The data are from the phase shift analyses KA84 [52] (open diamonds), SM95 [51] (open triangles) and SE-SM95 [51] (filled circles).

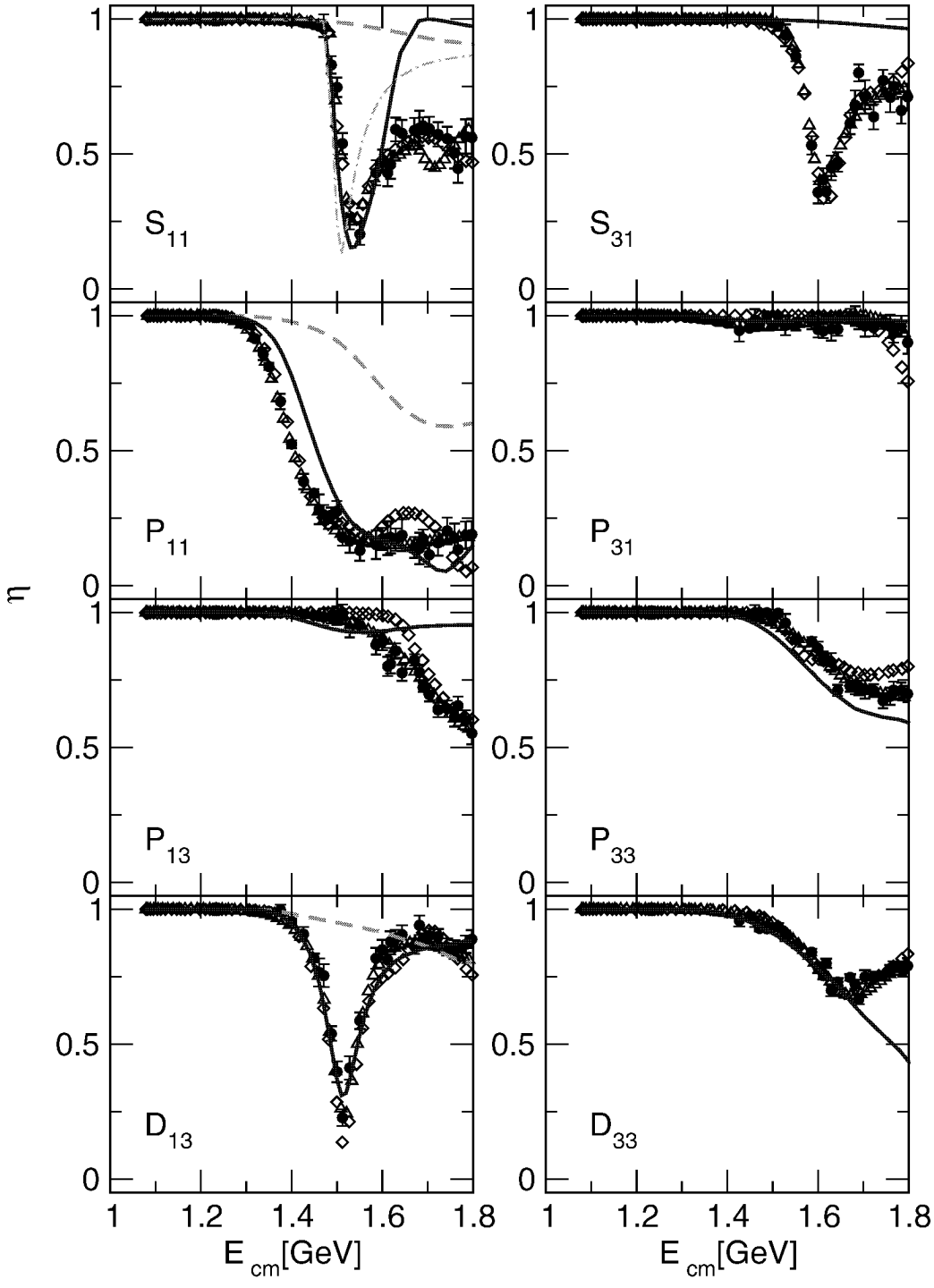

Figure 3.14: πN inelasticities. The solid lines show the results of our model. The dashed lines are calculated without the $N^\star$ resonances. The dot-dashed line is without the $S_{11}(1650)$. The data are from the phase shift analyses KA84 [52] (open diamonds), SM95 [51] (open triangles) and SE-SM95 [51] (filled circles).

i	c_i^σ	c_i^ρ	c_i^Δ	$c_i^{N^\star(1440)}$	$c_i^{N^\star(1520)}$	$c_i^{N^\star(1535)}$	$\sum c_i^{\text{res.}}$	[29]
1	-0.78	—	—	—	—	—	-0.78	-0.93 ± 0.10
2	—	—	1.79	0.09	0.001	0.02	1.90	3.34 ± 0.20
3	-0.21	—	-3.07	-0.11	-0.001	0.01	-3.17	-5.29 ± 0.25
4	—	0.57	1.54	0.22	0.001	-0.01	2.32	3.63 ± 0.10

Table 3.6: Values of the low-energy constants from resonance saturation and from the phenomenological determination in [29]. The values are given in units of GeV^{-1}.

by Bernard et al. [29]. Assuming that c_1 is saturated by scalar meson exchange, they find good agreement between the phenomenological values of the low-energy constants and the values from resonance exchange.

We compare our results for the resonance saturation of the low-energy constants with the phenomenological values in Table 3.6. We notice that our results go in the right direction but the absolute values are too small. Let us compare our results to those of [29] in more detail.

The vector part of ρ exchange in the t-channel already contributes at leading order. As already mentioned, it saturates the Weinberg-Tomazawa term, a $\pi\pi NN$ contact interaction. Assuming hadron universality ($g_{\rho\pi\pi} = 2g_{\rho NN} = g_\rho$[3]), the ρ mass and its coupling constant have to fulfil the KSFR-relation [54, 55]

$$m_\rho^2 = 2g_\rho^2 F_\pi^2 \,. \tag{3.47}$$

The coupling constants of our model fulfil this relation to an accuracy of 5%.

The contribution of ρ exchange to the low-energy constants at next-to-leading order in the pion-nucleon Lagrangian comes from the tensor coupling of the ρ to the nucleon,

$$c_4^\rho = \frac{g_{NN\rho} g_{\rho\pi\pi} F_\pi^2}{m_\rho^2} \cdot \frac{\kappa}{M_N} \,. \tag{3.48}$$

Using the KSFR relation, this expression simplifies to $c_4^\rho = \kappa/(4M_N)$, which is the expression given in [29]. They use $\kappa = 6.1$ and obtain $c_4^\rho = 1.63\ \text{GeV}^{-1}$, while we only get $c_4^\rho = 0.57\ \text{GeV}^{-1}$ with our lower value for κ.

[3]The factor of 2 in front of $g_{\rho NN}$ comes from our definition of the coupling constant. Usually, the ρNN Lagrangian is written $\mathcal{L} = \frac{1}{2} g_\rho \bar{\Psi} \ldots$ We have absorbed this factor of 2 into the coupling constant.

The t-channel σ exchange contributes to c_1 and c_3. In agreement with Bernard et al. [29] we find

$$c_1^\sigma = -\frac{g_{NN\sigma} g_1 F_\pi^2}{2m_\sigma^2} \tag{3.49}$$

$$c_3^\sigma = -\frac{g_{NN\sigma} g_2 F_\pi^2}{2m_\sigma^2}\,, \tag{3.50}$$

where the c_m of [29] has to be identified with $g_1 F_\pi^2/2$ and c_d with $g_2 F_\pi^2/4$. Bernard et al. start from the assumption that c_1 is completely saturated by the exchange of a scalar meson, so their value of $c_1^\sigma = -0.9\,\mathrm{GeV}^{-1}$ is an input quantity (from the phenomenologically determined low-energy constant). We find reasonable agreement between this value and our result, $c_1^\sigma = -0.78\,\mathrm{GeV}^{-1}$.
The value we obtain for c_3^σ is approximately a factor of seven lower than the value given by Bernard et al..

For the contribution of the Δ-isobar we obtain the expressions

$$c_2^\Delta = \left(\frac{f_{\pi N\Delta}}{m_\pi}\right)^2 \frac{4F_\pi^2}{9(M_\Delta - M_N)} \frac{M_N^2}{M_\Delta^2}\,, \tag{3.51}$$

$$c_3^\Delta = -2c_4^\Delta = -\left(\frac{f_{\pi N\Delta}}{m_\pi}\right)^2 \frac{4F_\pi^2}{9(M_\Delta - M_N)}\,. \tag{3.52}$$

We find agreement between these expressions and those in [29] if we drop the factor M_N^2/M_Δ^2 in our c_2^Δ and neglect the addend m_π^2 in the denominator of their formula. If we use the expression given in [29] for the Δ contribution, we obtain the values

$$c_2^\Delta = -c_3^\Delta = 2c_4^\Delta = \frac{4F_\pi^2}{9}\left(\frac{f_{\pi N\Delta}}{m_\pi}\right)^2 \frac{M_\Delta - M_N}{(M_\Delta - M_N)^2 - m_\pi^2} = 3.95\,\mathrm{GeV}^{-1}\,. \tag{3.53}$$

This would lead to a total of $c_2 = 4.06\ \mathrm{GeV}^{-1}$, $c_3 = -4.26\ \mathrm{GeV}^{-1}$ and $c_4 = 2.76\ \mathrm{GeV}^{-1}$, which is much closer to the phenomenological values.

The Roper resonance contributes as follows:

$$c_2^{P_{11}(1440)} = \frac{2M_N}{M_{P_{11}(1440)}^2 - M_N^2}\left(\frac{f_{P_{11}(1440)\pi N}}{m_\pi}\right)^2 F_\pi^2\,, \tag{3.54}$$

$$c_3^{P_{11}(1440)} = -\frac{1}{2}\,c_4^{P_{11}(1440)} = -\frac{1}{M_{P_{11}(1440)} - M_N}\left(\frac{f_{P_{11}(1440)\pi N}}{m_\pi}\right)^2 F_\pi^2\,. \tag{3.55}$$

These expressions agree with those given by Bernard et al., whereas the numerical values we obtain for the $c_i^{P_{11}(1440)}$ are almost a factor of two larger. The contribution of the Roper resonance is small compared to the contributions from the Δ. Contributions

from heavier resonances were not considered in [29] because their contributions should be even smaller than those of the Roper resonance.

For the sake of completeness, we also give the contributions of the $S_{11}(1535)$ and of the $D_{13}(1520)$ here:

$$c_2^{S_{11}(1535)} = \frac{2M_N}{M^2_{S_{11}(1535)} - M_N^2} \left(\frac{f_{S_{11}(1535)\pi N}}{m_\pi} \right)^2 F_\pi^2 , \tag{3.56}$$

$$c_3^{S_{11}(1535)} = -\frac{1}{2} c_4^{S_{11}(1535)} = \frac{1}{M_{S_{11}(1535)} + M_N} \left(\frac{f_{S_{11}(1535)\pi N}}{m_\pi} \right)^2 F_\pi^2 , \tag{3.57}$$

$$c_2^{D_{13}(1520)} = \frac{1}{M_{D_{13}(1520)} + M_N} \left(\frac{f_{D_{13}(1520)\pi N}}{m_\pi} \right)^2 \frac{2F_\pi^2}{3} \frac{M_N^2}{M^2_{D_{13}(1520)}} , \tag{3.58}$$

$$c_3^{D_{13}(1520)} = -2c_4^{D_{13}(1520)} = -\frac{1}{M_{D_{13}(1520)} + M_N} \left(\frac{f_{D_{13}(1520)\pi N}}{m_\pi} \right)^2 \frac{2F_\pi^2}{3} . \tag{3.59}$$

The contributions from these two resonances are indeed very small. The contributions from even heavier resonances should be completely negligible.

Let us summarise our findings for the resonance saturation of the low-energy constants from our model. We find that the major contribution comes from Δ exchange and agrees reasonably well with the Δ contribution given by Bernard et al. in [29]. c_1 is saturated to a good accuracy by the exchange of the scalar σ meson. The contributions of the σ to c_3 and of the ρ to c_4 are substantially smaller than the values given in [29] because our values for the corresponding coupling constants from the fit to πN data are smaller. However, the sum of the resonance contributions should agree with the phenomenological values for the low-energy constants. We find that our values for the c_i are of the same order of magnitude, but the difference to the phenomenological values amounts to nearly a factor of 2 for c_2. A part of this difference can be accounted for if we do not neglect terms of m_π^2 in the denominator of the Δ propagator. Anyway, we do not expect a 100% agreement because our model also accounts for higher orders and the phenomenological low-energy constants were determined with a fit of terms up to second order.

3.3.2 πN Initial and Final State Interaction in $\pi N \to \pi\pi N$

πN scattering contributes to $\pi N \to \pi\pi N$ as initial and final state interaction, see Fig. 3.15.

As in the case of $\pi\pi$ scattering, we decompose the T-matrix into a pole and a non-pole

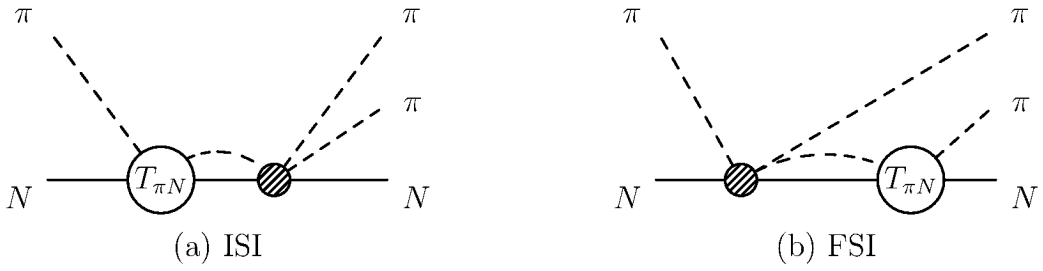

Figure 3.15: Contribution of the πN T-matrix to $\pi N \to \pi\pi N$. (a) Initial state interaction. (b) Final state interaction. Note that this decomposition into ISI and FSI is somewhat arbitrary and is just for illustrative purpose.

part,

$$T = \frac{f f^\dagger}{s - M_x^2 - \Sigma} + T^{NP}\,, \tag{3.60}$$

with the self-energy $\Sigma = f_0^\dagger G f$.
Because we deal with a coupled channel system for πN scattering, the dressed vertex functions f are given in terms of the bare vertex functions f_0 as

$$\begin{pmatrix} f_{\pi N} \\ f_{\sigma N} \\ \vdots \end{pmatrix} = \begin{pmatrix} 1 + T^{NP}_{\pi N} G_{\pi N} & T^{NP}_{\sigma N \to \pi N} G_{\sigma N} & \cdots \\ T^{NP}_{\pi N \to \sigma N} G_{\pi N} & 1 + T^{NP}_{\sigma N} G_{\sigma N} & \cdots \\ \vdots & \vdots & \ddots \end{pmatrix} \begin{pmatrix} f_{0\pi N} \\ f_{0\sigma N} \\ \vdots \end{pmatrix} . \tag{3.61}$$

The πN vertex for the nucleon or Roper pole diagram, for example, can be written as

$$\begin{aligned} f_{\pi N} &= f_{0\pi N} + T^{NP}_{\pi N} G_{\pi N} f_{0\pi N} + T^{NP}_{\sigma N \to \pi N} G_{\sigma N} f_{0\sigma N} + T^{NP}_{\pi\Delta \to \pi N} G_{\pi\Delta} f_{0\pi\Delta} \\ &= f_{0\pi N} \left(1 + G_{\pi N} T^{NP}_{\pi N} + \frac{T^{NP}_{\sigma N \to \pi N} G_{\sigma N} f_{0\sigma N}}{f_{0\pi N}} + \frac{T^{NP}_{\pi\Delta \to \pi N} G_{\pi\Delta} f_{0\pi\Delta}}{f_{0\pi N}} \right) \end{aligned} \tag{3.62}$$

with T^{NP} the non-pole T-matrix in the P_{11} partial wave. The term in brackets is just an energy-dependent complex number that can be regarded as a kind of 'form factor' that parametrises the inner structure of the vertex.
As an example, the form factor for the πN vertex of the Roper resonance is shown in Fig. 3.16. The real part of the form factor is 1 at the πN threshold, and the imaginary part vanishes. This behaviour is obvious from equation (3.62). The πN propagator and the propagators of the inelastic channels are zero at the πN threshold, so that

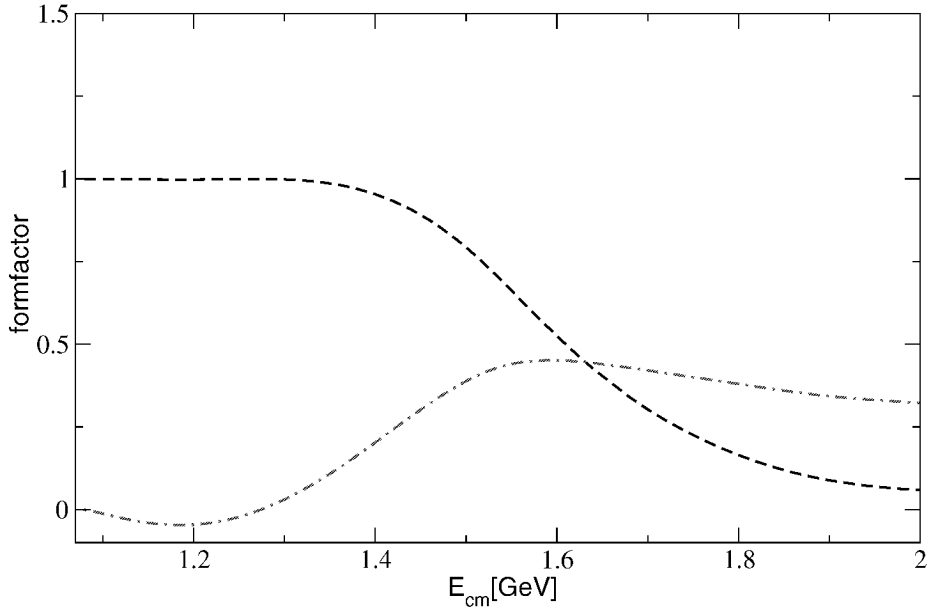

Figure 3.16: The form factor for the πN vertex of the Roper resonance. The dashed line shows the real part of the form factor, the dot-dashed line its imaginary part.

$f_{\pi N} = f_{0_{\pi N}}$. Above the threshold, the real part of the form factor decreases and the form factor acquires an imaginary part.

On the insertion of the dressed vertices into our model for $\pi N \to \pi\pi N$ we make a few approximations:

- At a vertex where a resonance decays into an off-shell intermediate πN state (see, e.g., Fig. 3.17a) we approximate the form factor in equation (3.62) with the value for the on-shell πN state at the same energy. We are forced to make an approximation at vertices with off-shell πN states because the K-matrix approximation, from which we calculate our form factors does not account for off-shell πN states.

- At a vertex with a resonance decaying into the $\pi\Delta$ or σN channel (see, e.g., Fig. 3.17b) we also make an approximation for the form factor. In principle, our coupled channels calculation for πN scattering allows us to extract values of the form factor for the decay into the unstable channels for any allowed invariant mass of the σ or the Δ. But for the present we work with just one form factor for the σN and $\pi\Delta$ channel, respectively. That reduces the calculational effort, but allows us to get an idea of the effect of the dressing of the vertices on the reaction $\pi N \to \pi\pi N$.
  For both decay channels we use the form factors of the largest transition matrix;

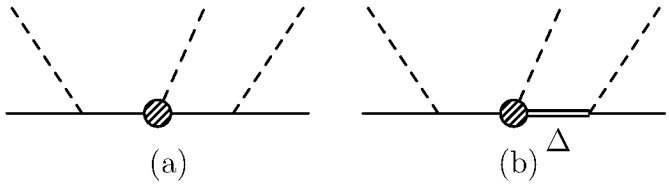

Figure 3.17: Examples for vertices at which we make approximations for the form factors.

this is the one with the smallest invariant mass of the Δ for the $\pi\Delta$ channel and the one with the largest invariant mass of the σ for the σN channel , respectively.

- For a decay into the $\pi\Delta$ state we take the form factor from the $\pi\Delta$ state with minimal angular momentum contributing to the partial wave of the resonance. In the $J = 1/2$ partial waves, there is only one possible angular momentum of the $\pi\Delta$ state, $L = 2$ for the πN s-waves and $L = 1$ for the πN p-waves. But in the P_{13}/P_{33}, the $\pi\Delta$ state can have $L = 1$ and $L = 3$. Here we take the form factor for the transition to the $L = 1$ state. The transition to the $L = 3$ state is suppressed because of its higher angular momentum. Similarly, we take the form factor for the D_{13} decay from the $L = 0$ $\pi\Delta$ state.

- At a vertex with a decay into the ρN channel we do not account for the dressing, because we have not taken into account the ρN channel in our coupled channels calculation for πN scattering and so cannot extract any value for the form factor from this calculation. The contribution of a resonance decay into the ρN channel should in any case only be small — also in $\pi N \to \pi\pi N$ — because the $\pi\pi$ interaction in the vector-isovector partial wave is still relatively small in the energy range considered.

We will investigate the effect of the dressed vertex functions on the pion production reaction $\pi N \to \pi\pi N$ by comparison to a tree-level model. In the tree-level model, the pole diagrams of resonances are described by expressions of the form

$$T_0^P = \frac{f_0 f_0^\dagger}{s - M_x^2 - \Sigma_0}\,, \tag{3.63}$$

with the self-energy $\Sigma_0 = f_0^\dagger G f_0$.

It is instructive to see how such an approximation works in the case of πN scattering. In Fig. 3.18 we compare expression (3.63) for the Roper resonance with the pole matrix T^P for the Roper resonance. Both real and imaginary part of T^P are well approximated by the expression for T_0^P. Above 1.3 GeV the real part of T_0^P starts

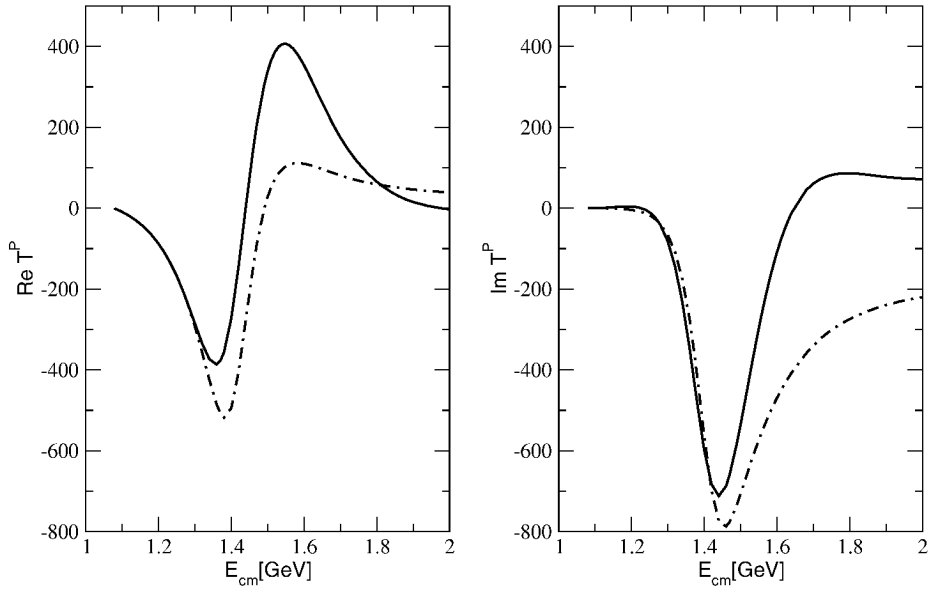

Figure 3.18: The pole T-matrix for the Roper resonance. The solid lines show the full T^P as in equation (3.60), the dot-dashed lines show the approximation (3.63).

to overestimate the absolute value of T^P. In this energy regime we can expect that the contribution of the Roper resonance is overestimated by expression (3.63). The imaginary part of T^P is nicely described by the approximation T_0^P up to 1.4 GeV.

At the tree-level, pion-nucleon scattering is described by an expression of the form

$$T = T_0^P + V^{NP} = \frac{f_0 f_0^\dagger}{s - M_x^2 - \Sigma_0} + V^{NP}\,, \tag{3.64}$$

or, if we take into account the effect of T^{NP} on the pole part of the T-matrix,

$$T = T^P + V^{NP} = \frac{f f^\dagger}{s - M_x^2 - \Sigma} + V^{NP}\,. \tag{3.65}$$

As long as the non-pole potential is weak, these tree-level approximations should be able to describe the data. If the non-pole potential becomes strong, higher order effects will also be important for the non-pole part of the interaction. The neglect of these higher order effects in the tree-level approximation will then lead to a violation of the unitarity bounds $0 \leq \eta \leq 1$.

In Fig. 3.19 we show the inelasticity parameter for a tree-level calculation of πN scattering in comparison with the inelasticity parameter for the unitary K-matrix model.

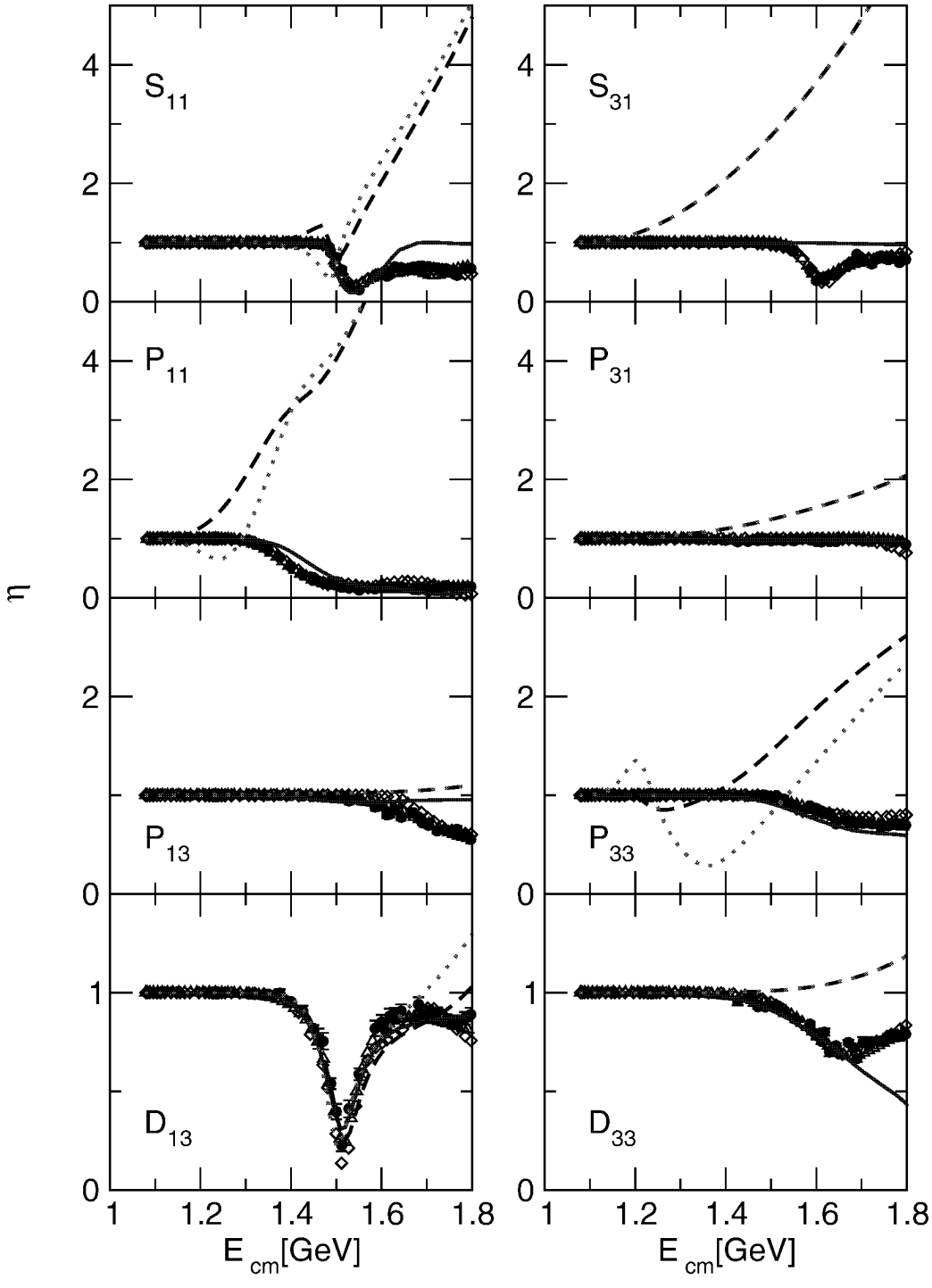

Figure 3.19: πN inelasticities. The solid lines show the results of the unitary K-matrix model. The dashed lines are calculated with the approximation $T = T^P + V^{NP}$. The dotted lines show the approximation $T = T_0^P + V^{NP}$. The data are from KA84 [52] (open diamonds), SM95 [51] (open triangles) and SE-SM95 [51] (filled circles).

In the partial waves for which we have not included any resonances (S_{31}, P_{31}, P_{13} and D_{33}), the expressions (3.64) and (3.65) give of course the same results because in these partial waves the interaction comes solely from the non-pole potential. For the S_{11} and the D_{13} the results for both approaches are also similar. In the P_{11}, the inelasticity parameter η starts to increase above one already at the $\pi\pi N$ threshold at ~ 1.2 GeV if one takes into account the effect of the non-pole T-matrix on T^P. If one works with expression (3.64), the inelasticity parameter first decreases before it also starts to rise above one at 1.3 GeV. Both approaches will certainly overestimate the P_{11} partial wave cross section above 1.3 GeV.
In the right panel of Fig. 3.21 we show the total cross sections for $\pi^- p$ scattering. We indeed observe an overestimation of the data already above 1.3 GeV for both approaches, equation (3.64) as well as equation (3.65). This overestimation can be attributed to the failure of the tree-level approximations in the description of the P_{11} partial wave.

In the P_{33} partial wave the inelasticity parameter starts to deviate significantly from one only above 1.4 GeV if we take into account the full pole potential. The approach with the undressed vertex functions for the pole matrix, equation (3.64), first oscillates around $\eta = 1$. Already at 1.2 GeV, the inelasticity parameter reaches a local maximum of $\eta = 1.4$. So expression (3.64) should already overestimate the interaction around the Δ peak. This can be seen clearly in the left panel of Fig. 3.21, where we show the total cross sections for $\pi^+ p$ scattering.

Also in the S_{31} partial wave η starts to deviate from one as early as 1.2 GeV. So also in this partial wave, the tree-level model for πN scattering will break down at energies slightly above the $\pi\pi N$ threshold already. In the P_{31}, P_{13} and in the D-waves, the inelasticity parameter η starts to leave the unitarity bounds only at relatively high energies above ~ 1.4 GeV. In these partial waves, the tree-level approximations (3.64) and (3.65) work quite well. This is not too surprising, because we found that the non-pole interaction in these partial waves is small. The phase shifts in these partial waves are of the size of a few degrees only, see the dashed line in Fig. 3.13.
It is remarkable that the description of the inelasticity parameter in the D_{13} partial wave is so good for both of the tree-level approximations. The coupling to the inelastic channels occurs only through the self-energy term in equation (3.64). This alone is enough to describe the inelasticity in the D_{13} partial wave correctly. Of course, such an approximation can only work so nicely because the non-pole potential in the D_{13} partial wave is so small.

In Fig. 3.20 we show the phase shifts obtained with the tree-level approximations, equations (3.64) and (3.65). In the S_{11} partial wave we have in all calculations omitted the contribution from the $S_{11}(1650)$. The tree-level approximations describe the phase

shifts obtained with the unitary K-matrix model reasonably well.
In the S_{31} partial wave we observe a large effect of the neglection of the unitarisation. The interaction in this partial wave is solely due to a non-pole potential in our model. This potential is relatively strong (it causes a phase shift of -20° at 1.2 GeV already). This explains the presence of large higher order effects in the scattering equation $T = V^{NP} + V^{NP}GV^{NP} + \ldots$.
With the exception of the P_{11} and the P_{33} partial waves, we find a good description of the phase shifts in both tree-level approximations.
In the P_{11} partial wave, approximation (3.64) already starts to differ from the data and the results of the K-matrix model at 1.2 GeV. Approximation (3.65) can describe the data up to 1.4 GeV, but above this point the phase shifts stay nearly constant at a value of $30° - 40°$. The resonant behaviour of the P_{11} is not reproduced by either of the two approximations.

In the P_{33} partial wave, the phase shifts are clearly better reproduced by the approximation using the full pole T-matrix. For the other approximation, equation (3.64), the resonance cannot be correctly described. The phase shifts rise to 90° like the data, but then the rise in the calculated phase shifts becomes smaller until the phase shifts start to go down again.

In summary we find that a tree-level approximation cannot describe πN scattering above 1.25 GeV (or 1.4 GeV for the isospin 3/2 channel). Based on this observation we would not expect the tree-level model to account for the pion-production reaction $\pi N \to \pi\pi N$ at higher energies.
Nevertheless, a good description of the total cross sections in all experimentally accessible reaction channels in $\pi N \to \pi\pi N$ is possible in the (extended) Oset–Vicente-Vacas model [24, 25, 56] up to nearly 1.4 GeV! Also a Chiral Perturbation Theory calculation at $\mathcal{O}(p^2)$ which consists only of tree-level contributions can give a good account of the $\pi N \to \pi\pi N$ data [23] over the same energy range.
The reason that a tree-level approximation works so well in the pion production reaction $\pi N \to \pi\pi N$, but not in πN scattering was given by Fettes et al. in [57]. They performed a one-loop calculation of $\pi N \to \pi\pi N$ in Chiral Perturbation Theory and found the unitarity corrections to be small. They found that the attachment of the additional pion line to the πN scattering contributions leads to large cancellations in the loop contributions that are present in πN scattering.

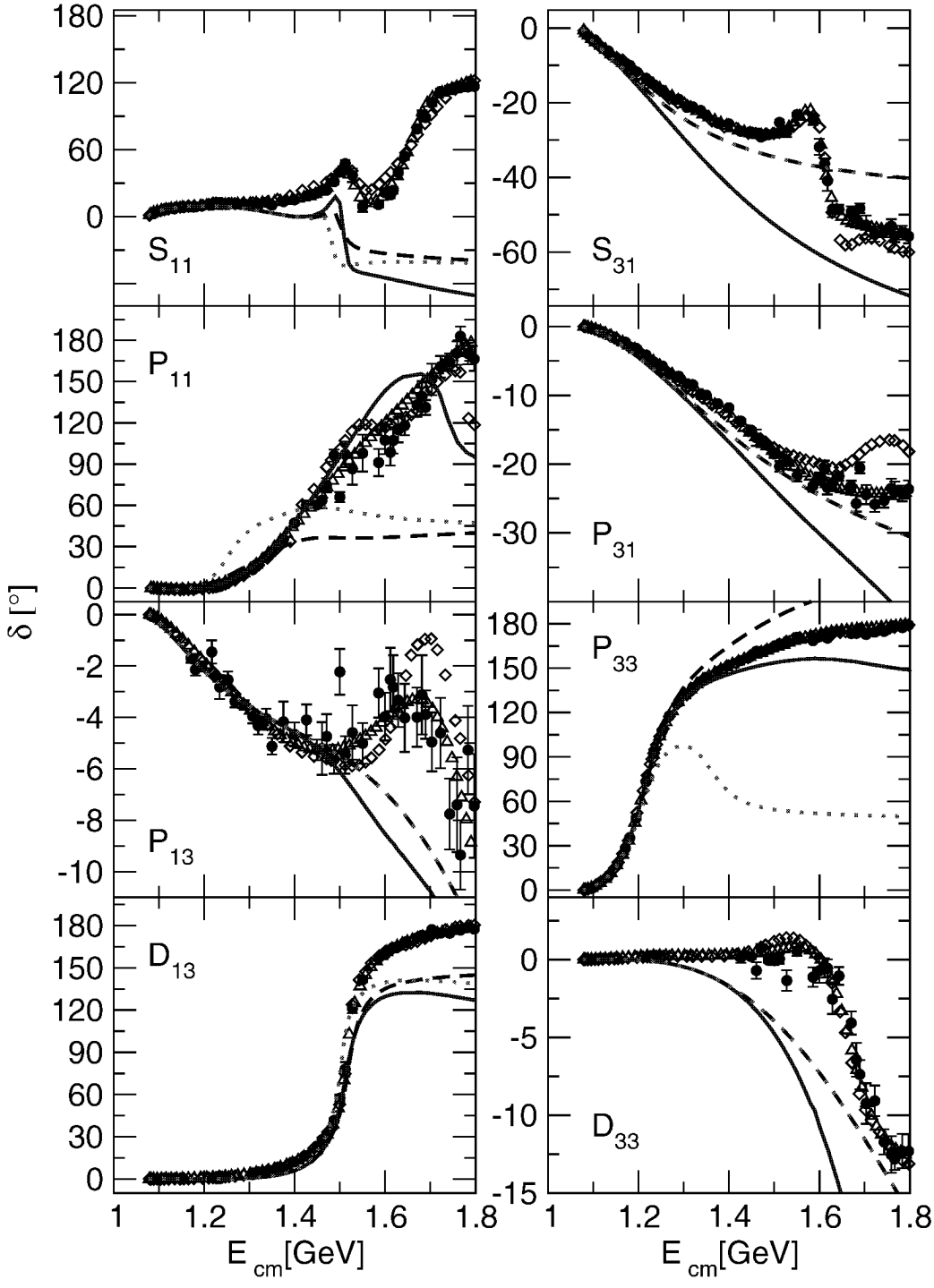

Figure 3.20: πN phase shifts. The solid lines show the results of the unitary K-matrix model. The dashed lines are calculated with the approximation $T = T^P + V^{NP}$. The dotted lines show the approximation $T = T_0^P + V^{NP}$. The data are from KA84 [52] (open diamonds), SM95 [51] (open triangles) and SE-SM95 [51] (filled circles).

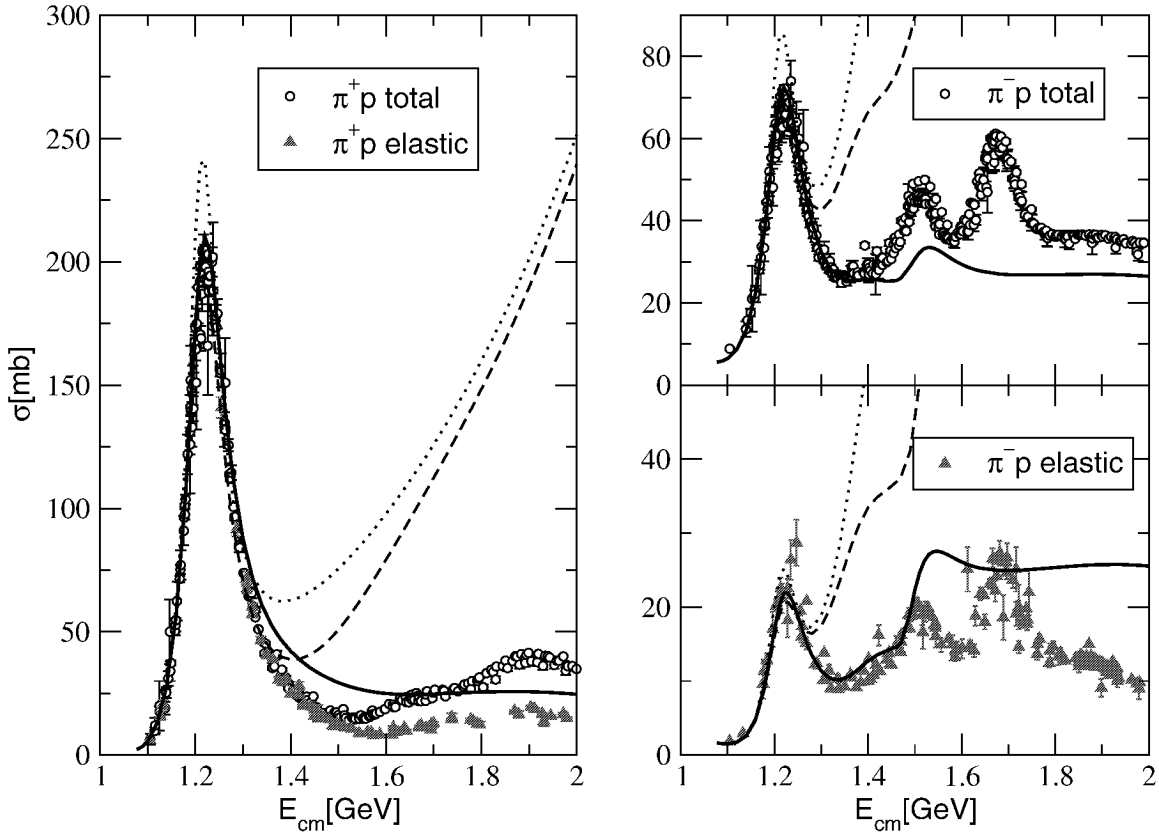

Figure 3.21: πN total cross sections. On the left hand side we show the total and elastic cross sections for $\pi^+ p$ scattering, the calculations being for elastic $\pi^+ p$ scattering. On the right hand side the total (upper panel) and elastic (lower panel) cross sections for $\pi^- p$ scattering. The calculations for the total cross section in $\pi^- p$ scattering comprise the sum of the $\pi^- p$ and $\pi^0 n$ final states. The solid lines show the results of the unitary K-matrix model. The dashed lines are calculated with the approximation $T = T^P + V^{NP}$. The dotted lines show the approximation $T = T_0^P + V^{NP}$. The data are from the Particle Data Group [31].

Chapter 4

The Reaction $\pi N \to \pi\pi N$

In this chapter we present the results of our model for the pion production reaction $\pi N \to \pi\pi N$.

We use two variants of our model that differ in the description of the pole diagrams:

- Model A uses the bare vertex functions f_0 for the pole diagrams, and the self-energy is calculated from the expression $\Sigma_0 = f_0^\dagger G f_0$ which includes only loops without any non-pole interaction.
- Model B uses the dressed vertex functions $f = (1+T^{NP}G)f_0$, and the expression for the self-energy contains non-pole interactions, $\Sigma = f_0^\dagger G f$, as discussed in sections 3.2.2 and 3.3.2.

4.1 Total Cross Sections

Fig. 4.1 shows the total cross sections in the five reaction channels of pion-induced pion production that are accessible to experiment,

$$\begin{aligned} \pi^\pm p &\to \pi^\pm\pi^+ n\,, \\ \pi^\pm p &\to \pi^\pm\pi^0 p\,, \\ \text{and } \pi^- p &\to \pi^0\pi^0 n\,. \end{aligned}$$

The data are shown as a function of the kinetic energy of the initial state pion in the laboratory frame T_π, which is related to the invariant mass $\sqrt{s}$ of the reaction via

$$T_\pi = \frac{s - (M_N + m_\pi)^2}{2M_N}\,. \tag{4.1}$$

	ΔT[MeV]
$\pi^- p \to \pi^- \pi^+ n$	0.0039
$\pi^- p \to \pi^0 \pi^0 n$	−0.008
$\pi^- p \to \pi^0 \pi^- p$	−0.0037
$\pi^+ p \to \pi^+ \pi^+ n$	0.0039
$\pi^+ p \to \pi^0 \pi^+ p$	−0.0037

Table 4.1: Threshold correction for each reaction channel.

As an orientation, the largest energy shown in Fig. 4.1, $T_\pi = 0.4$ GeV corresponds to $\sqrt{s} = 1.38$ GeV, which is below the Roper resonance. The Δ isobar lies at $T_\pi = 0.19$ GeV.

The observables are calculated in the isospin-symmetric limit in our model. The cross sections are however sensitive to isospin breaking through the masses in the final states, as the cross sections rise proportionally to the square of the energy above the reaction threshold. It is thus important to correct the threshold energy for each of the reaction channels. This is done by shifting the isospin symmetric threshold

$$T_\pi^{\text{thr.}} = m_\pi - \frac{3m_\pi^2}{M_N} = 0.168\,\text{GeV} \tag{4.2}$$

to its correct value for each reaction channel [23]. The difference ΔT for each reaction channel is given in Table 4.1.

In all five reaction channels both of our model variants give a reasonable description of the data. There are hardly any differences between Model A and B. In the $\pi^- p \to \pi^+ \pi^- n$ and $\pi^- p \to \pi^0 \pi^0 n$ reactions, Model A gives results that are on the upper edge of the data, while model B gives even a little larger results for the cross sections. In $\pi^- p \to \pi^0 \pi^0 n$ both models overestimate the data between 0.17 and 0.2 GeV by almost a factor of two.
For $\pi^+ p \to \pi^+ \pi^0 p$ the cross sections obtained with Model A also lie on the upper edge of the data above ~ 0.25 GeV. In this case, Model B gives lower results, which leads to a good description of the data.
The cross sections in the $\pi^- p \to \pi^- \pi^0 p$ and $\pi^+ p \to \pi^+ \pi^+ n$ channels are well reproduced by both models, though in the $\pi^+ p \to \pi^+ \pi^+ n$ reaction we start to overestimate the data above $T_\pi \sim 0.3$ GeV.

For comparison, we also show the results of a calculation in Chiral Perturbation Theory up to $\mathcal{O}(p^3)$ [57]. Chiral Perturbation Theory works well for $\pi N \to \pi\pi N$

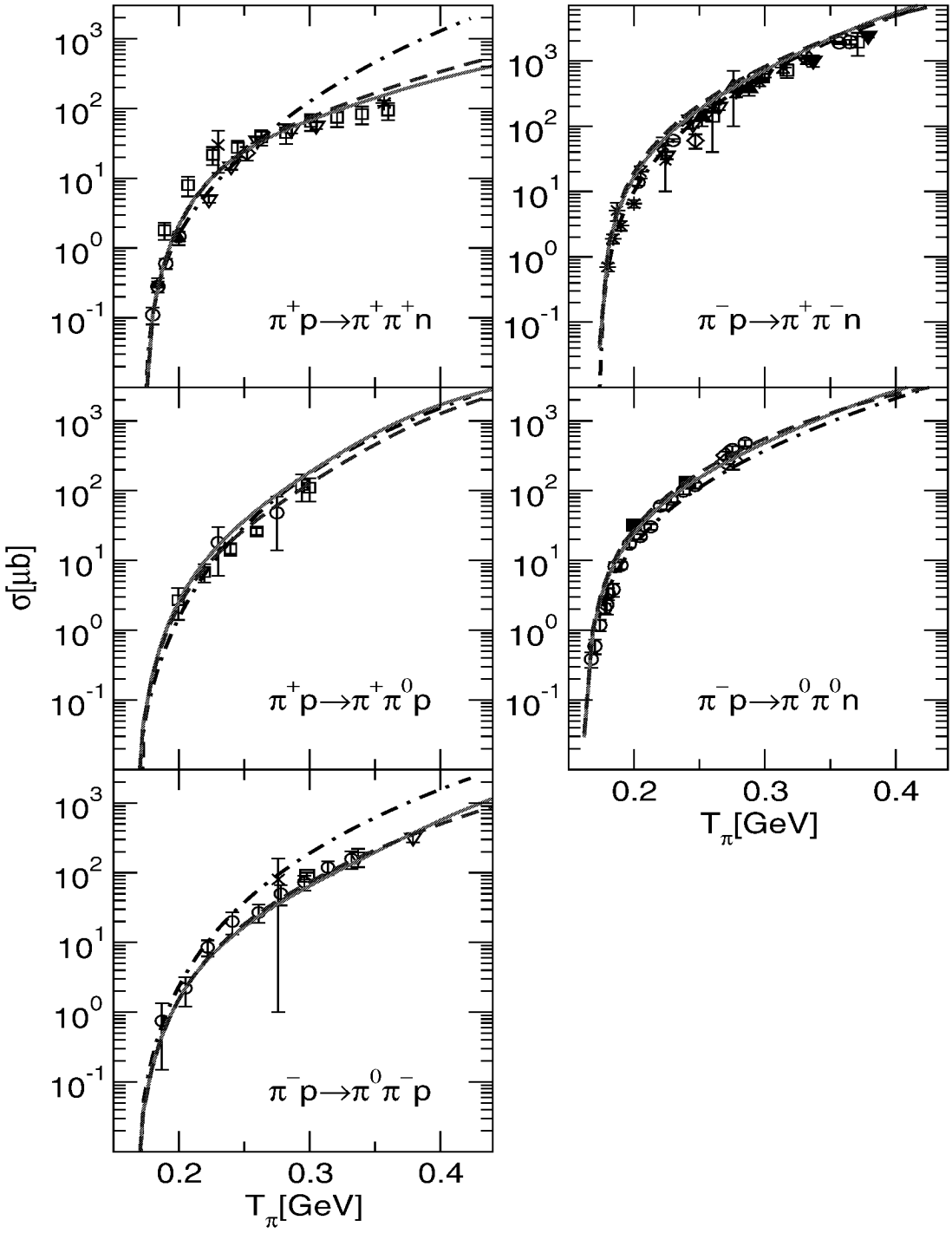

Figure 4.1: Total cross sections for $\pi N \to \pi\pi N$. The solid lines show the results of Model A (as described in the text), the dashed lines the results of Model B. For comparison we also show the results of Chiral Perturbation Theory [57] (dot-dashed lines). The data are taken from the compilation in [58] and from [26].

despite the presence of the Δ isobar already at T_π =0.19 GeV. The description of the $\pi^- p \to \pi^+\pi^- n$ and $\pi^- p \to \pi^0\pi^0 n$ data at low energies is certainly better than in our model. Note however, that the $\pi N \to \pi\pi N$ data up to 250 MeV have been used to fix six of the dimension three low-energy constants, while we have fixed all of our model parameters to πN and $\pi\pi$ scattering. In the reaction channels $\pi^- p \to \pi^0\pi^- p$ and $\pi^+ p \to \pi^+\pi^+ n$ the cross sections are clearly overestimated above 0.3 GeV in the Chiral Perturbation Theory approach.

It should be mentioned that our results for the total cross sections are also similar to those obtained with the extended Oset–Vicente-Vacas model [56].

In Figure 4.2 we investigate the effect of different mechanisms on the total cross sections for Model A. The results for Model B are very similar, so we refrain from showing them also.

Let us first discuss the contribution of the Δ isobar. We observe a large contribution of the Δ in $\pi^+ p \to \pi^+\pi^0 p$. This is not too surprising: because the initial $\pi^+ p$ state has isospin 3/2 and the Δ isobar lies already at T_π = 1.9 GeV, we expect a large contribution from the Δ already in the threshold region of this reaction channel. Following this reasoning, we do also expect a large contribution of the Δ in $\pi^+ p \to \pi^+\pi^+ n$, but there the effect of switching off the Δ contribution is almost negligible. We find that also in the $\pi^+ p \to \pi^+\pi^+ n$ channel the contribution of the diagrams with intermediate Δ states by itself is large, but there is destructive interference between the Δ contributions and the rest of the diagrams. So adding the Δ contribution to the remaining contributions only has a small effect in this reaction channel.
The contributions from Δ intermediate states are sizeable in the reaction channels with a $\pi^- p$ initial state.

We find that the impact of the $N^\star$ resonances $S_{11}(1535)$ and $D_{13}(1520)$ on the total cross sections is negligible in each of the five reaction channels in this energy regime up to $\sim$1.4 GeV. The contribution from the $N^\star$ resonances comes almost exclusively from the Roper resonance.

The contribution of the $N^\star$ resonances in the isospin 3/2 channels is negligible, and comes solely from the Roper resonance via the diagrams (K.3)–(K.6) (see Fig. 2.3 on page13). Also in $\pi^- p \to \pi^0\pi^- p$ the contribution from $N^\star$ resonances is small and only has an effect above $\sim$ 0.4 GeV.
In $\pi^- p \to \pi^+\pi^- n$ and $\pi^- p \to \pi^0\pi^0 n$ we observe the largest effect of the $N^\star$ contributions. In these two reaction channels the final pions can be in the scalar-isoscalar partial wave and so the decay of the Roper resonance into the σ N state is possible. This decay channel is favoured at lower energies versus the $\pi N(\to \pi\pi N)$ or $\pi\Delta$ decay because it allows all final state particles to be in relative s-waves. For $\pi^- p \to \pi^0\pi^- p$

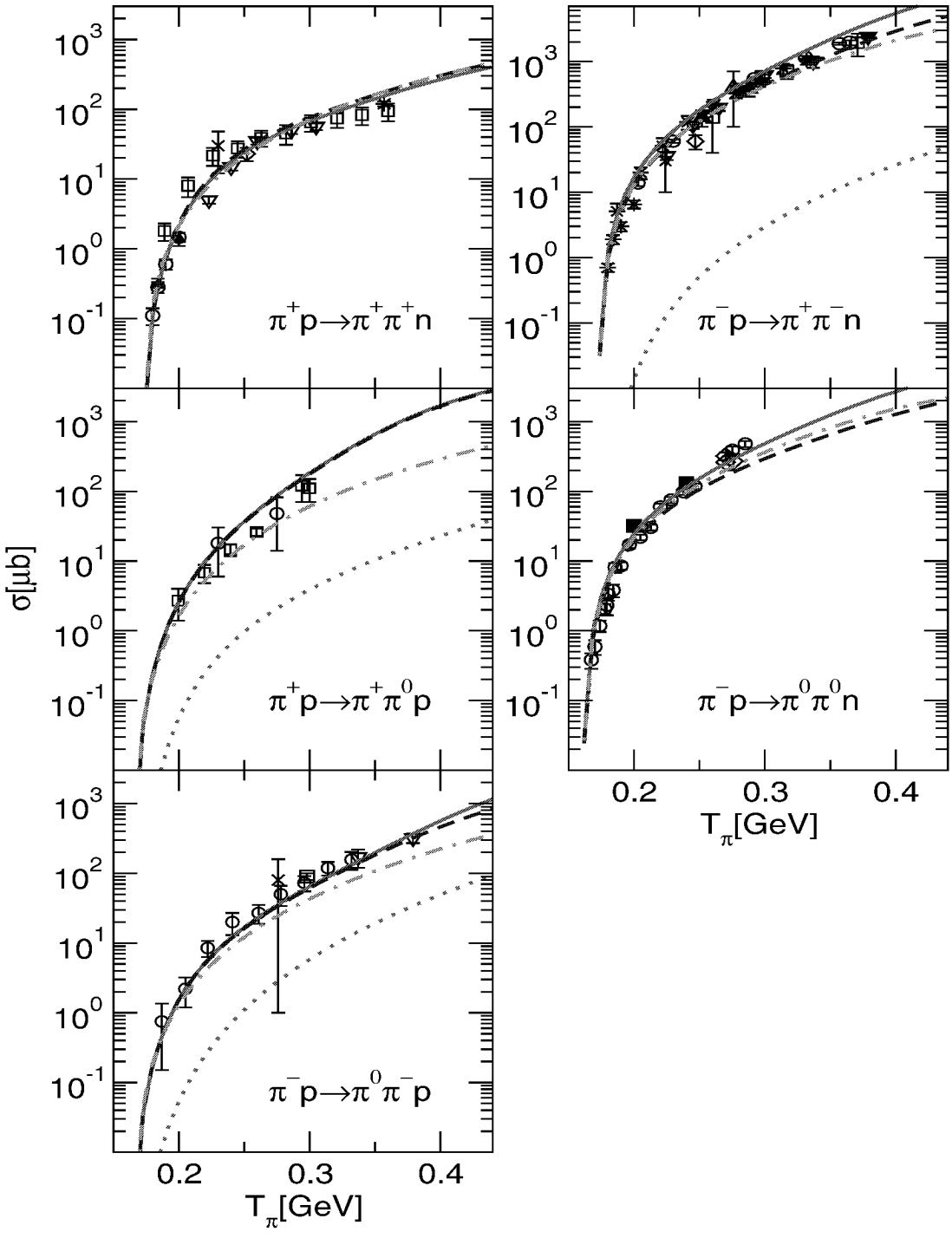

Figure 4.2: Total cross sections for $\pi N \to \pi\pi N$. The solid lines show the results of Model A. The dot-dashed line has been calculated without the Δ isobar, the dashed line is without the $N^\star$ resonances. The dotted line shows the contribution of diagrams with a ρ decaying to the final state pions.

the σN decay channel is not allowed, and so the Roper resonance contributes only at larger energies.

Finally, we also show the contribution of diagrams (C.3)–(D.2) and (H.1/2), where the final state pions are correlated via ρ exchange. We mentioned that we do not account for the dressing of the decay vertices to the ρN channel in model B and argued that the contribution of the ρN channel is only small because the pion interaction in the ρ partial wave is small in the relevant energy regime. Here we see that these contributions are indeed small for $\pi N \to \pi\pi N$. For the $\pi^+\pi^+ n$ and $\pi^0\pi^0 n$ final states, these contributions are zero, because the ρ cannot decay to $\pi^+\pi^+$ or $\pi^0\pi^0$. In the other reaction channels, the contribution of the ρN channel is down by at least one order of magnitude.

4.2 Differential Cross Sections

The investigation of differential cross sections allows to study the dynamics of the reaction $\pi N \to \pi\pi N$ in more detail. The final state is characterised by four independent kinematical variables which can be chosen to be the invariant mass of the two pions $M_{\pi\pi}$, the momentum transfer t between the nucleons, the angle θ between the initial state pion and one of the final state pions and the angle ϕ between a final state pion and the reaction plane defined by the initial state pion and the nucleons, see also Fig. E.1 in Appendix E. In this appendix, the formulae for the calculation of the differential cross sections are also given.

Differential cross sections $d\sigma/dt$, $d\sigma/dm^2_{\pi\pi}$ and $d\sigma/d\cos\theta$ have been measured at TRIUMF for the reaction channels $\pi^\pm p \to \pi^\pm\pi^+ n$ [26]. Their focus was on the threshold region up to $T_\pi \sim 300$ MeV.

In Figs. 4.3 – 4.5 we compare Models A and B to the differential cross sections in the $\pi^+ p \to \pi^+\pi^+ n$ channel.

The description of the cross sections in the isospin 3/2 reaction channels $\pi^+ p \to \pi^+\pi^+ n$ and $\pi^+ p \to \pi^+\pi^0 p$ provides an important test of our model for the background below the $N^\star$ resonances, because the contributions of $N^\star$ resonances in these reaction channels are minimal. In our model only the Roper resonance can make a contribution in the isospin 3/2 channels via the diagrams (K.3)–(K.6) (see Fig. 2.3 on page 13), but this turns out to be negligible (see Fig. 4.2).

In the $d\sigma/dM^2_{\pi\pi}$ distributions, the data show an enhancement over phase space at intermediate values of $M^2_{\pi\pi}$. Both of our models predict an enhancement at low $M^2_{\pi\pi}$. Also the Chiral Perturbation Theory calculation [57] and the extended Oset–Vicente-

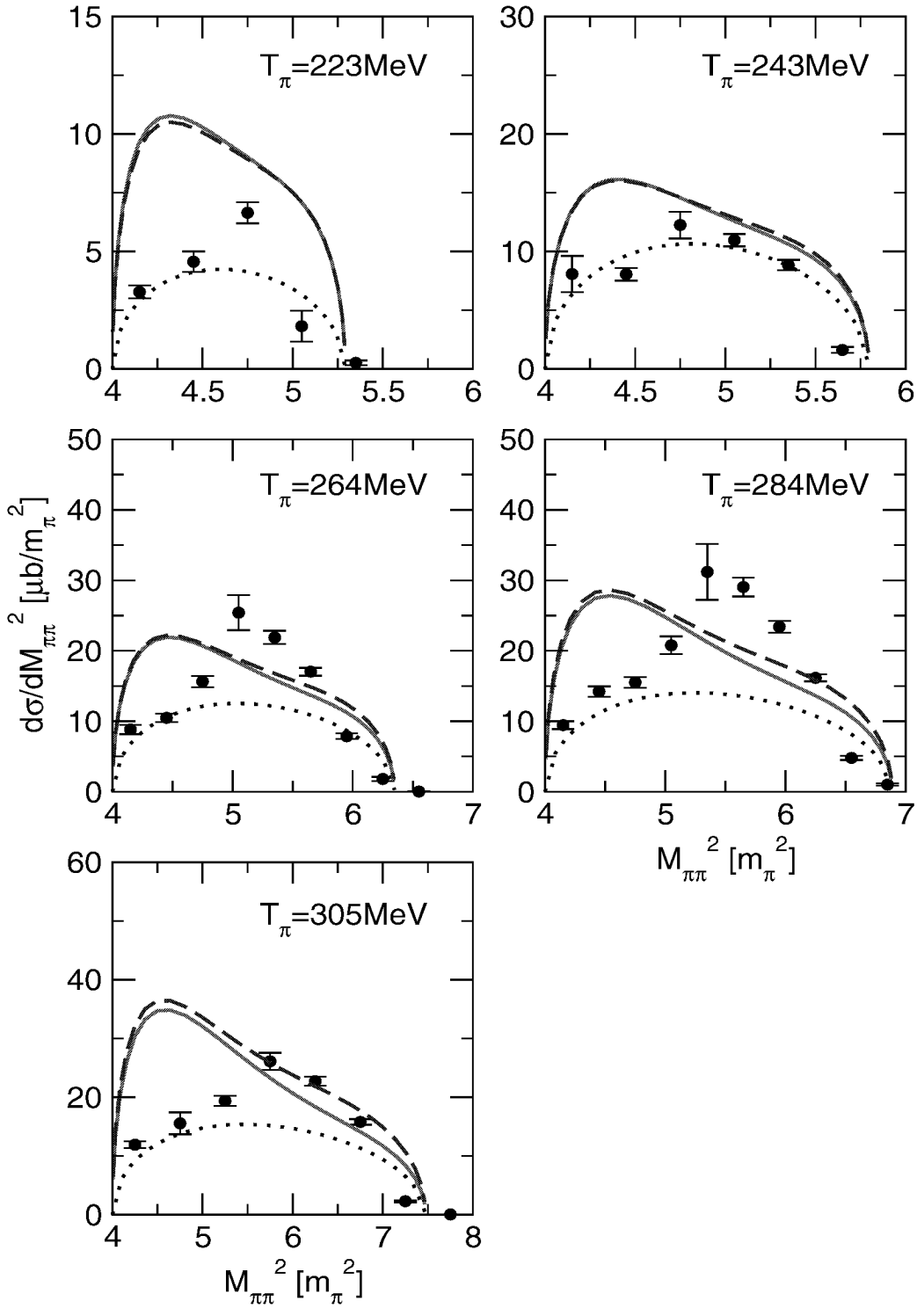

Figure 4.3: Differential cross sections $d\sigma/dM^2_{\pi\pi}$ for $\pi^+p \to \pi^+\pi^+n$. The solid lines show the results of Model A, the dashed lines are for Model B. The dotted line shows the phase space distribution. The data are from [26].

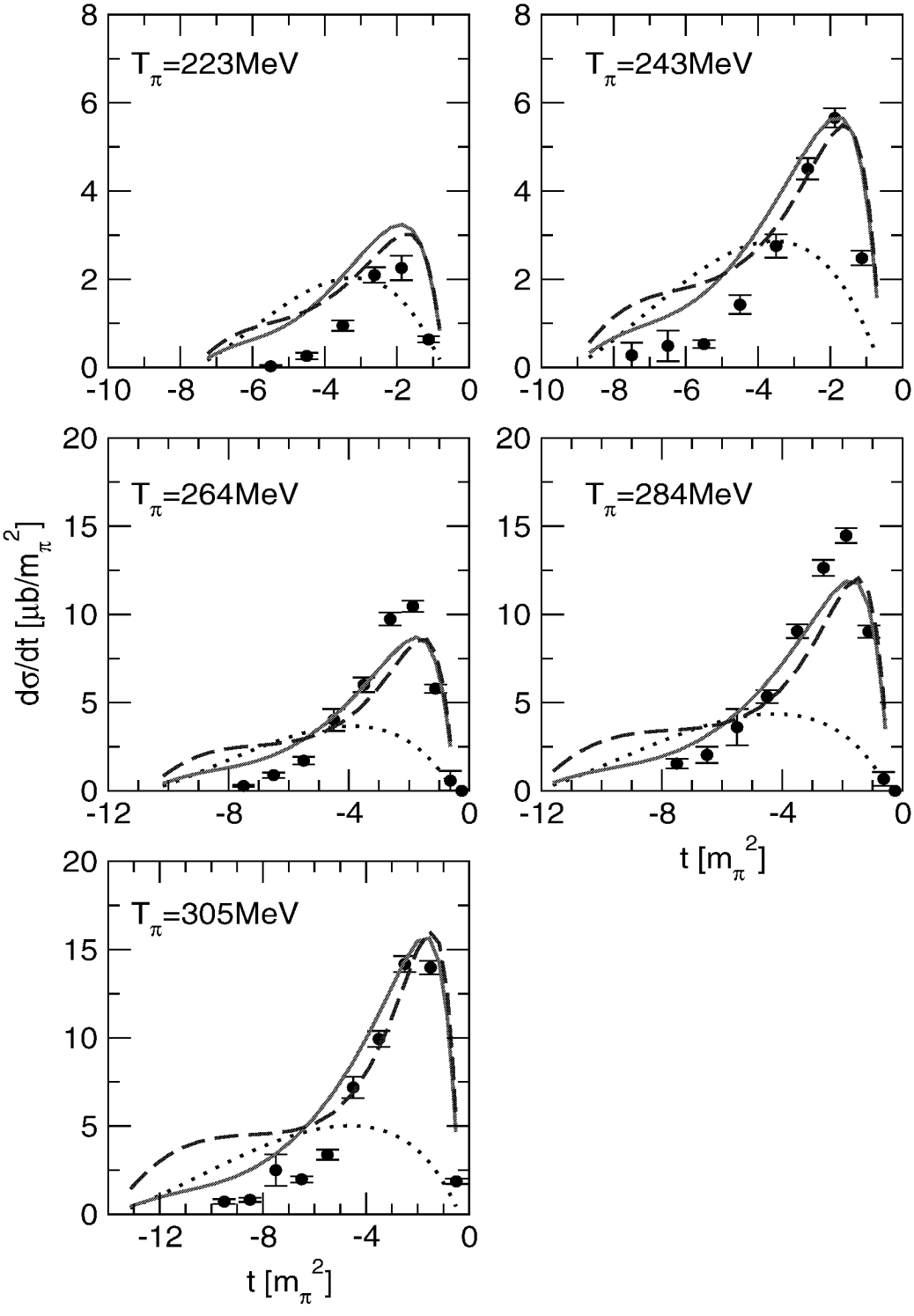

Figure 4.4: $d\sigma/dt$ for $\pi^+ p \to \pi^+\pi^+ n$. The lines denote the same as in Fig. 4.3.

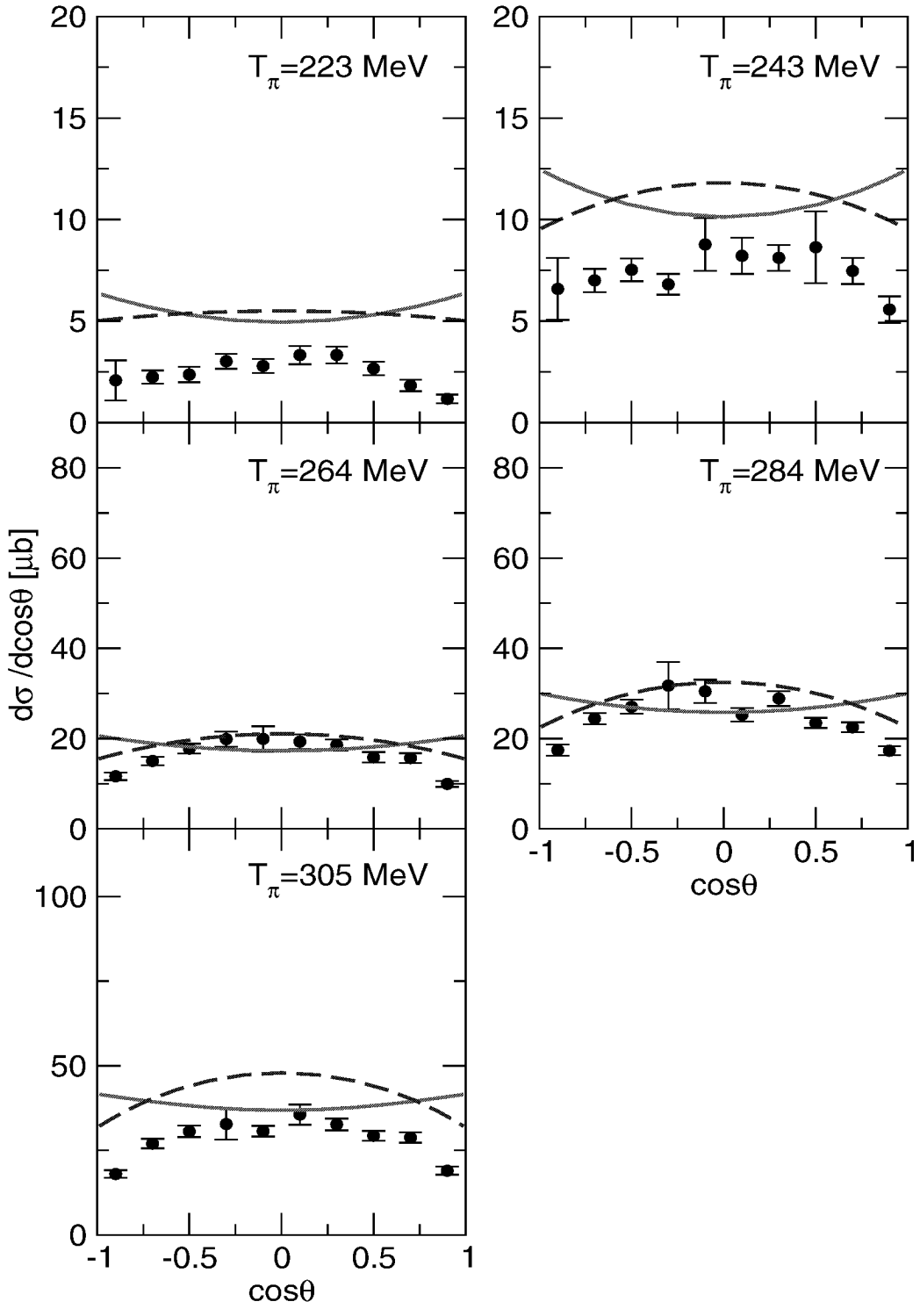

Figure 4.5: $d\sigma/d\cos\theta$ for $\pi^+p \to \pi^+\pi^+n$. The lines denote the same as in Fig. 4.3.

Vacas model [26] predict a similar enhancement at low $M^2_{\pi\pi}$. It is not clear how the shape of the experimental distributions can be described.

The differential cross sections $d\sigma/dt$ show a peak at low $|t|$. This is also present in our models. Model A can describe also the tail of the peak quite well, whereas Model B produces a shoulder at large $|t|$.

In Fig. 4.5 we show the differential cross sections $d\sigma/d\cos\theta$ as a function of the angle between one final pion and the initial pion in the centre-of-momentum frame of the final state pions. This angular cross section has to be symmetric about $\cos\theta = 0$ for the $\pi^+\pi^+n$ final state because of the symmetry of the reaction under the exchange of the final state pions. The experimental $\cos\theta$ distributions show a maximum at $\cos\theta = 0$. The distributions obtained with Model A are bent in the opposite direction whereas Model B gives the correct curvature. For Model A it is possible to change the curvature by increasing the $\sigma\pi\pi$ gradient coupling g_2 by a factor of seven and simultaneously increasing the $\pi\pi\Delta$ coupling by a factor of three. But increasing g_2 by such an amount leads to a shape similar to phase space for the $d\sigma/dt$ distributions which would completely spoil the description of these distributions. So we conclude that there is no way to simultaneously describe the t-distributions and the $\cos\theta$-distributions in Model A.

No calculations have been published for the angular distributions from the Oset–Vicente-Vacas model. The only calculation of these angular distributions that we are aware of is the Chiral Perturbation Theory calculation by Fettes [59]. This calculation finds the opposite curvature as compared to the data.

In the angular distributions we have found a quantity that is sensitive to higher order loop effects as are contained in the dressed vertex functions of Model B. The importance of final state interaction effects in the description of this quantity questions the applicability of tree-level models for the analysis of these data. However, there are a few points that need further investigation: we cannot fully exclude the possibility that a refit of those parameters of our model that are not too much constrained by $\pi\pi$ and πN scattering, e.g. the $\pi\pi\Delta$ and $\rho N\Delta$ coupling constants to the $\pi N \to \pi\pi N$ differential cross sections could lead to at least a qualitative agreement with the observables in the $\pi^+p \to \pi^+\pi^+n$ reaction channel. Secondly, there is the possibility that other mechanisms, for example a contribution of the $S_{31}(1620)$, have an influence on the shape of the angular distributions.

Let us now proceed to the $\pi^-p \to \pi^+\pi^-n$ reaction. The differential distributions for this reaction channel are displayed in Figs. 4.6 – 4.8.

The magnitude of the differential cross sections is overestimated by both of our models,

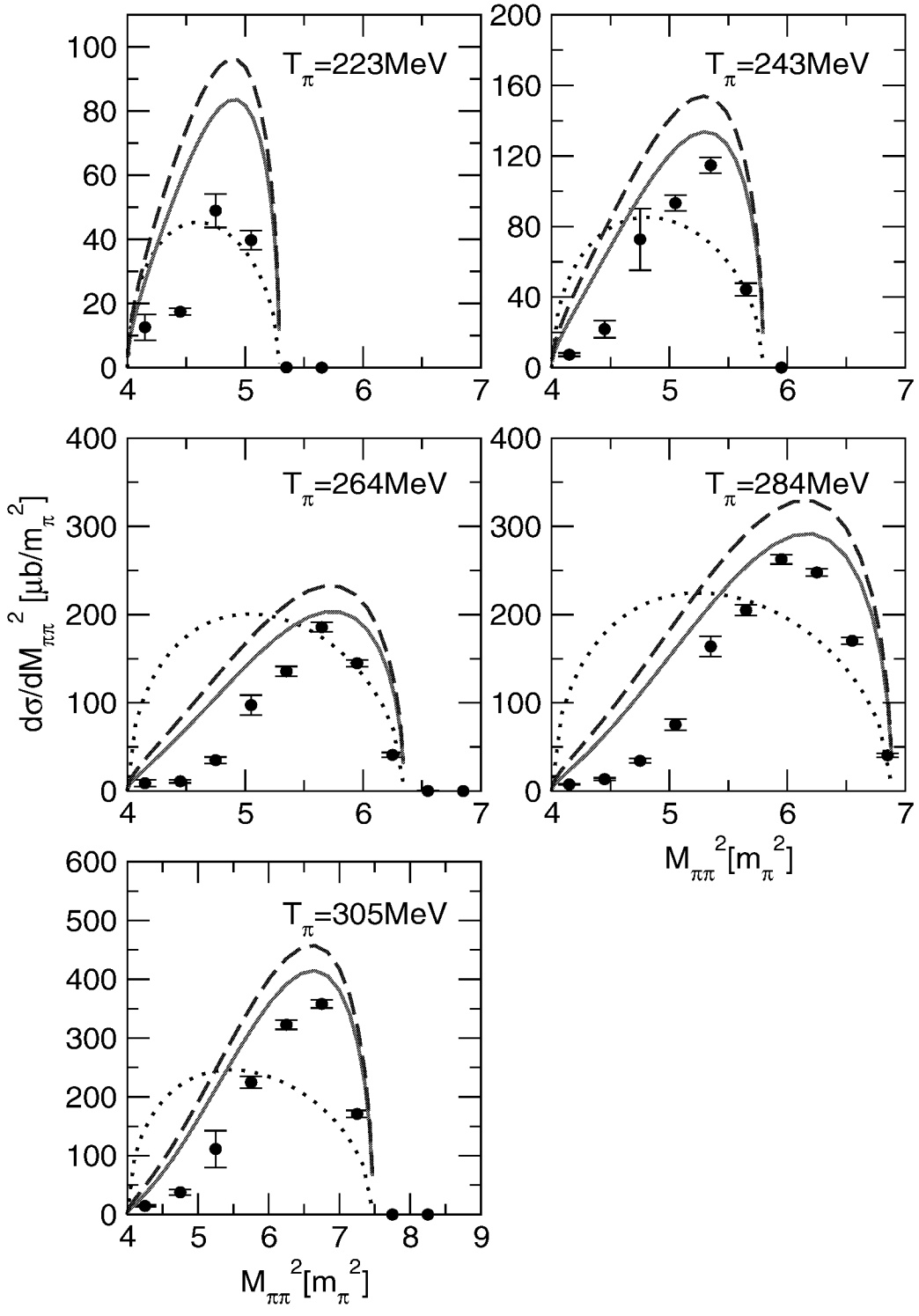

Figure 4.6: Differential cross sections $d\sigma/dM^2_{\pi\pi}$ for $\pi^- p \to \pi^+\pi^- n$. The solid lines show the results of Model A, the dashed lines are for Model B. The dotted line shows the phase space distribution. The data are from [26].

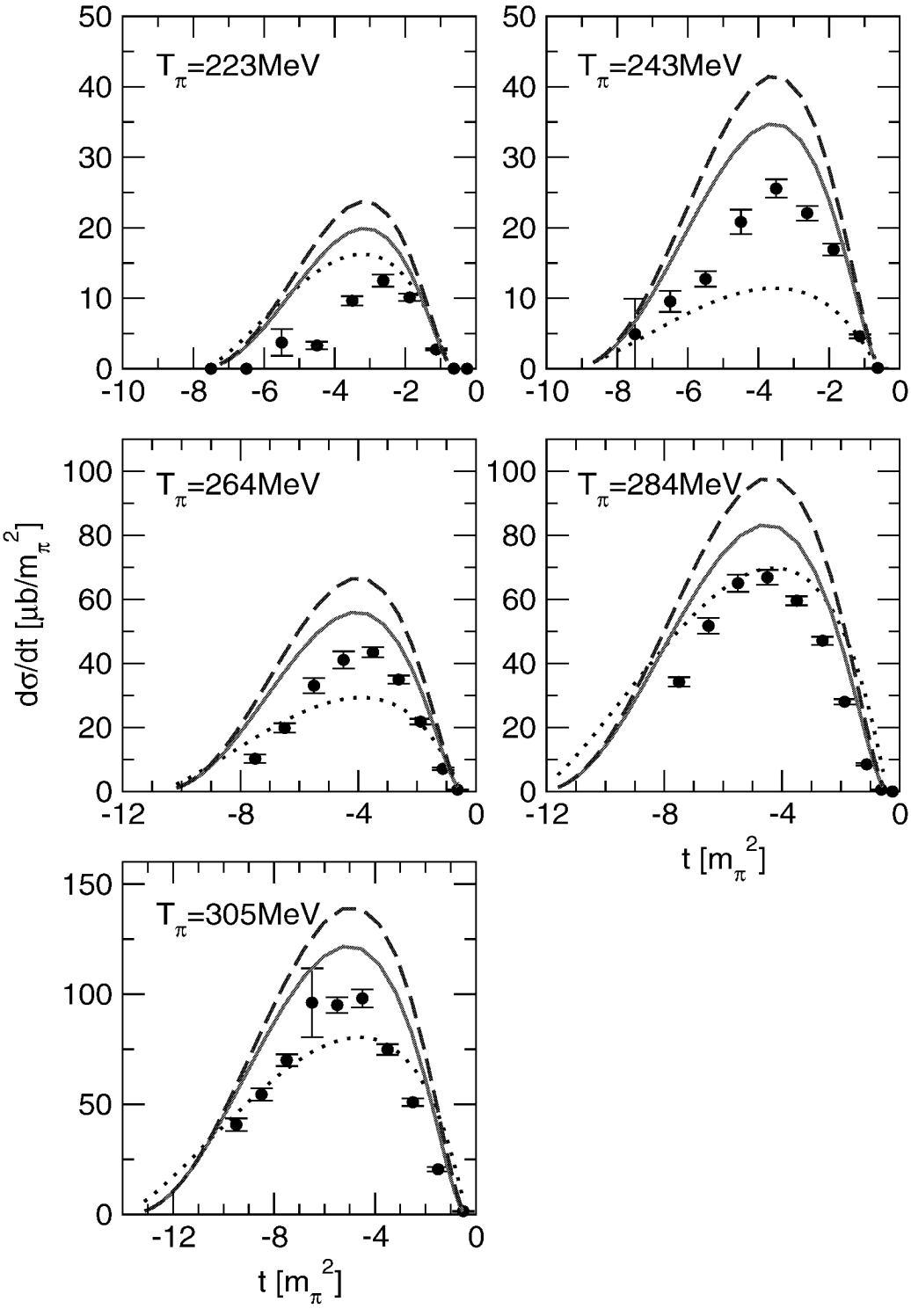

Figure 4.7: $d\sigma/dt$ for $\pi^- p \to \pi^+\pi^- n$. The lines denote the same as in Fig. 4.6.

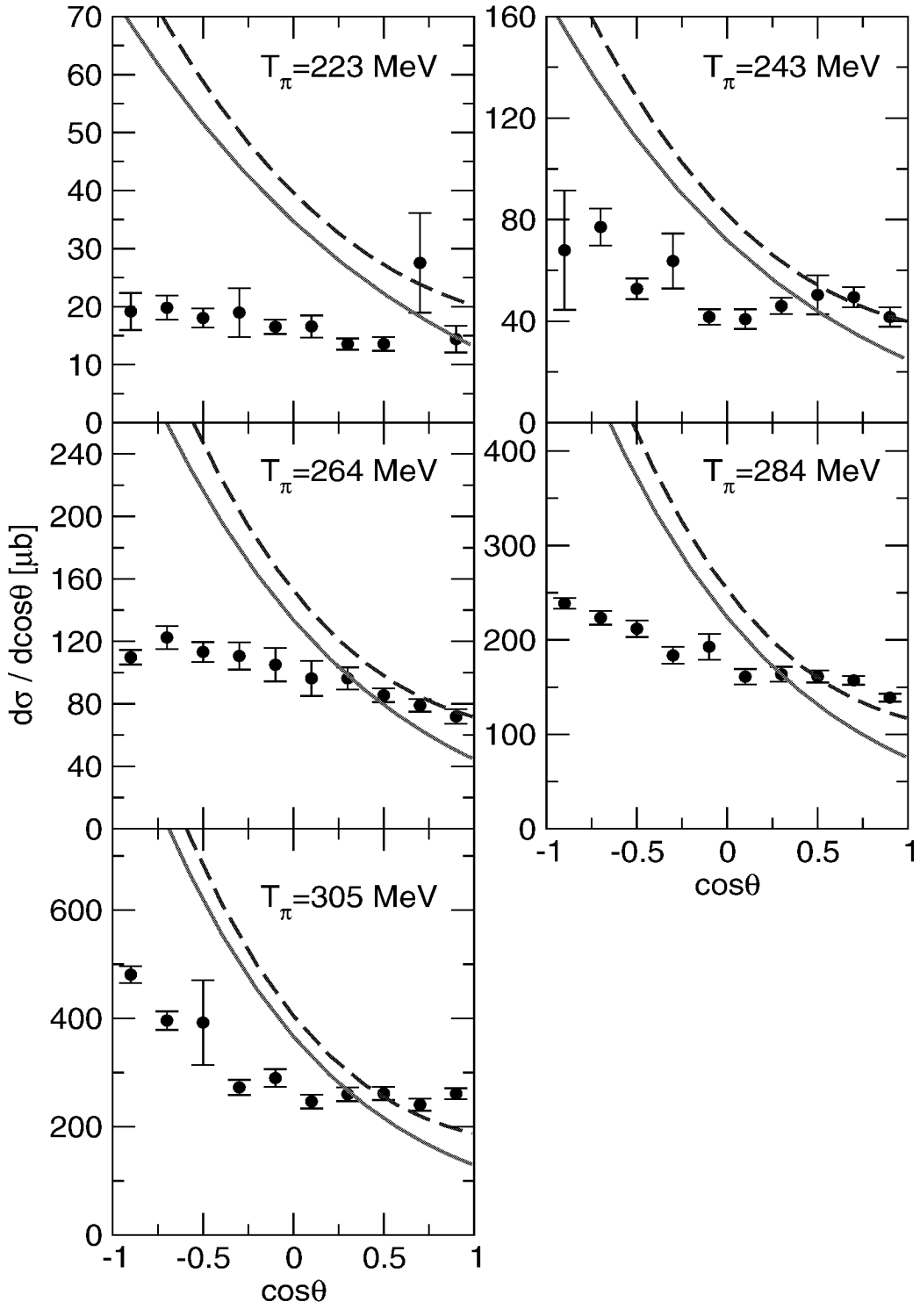

Figure 4.8: $d\sigma/d\cos\theta$ for $\pi^- p \to \pi^+\pi^- n$. The lines denote the same as in Fig. 4.6.

at the lowest energy $T_\pi = 223$ MeV approximately by a factor of two. But the shape of the differential cross sections is largely in agreement with the data for the $M^2_{\pi\pi}$ and t distributions.

For the angular distributions we find a large overestimation of the data at backward angles. In this reaction channel, the dressing of the vertices in Model B has no effect on the shape of the distributions.

In Fig. 4.9 we show the effect of the resonance contributions on the differential cross sections $d\sigma/dM^2_{\pi\pi}$ for Model B. The neglect of the resonances in Model A leads to similar results. Switching off the contribution of the Δ isobar leads to a reduction in the size of the differential cross sections but the shape of the distributions remains practically unchanged. The same goes for the contribution of the Roper resonance.

In order to obtain more information on the effect of the Roper resonance on the distributions, we study its effect at larger energies, in the resonance region. Recently, detailed differential distributions have been measured for the $\pi^- p \to \pi^0\pi^0 n$ reaction [22] at energies from threshold up to 1.53 GeV. Figs. 4.10 and 4.11 show our results in comparison to the differential distributions in the energy range from 1.35 GeV to 1.5 GeV. Note that the data were given without normalisation; we scaled them to the results of Model A.

We find that the shapes of the $d\sigma/dM_{\pi^0 n}$ distributions are very well reproduced by Model A and Model B. Above 1.47 GeV one clearly sees an enhancement at the mass of the Δ. Switching off the contribution of the Roper resonance (we show here the results for Model B) only leads to a change in the size of the $M_{\pi^0 n}$ distributions, but no qualitative change in the shape can be found. It is also interesting to observe, that above 1.47 GeV the effect of the Roper resonance is nearly negligible. Physically, one would expect a large contribution of the Roper resonance especially in this energy region, because in this energy region the resonance is observed in pion-nucleon scattering. In our model, the contribution of the Roper resonance however vanishes in the background for the pion production reaction.
In the t-distributions one observes the evolution of a broad shoulder at low $|t|$ with increasing energy. At even larger energies, this enhancement becomes a peak [22]. Such a peak structure can be explained with the pion-exchange diagrams (C.1)–(C.4) (see Fig. 2.1 on page 11) becoming important. We do not see such a structure in our Model A. Model B however displays a similar shape as the data. Maybe the resonance contributions are overestimated in this energy regime in Model A and so hide the effect of the pion-exchange.

Also in this reaction channel our models cannot correctly reproduce the angular dis-

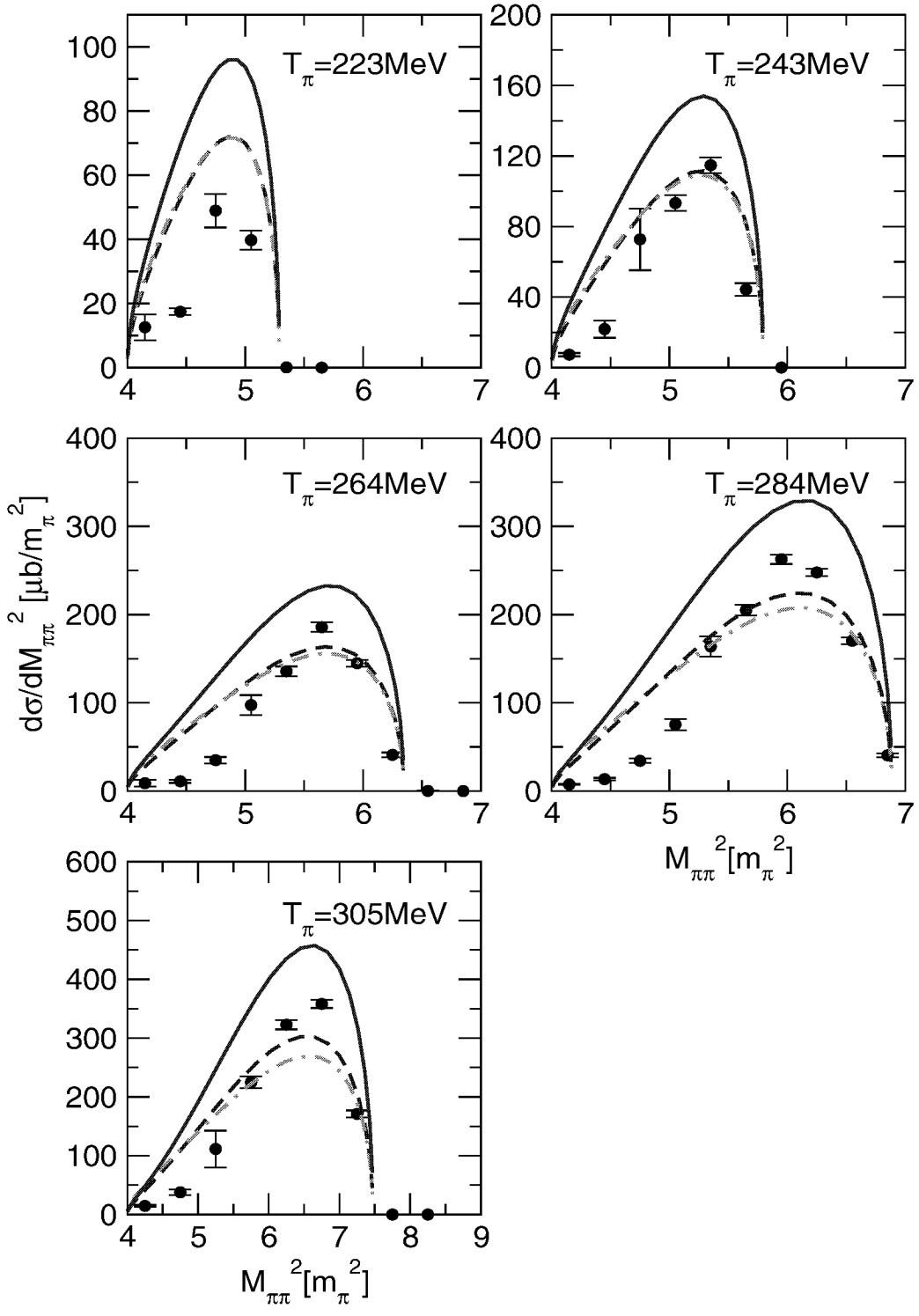

Figure 4.9: Effect of resonance contributions on $d\sigma/dM^2_{\pi\pi}$ for $\pi^- p \to \pi^+\pi^- n$. The solid line is for the full Model B, the dashed line is without Roper resonance contributions and the dot-dashed line without Δ contributions. The data are from [26].

tributions. Model A can roughly describe the ϕ distributions, see Fig. 4.11. The $\cos\theta$ distributions can only be described at the lowest energy, at larger energies, our model results remain comparatively flat and have rather the opposite curvature compared to the experimental distributions. Model B results in even more unacceptable distributions. The contributions from the Roper resonance have no influence on the shape of the angular distributions.

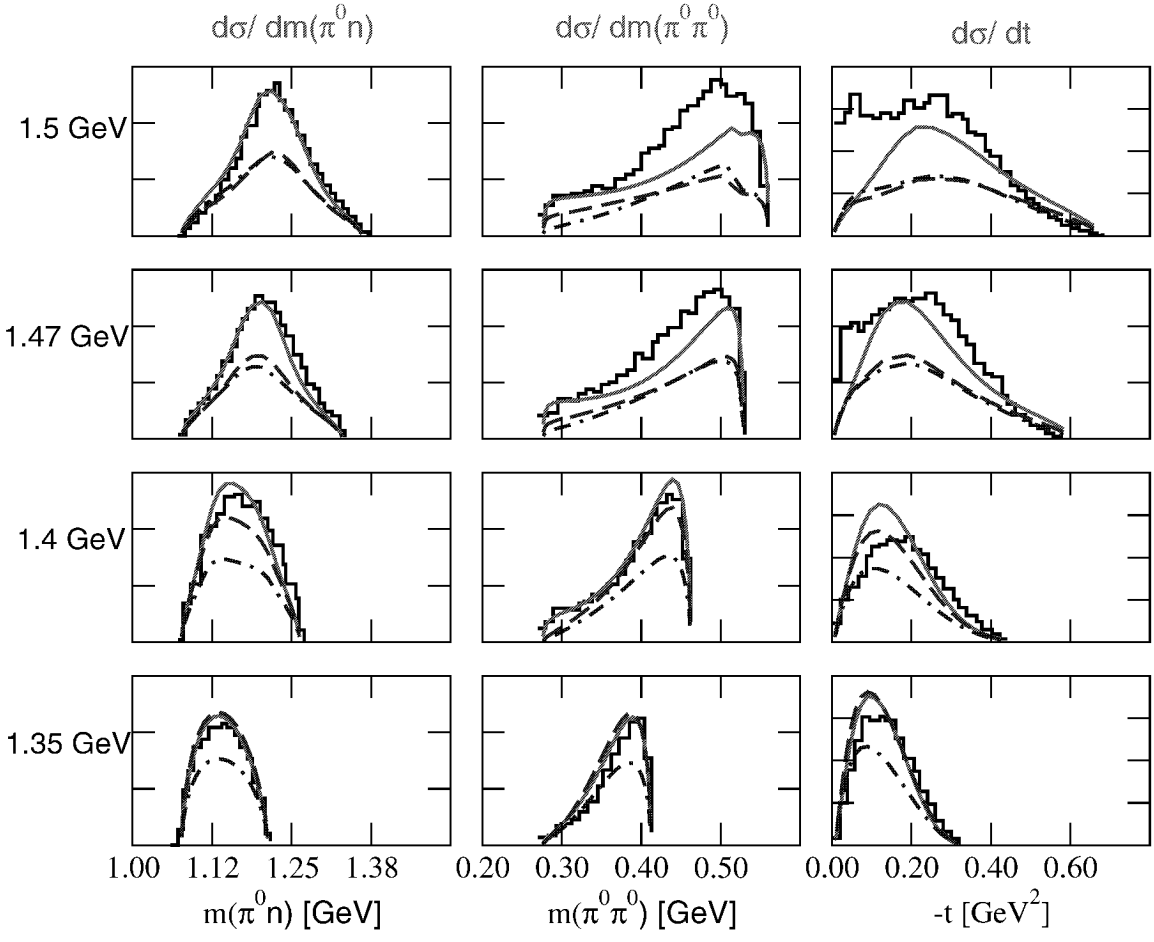

Figure 4.10: Differential distributions for the $\pi^- p \to \pi^0\pi^0 n$ reaction for energies from 1.35 GeV up to 1.5 GeV. The solid lines show the results from Model A, the dashed lines those of Model B. The dot-dashed lines show the results of Model B without contribution of the Roper resonance. The data are from [22] and have been normalised to the results of Model A.

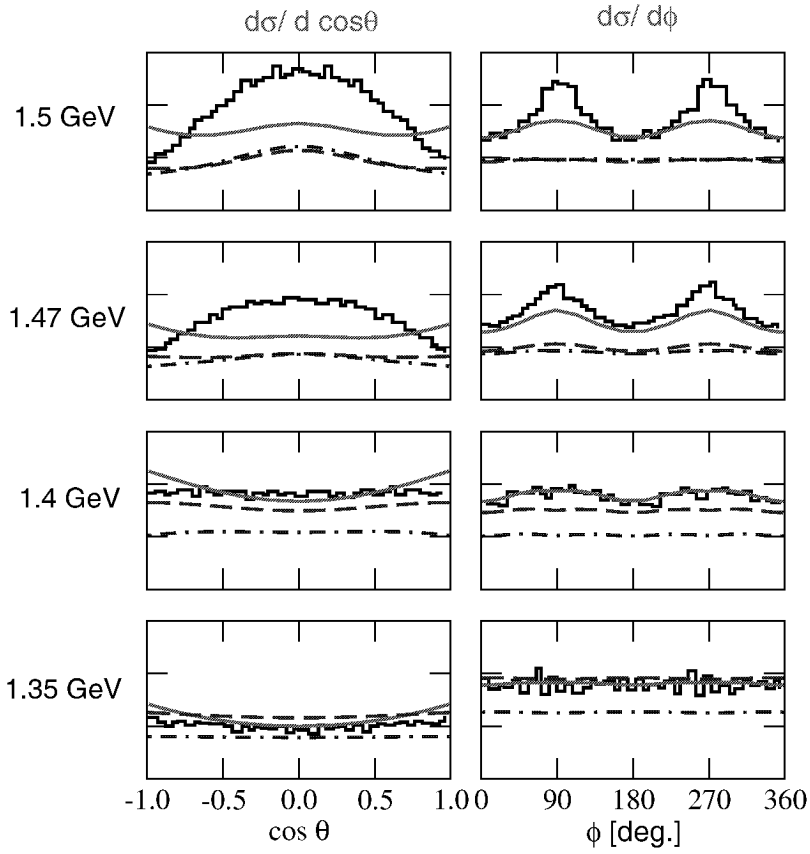

Figure 4.11: Angular distributions for the $\pi^- p \to \pi^0\pi^0 n$ reaction for energies from 1.35 GeV up to 1.5 GeV. The solid lines show the results from Model A, the dashed lines those of Model B. The dot-dashed lines show the results of Model B without contribution of the Roper resonance. The data are from [22] and have been normalised to the results of Model A.

Chapter 5

Summary and Outlook

We have studied pion-induced two-pion production on the nucleon in the framework of a meson-exchange model. In the limit of low energies, this model is constrained by Chiral Perturbation Theory. The parameters of the model were fitted to pion-pion and pion-nucleon scattering in a unitary K-matrix approximation.

The model gives reasonable results for the mass and t-distributions over a wide energy range from threshold up to 1.5 GeV. Our model obviously contains the essential mechanisms to describe the reaction. So our model forms a good starting point for the analysis of the $\pi N \to \pi\pi N$ reaction.

The success in the description of pion-induced pion production encourages a test of this model also in other pion production reactions. One possibility would be to replace the initial pion by a photon and investigate two-pion photoproduction. For this reaction, detailed differential distributions were measured to a high accuracy at the MAMI facility at Mainz [16–18]. The comparison of these data with the model could help to further constrain the model parameters.

The description of the angular distributions in the $\pi^- p \to \pi^+\pi^- n$ and $\pi^- p \to \pi^0\pi^0 n$ channels turns out to be difficult for our model. Another problematic distribution is the mass distribution $d\sigma/dM^2_{\pi\pi}$ for the $\pi^+\pi^+ n$ final state. These distributions are also not described by Chiral Perturbation Theory [57]. It needs to be checked whether a refit of some of our model parameters, that are not too well constrained from $\pi\pi$ and πN scattering, directly to the $\pi N \to \pi\pi N$ differential cross sections leads to more satisfactory results or whether the inclusion of other mechanisms is needed.

We observe a contribution of $N^\star$ resonances in the reaction channels $\pi^- p \to \pi^+\pi^- n$ and $\pi^- p \to \pi^0\pi^0 n$. In the energy range considered, the contribution comes mainly from the Roper resonance. The contribution of the Roper resonance does however

not manifest itself in a qualitative change in any of the studied observables for the $\pi N \to \pi\pi N$ reaction.

One aim was to investigate the impact of unitarisation effects on the $\pi N \to \pi\pi N$ observables. For this we use two model variants: Model A is a "pure" tree-level model. The bare vertices are used for the pole diagrams, and the self-energy is calculated from loops without any non-pole interaction. Model B takes into account some unitarisation effects by using dressed vertex functions for the pole diagrams and taking into account a contribution from non-pole interactions to the self-energies. These unitarisation effects have been determined from our K-matrix models for $\pi\pi$ and πN scattering.

We find qualitative differences between the models in the angular distributions for the reaction channel $\pi^+ p \to \pi^+\pi^+ n$. These data cannot be reproduced with Model A without destroying the description of the t-distributions in this reaction channel. The inclusion of higher order loop effects that are present in the dressed vertices of Model B allows for a reasonable description of both distributions. This hints at the need of initial and final state interaction effects to describe the data. One should however investigate whether other contributions can change the shape of the differential cross sections within Model A. A possible candidate may be a contribution from the $S_{31}(1620)$ resonance that we have not included in our model at present.

Chapter 6

π^+ absorption on ^{3}He in quasifree kinematics[1]

Over the last decades much work has been devoted to the study of pion production and absorption on nucleons. One aim was to gain information about the short-range part of the nuclear wave functions and to probe many-body correlations inside the nucleus [61]. But already the pion interaction with the two-nucleon system proved to be a challenge to the theoretical understanding, and so most of the work concentrated on the two-nucleon system.

Pion production and absorption processes in few-nucleon systems like ^{3}He offer the possibility to investigate to what extent the pionic inelasticities in a "many-body" environment can be described by the elementary two-body amplitude in a system that can be theoretically handled. Such investigations are a necessary step towards understanding the pion interaction with heavier nuclei and maybe using the pions as probes of nuclear wave functions.

For pion absorption on ^{3}He, the elementary two-body process should be most emphasised in pion absorption in the quasifree region. In this case, one of the protons does not absorb momentum from the pion and thus leaves the reaction volume with only its Fermi momentum. This proton is believed not to actively participate in the reaction, so that pion absorption can be treated as a two-body absorption process on a nucleon pair. The initial state wave function of the ^{3}He is in principle known from Faddeev calculations and the final state wave function is similar to the two-nucleon case.

Differential cross sections for quasifree pion absorption on ^{3}He have been measured at LAMPF [62], TRIUMF [63] and PSI [64]. Scarce data also exist for the polarisation

[1]The results of this investigation were published in [60].

of the fast protons in the final state [65,66].

Previous theoretical work on quasifree π^+ absorption on ^{3}He used the simple ansatz of range-corrected deuteron wave functions and completely neglected exchange terms with respect to the spectator proton [67,68]. That model could qualitatively reproduce the differential cross sections but had problems with the polarisation data: for a qualitative description of the data it was necessary to use different models for the two energies $T_\pi = 120$ MeV and $T_\pi = 250$ MeV for which the polarisation has been measured [66].

In the present approach, we employ a new parameterisation of the three-nucleon bound state wave function [69]. This parameterisation is similar in philosophy to the one presented in [70], but it differs in two important aspects. First of all, the new parameterisation fits directly the antisymmetrised wave function and not just the single Faddeev amplitude. This is particularly convenient for the evaluation of any two-body operator since contributions from all of the three NN pairs are automatically included although the actual calculation has to be performed for only one pair. In addition, the parameterisation of [69] goes beyond the separable ansatz in terms of the pair and spectator momenta and allows for correlations between them. This leads to an improvement in the fit of the wave functions obtained from Faddeev calculations especially when both momenta are large. The parameterisation was used successfully to describe low-momentum observables such as the $\pi\,^3$He scattering length [69].

The aim of this study is twofold. Firstly, we want to test the reliability of the new parameterisation of the three-nucleon wave function in a reaction involving high momentum transfer. And secondly we want to investigate whether a two-nucleon calculation can describe the data, in particular the polarisation data of [66], or whether the data demand for additional mechanisms such as a more active participation of the spectator even in quasifree kinematics.

6.1 Description of the Model

In this section we briefly introduce the parameterisation of the ^{3}He wavefunction of Ref. [69] and the pion absorption mechanisms in the two-nucleon system.

6.1.1 The Parameterisation of the ^{3}He Wave Function

The fully antisymmetric three-nucleon wave function can be written as the sum over three Faddeev components,

$$|\mathbf{\Psi}\rangle = \left|\Psi_{(12)3}\right\rangle + \left|\Psi_{(23)1}\right\rangle + \left|\Psi_{(31)2}\right\rangle . \tag{6.1}$$

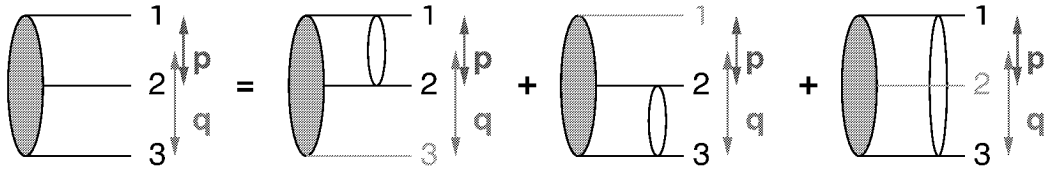

Figure 6.1: Diagrammatic representation of the three-nucleon antisymmetric wave function in terms of the three Faddeev components.

This equation is represented diagrammatically in Fig. 6.1. The Faddeev components $\left|\Psi_{(ij)k}\right\rangle$ correspond to different permutations of the nucleons. In coordinate space, they can be expressed as

$$\Psi^{\nu}(r_{ij},\rho_k) = \left\langle r_{ij}\rho_k\nu \,\middle|\, \Psi_{(ij)k} \right\rangle , \tag{6.2}$$

with the pair coordinate $\vec{r}_{ij}$ and spectator coordinate $\vec{\rho}_k$. The index ν denotes the angular momentum quantum numbers of the pair and spectator. The relevant partial waves ν in quasifree pion absorption on ^{3}He are the states where the spectator is in a relative s-wave. States with larger spectator angular momentum are assumed to be less important because the spectator remains essentially at rest in the quasifree reaction. So the index $\nu = 1,2,3$ denotes in this case the three possible states of the pair wave function[2], $^1S_0$, $^3S_1$ and $^3D_1$.

The action of a two-body operator (e.g. that of pion absorption on a nucleon pair) on the fully antisymmetric state does not depend on the choice of the active pair, so let us choose the pair (12) as the active pair. Then the action of the two-body operator on the first Faddeev component in equation (6.1) is simple but in the remaining two terms the pair and spectator coordinates of the Faddeev component would have to be reexpressed in terms of the pair coordinate of the active pair, e.g. $\vec{r}_{23} = -1/2\vec{r}_{12} - \vec{\rho}_3$ and likewise the angular momenta would have to be recoupled.

To avoid such complications, the full antisymmetric wave function was parametrised directly in terms of $\vec{r}_{12}$ and $\vec{\rho}_3$ in Ref. [69]. The full antisymmetric wave function was calculated from the CD Bonn [71] and Paris [72] potentials and then expressed as a product of functions separable in the pair and spectator momenta p and q,

$$v_1^{\nu}(p) = \sum_j \frac{a_j^{\nu}}{p^2 + (m_j^{\nu})^2} \, , w_1^{\nu}(q) = \sum_j \frac{b_j^{\nu}}{q^2 + (M_j^{\nu})^2} \, . \tag{6.3}$$

To improve the quality of the fit, a second product term was added. So finally the

[2]We use the notation $^{2S+1}L_J$ with S, L and J the total spin, the orbital angular momentum and the total angular momentum of the pair.

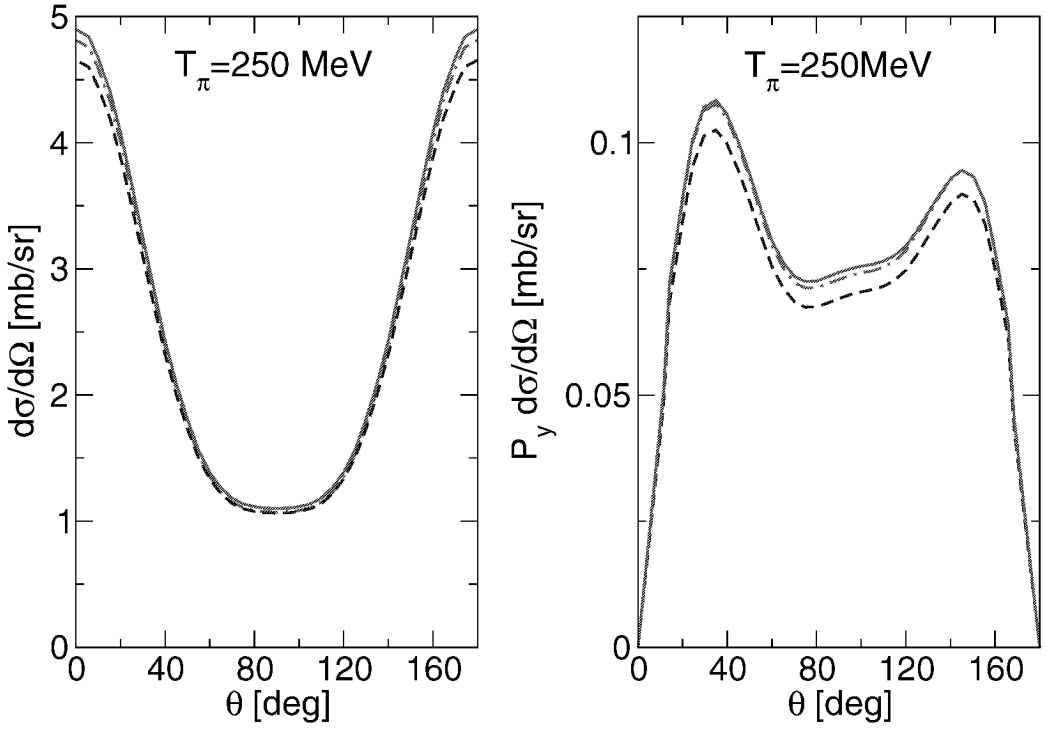

Figure 6.2: The differential absorption cross section and its "asymmetry" $P_y \cdot d\sigma/d\Omega$. The dashed line shows the result of a single-term separable fit to the CD-Bonn trinucleon wave function, the solid line shows the result for a two-term fit, and the dotted line the result for a three-term fit.

wave function was parametrised as

$$\mathbf{\Psi}^\nu(p,q) = v_1^\nu(p) w_1^\nu(q) + v_2^\nu(p) w_2^\nu(q)\,, \tag{6.4}$$

with the normalisation

$$\sum_\nu \int_0^\infty dp\, dq\, p^2\, q^2 |\Psi^\nu(p,q)|^2 = 1\,. \tag{6.5}$$

Here, the sum over ν comprises the five most important Faddeev components, where the NN pair is in a $^1S_0$, $^3S_1$ or $^3D_1$ state.

The inclusion of the second term allows for correlations between the pair and spectator momenta. At large momenta, relevant to meson production and absorption, the quality of the parameterisation was significantly improved through the second term [69].

It remains to investigate the effect of the non-separability on physical observables. For this, we look at the cross sections and polarisation in π^+ absorption on ^{3}He at

the largest energy at which polarisation data are available, which is $T_\pi = 250$ MeV. We study the convergence of a systematic expansion of the wave function for up to three product terms. The results of this study are displayed in Fig. 6.2. We notice a visible effect of the non-separability when going from a single term separable form to the two-term parameterisation. However, compared to the model uncertainties and given the quality of the data this effect is not really significant. The inclusion of a third term leads only to minor changes in the observables. The parameterisation is already well converged for the two-term expression (6.4).

6.1.2 The Pion Absorption Potential

The potential for pion absorption on a nucleon pair is shown diagrammatically in Fig. 6.3. First of all we take into account the direct absorption on one nucleon. This is described by a pseudo-vector πNN coupling in the Galilean invariant form

$$H_{\pi NN} = \frac{f_{\pi NN}}{m_\pi} \sum_{i=1,2} \vec{\sigma}_i \left(\vec{q}\,(\vec{\tau}_i \vec{\pi}) - \frac{\omega_q}{2M_N} \left[\vec{p}_i\,(\vec{\tau}_i \vec{\pi}) + (\vec{\tau}_i \vec{\pi})\,\vec{p}_i \right] \right) . \tag{6.6}$$

Here, $\vec{\sigma}_i$ and $\vec{\tau}_i$ are the spin and isospin operators acting on the ith nucleon, $\vec{p}_i$ is the momentum of nucleon i. $\vec{q}$ denotes the momentum of the pion and ω_q its energy. For the coupling constant we use the value $f^2_{\pi NN}/(4\pi) = 0.076$.

The direct absorption is generalised to include also resonant p-wave πN rescattering through the $\Delta(1232)$. The interaction Hamiltonian that describes direct absorption involving the excitation of the Δ isobar in the final state is obtained by replacing the coupling constant and the spin and isospin operators by the corresponding coupling constant $f_{\pi N\Delta}$ and the transition spin and isospin operators $\vec{S}_i$ and $\vec{T}_i$.

The direct absorption involving a $N\Delta$ pair in the final state is treated on the same footing as the direct absorption with a final NN pair. The wave function of the

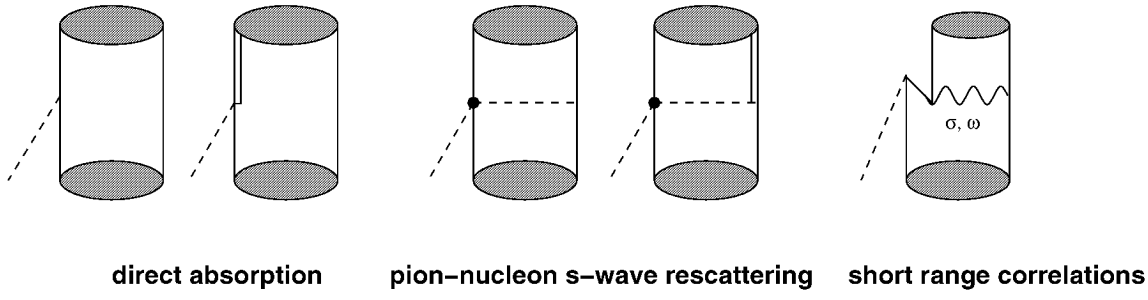

Figure 6.3: The potential for pion absorption on a nucleon pair.

final state pair contains an admixture of $N\Delta$ states as it is calculated for the coupled channels system $NN - N\Delta$. With the coupling constant $f^2_{\pi N\Delta}/(4\pi) = 0.35$ the peak in the cross section of π^+ absorption on the deuteron can be reproduced.

The interaction of the high-energy final state baryon pair is based on the Reid soft core potential [73]. At such high energies, the sensitivity to the details of the potential are expected to be small. Furthermore, the potential has to be modified to avoid a double counting of the $N\Delta$ intermediate states, that in our approach are treated explicitely through the coupled channels method.

Pion production (as well as absorption) in the two-nucleon system is at threshold dominated by the contribution from pion-nucleon s-wave rescattering. For the description of this contribution we use the phenomenological interaction

$$H_s = 4\pi\frac{\lambda_1}{m_\pi}\vec{\pi}\vec{\pi} + 4\pi\frac{\lambda_2}{m_\pi^2}\vec{\tau}\,\vec{\pi}\times\partial_0\vec{\pi} \tag{6.7}$$

at the $\pi\pi NN$ vertex. The parameters λ_1 and λ_2 are energy-dependent and are fitted to pion-nucleon scattering [74]. We include a monopole form factor for the pion exchange which is fitted to describe the analysing power A_y in pion production $pp \to d\pi^+$ at 515 MeV, see Fig. 6.4.

The abovementioned contributions are sufficient to describe positive pion absorption and production in the two-nucleon system. But for neutral pion production $pp \to pp\pi^0$ it is known that additional mechanisms are needed to describe the cross section data [75]. One possibility is the inclusion of short-range contributions of the NN interaction, such as the exchange of the heavy mesons σ and ω shown in Fig. 6.3 [76–78]. These heavy meson exchanges constitute also an important contribution in π^- absorption on $^1S_0$ pp pairs in ^{3}He [74]. The short-range effects are also included here for two reasons. Firstly, the pair wave function in ^{3}He is more condensed than in the deuteron. This could enhance the effect of short-range correlations. Secondly, π^+ absorption can not only happen on a quasideuteron pair inside ^{3}He, but also on a neutron-proton pair in the $^1S_0$ state.

First, let us show how this absorption potential describes the elementary two-nucleon reaction. In Fig. 6.4 we show the transverse analysing power A_y for $\vec{p}p \to d\pi^+$. A_y is given by

$$A_y(\theta) = \frac{d\sigma_\uparrow/d\Omega(\theta) - d\sigma_\downarrow/d\Omega(\theta)}{d\sigma_\uparrow/d\Omega(\theta) + d\sigma_\downarrow/d\Omega(\theta)}\,, \tag{6.8}$$

where $d\sigma_\uparrow/d\Omega(\theta)$ and $d\sigma_\downarrow/d\Omega(\theta)$ are the cross section for the polarisation of the proton perpendicular to the reaction plane. This quantity corresponds to the proton polarisation P_y of one of the fast final protons in the absorption process $\pi^+\,{}^3\mathrm{He} \to \vec{p}\,p\,p_{\mathrm{spec}}$.

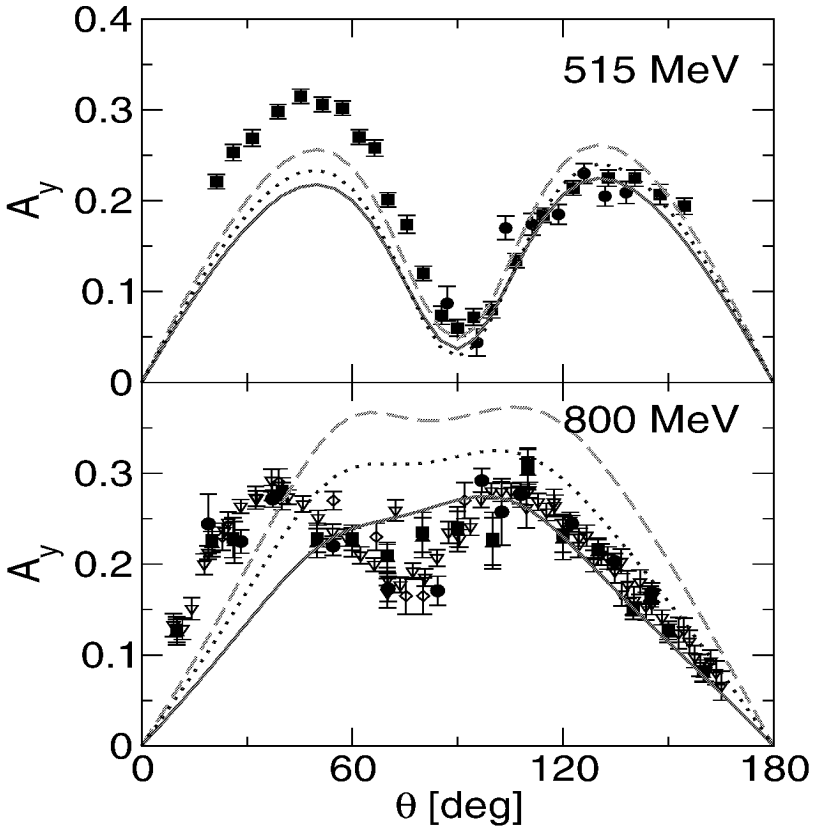

Figure 6.4: The analysing power in $pp \to d\pi^+$ at energies corresponding closely to the π^+ ^{3}He energies of [66]. We show the results for the different deuteron wave functions from the CD-Bonn (solid lines), Paris (dotted lines) and Reid soft core (dashed lines) potentials.

The analysing power is shown at energies that correspond closely to the energies of the polarisation measurements for π^+ absorption on ^{3}He.
In the calculations for the different deuteron wave functions, the form factor for the s-wave rescattering contribution has been adjusted to fit the dip in the analysing powers at 515 MeV. The fitting leads to three different values of the cutoff mass for the three different wave functions: $\Lambda = 3m_\pi$ for the CD-Bonn wave function, $\Lambda = 4m_\pi$ for the Paris wave function and $\Lambda = 5m_\pi$ for the Reid wave function. In spite of this fitting at 515 MeV, there are differences between the analysing powers for different wave functions at the higher energy of 800 MeV. The data seem to favour the newer Bonn and Paris wave functions over the Reid wave function. Furthermore we notice that A_y is correlated to the D-state probability of the deuteron wave function: the magnitude of A_y increases with the D-state probability.

For the investigation of π^+ absorption on ^{3}He, the two-nucleon absorption operator

has to be evaluated between the initial ^{3}He wave function and the final state wave function,

$$\langle\, p_{\rm spec}\Psi_{NN,f}\,|\,\mathcal{M}\,\delta_{\rm spec}\,|\Psi_{^3{\rm He}}\rangle\,. \tag{6.9}$$

$\delta_{\rm spec}$ indicates that the quantum numbers of the final state spectator proton $p_{\rm spec}$ are the same as for the third nucleon of the ^{3}He wave function.
For the final state proton we use a plane wave, the wave function of the final NN pair is the same as in the two-nucleon reaction: a NN wave function with explicit $N\Delta$ admixture based on the Reid soft core potential [79]. For the final NN pair, partial waves up to $J = 5$ are taken into account.
With the abovementioned parameterisation of the ^{3}He wave function

$$\Psi^\nu(r,\rho) = \sum_{\lambda=1,2} v^\nu_\lambda(r) w^\nu_\lambda(\rho) \tag{6.10}$$

we obtain, e.g. for the differential cross section the following expression

$$\frac{d\sigma}{d\Omega} = {\rm Tr} \sum_{\lambda\lambda'\,\nu\nu'} (\mathcal{M}^{\nu'}_{\lambda'})^*\,\mathcal{M}^\nu_\lambda\,\mathcal{W}^{\nu'\nu}_{\lambda'\lambda}\delta_{\nu\nu'}\,. \tag{6.11}$$

The trace is over spin orientations. The effect of the spectator is contained in the overlap integral

$$\mathcal{W}^{\nu'\nu}_{\lambda'\lambda} = \int d\rho\, w^{\nu'}_{\lambda'}(\rho) w^\nu_\lambda(\rho)\,. \tag{6.12}$$

Notice, that in this treatment the minor effect in kinematics from the variation of the spectator kinetic energy is neglected. The effect of the spectator on the kinematics is to absorb an average kinetic energy of 5 MeV (due to its Fermi motion). This is accounted for by the "effective" binding energy of the pair in ^{3}He. This binding energy is taken to be 10 MeV more than that of the free deuteron: 5 MeV for the kinetic energy carried away by the spectator and 5 MeV for the actual difference in binding energy.

6.2 Results

In Figs. 6.5 and 6.6 we show the differential cross sections and proton polarisations for positive pion absorption on ^{3}He. Our aim is to study the dependence of the observables on the wave function employed for the bound state.

Let us first discuss the results obtained with the new parameterisation of the ^{3}He wave function. We show the results based on the Bonn and Paris potentials. Both

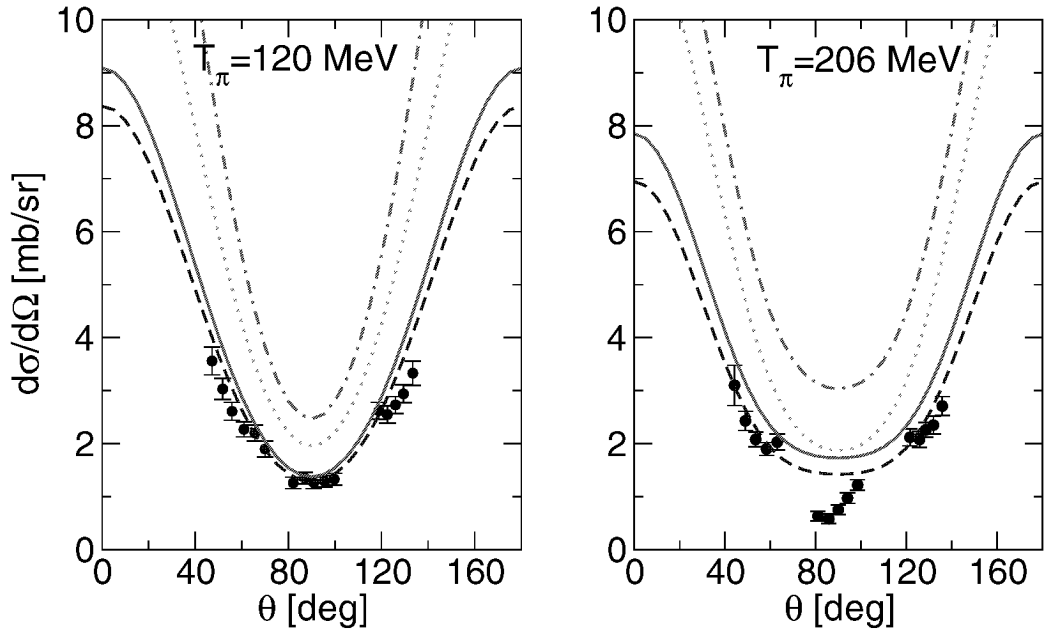

Figure 6.5: The differential cross sections for π^+ absorption on ^{3}He. We show the dependence on the ^{3}He wave function: CD Bonn (solid), Paris (dashed), single Faddeev amplitude normalised to one for the CD Bonn wave function (dot-dashed) and result using a wave function based on the correlation function as in [67, 68](dotted). The data are from [64].

can describe the shape of the differential cross sections as well as their magnitude at $T_\pi = 120$ MeV. At the larger energy of $T_\pi = 206$ MeV, both potentials lead to a similar shape, but the difference in the magnitude of the cross sections amounts to $\sim 10\%$. Note, that the amplitudes for both potentials have been adjusted individually to fit the analysing power in $pp \to d\pi^+$ at 515 MeV. Without this adjustment, the difference would be of the order of $20-30\%$. This is compatible with the spread obtained in [80] for the use of different deuteron wave functions in the reaction $pp \to d\pi$.
The shape of the polarisation can be roughly reproduced with the new bound state wave functions for both energies.

In order to compare with the earlier results of [66], we also show the results obtained with a wave function based on the correlation function of the proton pair in ^{3}He given in [81]. These results are very similar to the results of [66]. Note, however, that our calculation includes in addition the heavy-meson exchange as well as the absorption on a $^1S_0$ pair, so that any difference between the dotted line and the other lines is due to the effect of the different wave function.

The use of the new bound state wave functions clearly leads to an improvement in

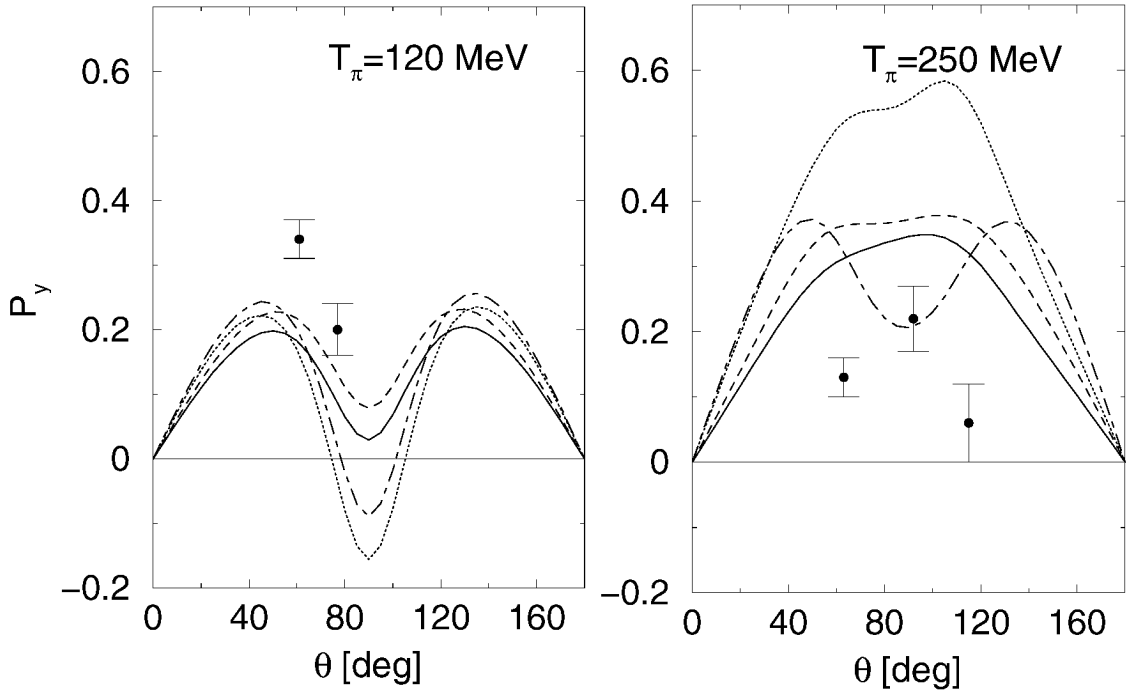

Figure 6.6: The proton polarisation P_y. The lines are the same as in Fig. 6.5. The data are from [66].

the description of the polarisation compared to the older calculation. At the lower energy of $T_\pi = 120$ MeV, the two data points do not allow to distinguish between the different wave functions, but at the higher energy, the data favour the results obtained with the new wave functions. The magnitude of the polarisation is much smaller, and the slight dip of the earlier results at 90° becomes flatter for the new wave functions, although it is still present.
The success of the new bound state wave functions may be partly attributed to the lower D-state probability of the quasideuteron. It was shown in the earlier calculations [66] that the polarisation data at 250 MeV could be reproduced by neglecting the D-state of the deuteron. This, however, destroyed the agreement at the lower energy.

The use of the parameterisation of a single Faddeev amplitude from [69] leads to a striking disagreement with the polarisation at the larger energy. The results for the total cross sections are larger than the cross sections obtained with the parameterisation of the fully antisymmetric wave function and qualitatively more similar to the results obtained with the Gibson correlation wave function. Here reflects the shorter range of the single Faddeev amplitude [69] and the Gibson correlation wave function

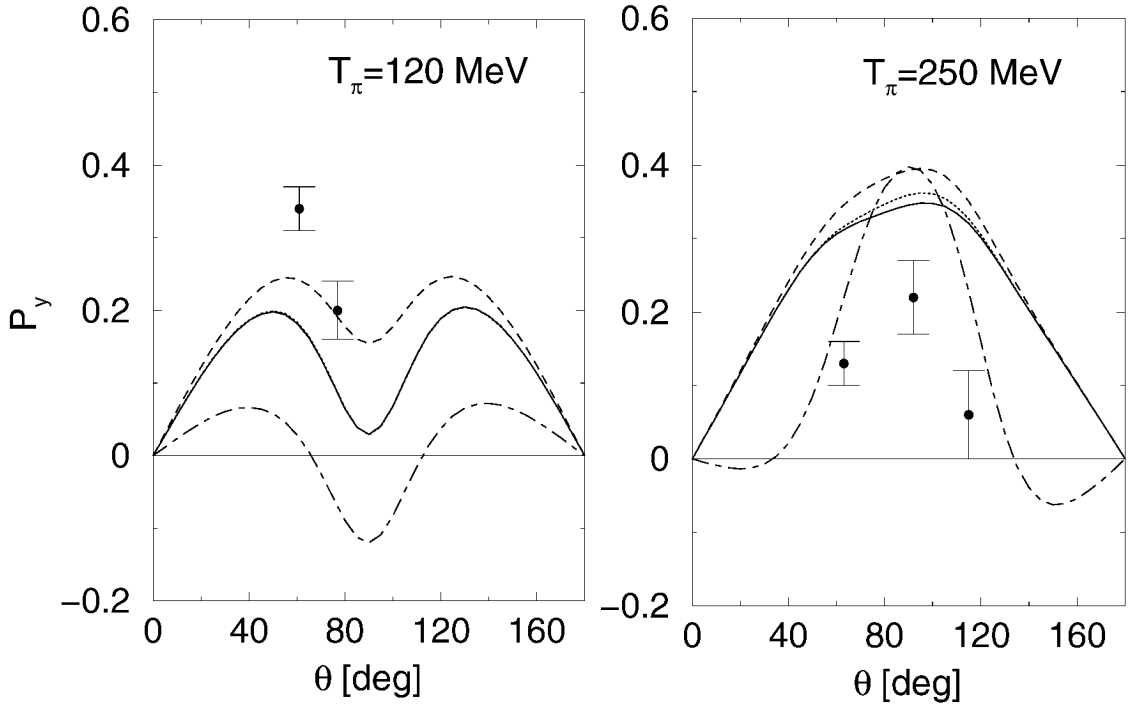

Figure 6.7: The proton polarisation P_y. The solid line shows our result for the CD-Bonn potential as in Fig. 6.6. For the dotted line, the absorption on the $^1S_0$ pair is neglected, for the dashed line we neglect the contributions from heavy meson exchange. The dash-dotted line was calculated without the D state of the quasideuteron. The data are from [66].

compared to the fully antisymmetric wave function. The longer ranged antisymmetric wave functions put less weight on the short distances that are probed with the high momentum transfer pion absorption, and so the cross sections obtained with these wave functions are smaller.

In Fig. 6.7 we study the contributions to our model in more detail. We find that the pion absorption on a $^1S_0$ pair only plays a negligible role. So the absorption process takes mainly place on the two components of the quasideuteron pair, $^3S_1$ and $^3D_1$. We find that the effect of heavy meson exchange is larger than in the two-body reaction $pp \to d\pi^+$, but its effect does not change the results qualitatively.
Switching off the D-state component of the quasideuteron has a drastic effect on the polarisation observables. As was also seen in [66], the polarisation data at 250 MeV can be well reproduced without the D state, but then the data at the lower energy cannot be described any more.

6.3 Conclusion

We have studied positive pion absorption on ^{3}He using a parameterisation of the three-nucleon wave function obtained from realistic NN potentials. We find that the non-separability of the new wave functions in terms of the pair and spectator coordinates has a minor effect on the observables, but the use of the fully antisymmetrised wave functions was necessary to describe the differential cross sections quantitatively and to obtain qualitative agreement with the polarisation data.

The success in the description of the polarisation data at $T_\pi = 250$ MeV can partly be attributed to the lower D-state probability of the quasideuteron in the new wave functions. As was already observed in [66], switching off the D-state component leads to a good description of the polarisation at $T_\pi = 250$ MeV but spoils the agreement at the lower energy. The new wave functions form a compromise between the previously used wave functions and the wavefunctions without the D-state.

For further improvements, a more active participation of the spectator even in quasifree kinematics may be needed. This can be seen from a comparison of the two-body and quasi two-body results. From a look at the analysing power for $pp \to d\pi^+$ in Fig. 6.4 and the polarisation for π^+ absorption on ^{3}He in Fig. 6.6 we find that the shapes of the calculated distributions are in one-to-one correspondence for the corresponding energies. The success in describing the polarisation observables in π^+ absorption on ^{3}He may be attributed to the failure of the model in describing the dip in the $pp \to d\pi^+$ data. If we take the dip in the $pp \to d\pi^+$ data seriously and if the assumption of quasifree mechanisms is correct, then it is hard to understand why there should be a peak in the ^{3}He data. The indication of a peak in the ^{3}He data thus lends support to the need of other mechanisms, probably a more active participation of the spectator.

However, the structural difference is at present only based on three data points. It would be desirable to confirm the peak structure at 250 MeV and also to measure the polarisation at intermediate pion energies to investigate the development of the structural changes.

Appendix A

Definitions and Conventions

1. Minkowski Metric

$$g_{\mu\nu} = g^{\mu\nu} = \begin{pmatrix} 1 & 0 & 0 & 0 \\ 0 & -1 & 0 & 0 \\ 0 & 0 & -1 & 0 \\ 0 & 0 & 0 & -1 \end{pmatrix}$$

2. Dirac Matrices, Pauli Matrices

$$\gamma^0 = \begin{pmatrix} I & 0 \\ 0 & -I \end{pmatrix} \qquad \vec{\gamma} = \begin{pmatrix} 0 & \vec{\sigma} \\ -\vec{\sigma} & 0 \end{pmatrix} \qquad \gamma_5 = \begin{pmatrix} 0 & I \\ I & 0 \end{pmatrix} \tag{A.1}$$

$$\sigma^1 = \begin{pmatrix} 0 & 1 \\ 1 & 0 \end{pmatrix} \qquad \sigma^2 = \begin{pmatrix} 0 & -i \\ i & 0 \end{pmatrix} \qquad \sigma^3 = \begin{pmatrix} 1 & 0 \\ 0 & -1 \end{pmatrix} \tag{A.2}$$

$$\sigma_{\mu\nu} = \frac{i}{2}[\gamma_\mu, \gamma_\nu] \tag{A.3}$$

3. Dirac Spinors

To describe a spin $\frac{1}{2}$ particle of mass m and momentum k we use the helicity spinors

$$u(\vec{k}, \lambda) = \sqrt{E_k + m} \begin{pmatrix} 1 \\ \frac{\vec{\sigma}\vec{k}}{E_k + m} \end{pmatrix} |\lambda\rangle \,. \tag{A.4}$$

These are normalised such that $\bar{u}(\vec{k},\lambda)u(\vec{k},\lambda) = 2m$.

$|\lambda\rangle$ is an eigenvector of the helicity operator $\frac{\vec{\sigma}\vec{k}}{2k}$ and can have the eigenvalues $\pm\frac{1}{2}$. For a particle with momentum $\vec{k}$ in the direction (θ,ϕ) the eigenvectors can be written as

$$|\lambda = +\frac{1}{2}\rangle = \begin{pmatrix} \cos\frac{\theta}{2}\exp(-i\frac{\phi}{2}) \\ \sin\frac{\theta}{2}\exp(i\frac{\phi}{2}) \end{pmatrix} , \tag{A.5}$$

$$|\lambda = -\frac{1}{2}\rangle = \begin{pmatrix} -\sin\frac{\theta}{2}\exp(-i\frac{\phi}{2}) \\ \cos\frac{\theta}{2}\exp(i\frac{\phi}{2}) \end{pmatrix} . \tag{A.6}$$

4. Rarita-Schwinger spinor and Rarita-Schwinger propagator

The spinor of a particle of spin $\frac{3}{2}$ can be described by the coupling of a spin $\frac{1}{2}$ spinor and a spin 1 polarisation vector:

$$u^\mu(\vec{k},\lambda) = \sum_{\lambda_1,\lambda_2} \langle 1\,\lambda_1\,\frac{1}{2}\,\lambda_2|\frac{3}{2}\,\lambda\rangle\,\epsilon^\mu(\vec{k},\lambda_1)u(\vec{k},\lambda_2) . \tag{A.7}$$

The Rarita-Schwinger propagator is given by

$$\begin{aligned} D^{\mu\nu}(q) &= \frac{\not{q}+m}{q^2-m^2}P^{\mu\nu}_{\rm rs} \\ &= \frac{\not{q}+m}{q^2-m^2}\left[-g^{\mu\nu}+\frac{1}{3}\gamma^\mu\gamma^\nu+\frac{2}{3m^2}q^\mu q^\nu-\frac{1}{3m}(q^\mu\gamma^\nu-q^\nu\gamma^\mu)\right] \end{aligned} \tag{A.8}$$

The propagator can be reexpressed in terms of the spin-3/2 and spin-1/2 projectors

$$\left(P^{3/2}\right)^{\mu\nu} = -g^{\mu\nu}+\frac{1}{3}\gamma^\mu\gamma^\nu+\frac{1}{3q^2}(\not{q}\gamma^\mu q^\nu+q^\mu\gamma^\nu\not{q}) \tag{A.9}$$

$$\left(P^{1/2}_{22}\right)^{\mu\nu} = -\frac{q^\mu q^\nu}{q^2} \tag{A.10}$$

$$\left(P^{1/2}_{12}+P^{1/2}_{21}\right)^{\mu\nu} = -\frac{1}{\sqrt{3}q^2}\not{q}\,(q^\mu\gamma^\nu-\gamma^\mu q^\nu) , \tag{A.11}$$

which leads to

$$D^{\mu\nu}(q) = \frac{\not{q}+m}{q^2-m^2}\left(P^{3/2}\right)^{\mu\nu}-\frac{2(\not{q}+m)}{3m^2}\left(P^{1/2}_{22}\right)^{\mu\nu}+\frac{1}{\sqrt{3}m}\left(P^{1/2}_{12}+P^{1/2}_{21}\right)^{\mu\nu} \tag{A.12}$$

The first term on the right hand side of this equation gives rise to the Δ pole in the P_{33} partial wave of πN scattering while the remaining two terms amount to

a $\pi\pi NN$ contact interaction in the $J = 1/2$ partial waves. Only the first term acquires a finite self-energy through the dressing,

$$D^{\mu\nu}(q) = \frac{\not{q} + m}{q^2 - m^2 - \Sigma} \left(P^{3/2}\right)^{\mu\nu} + D^{\mu\nu}_{1/2}\,, \tag{A.13}$$

with $D^{\mu\nu}_{1/2}$ given by

$$D^{\mu\nu}_{1/2} = -\frac{2(\not{q} + m)}{3m^2} \left(P^{1/2}_{22}\right)^{\mu\nu} + \frac{1}{\sqrt{3}m} \left(P^{1/2}_{12} + P^{1/2}_{21}\right)^{\mu\nu}\,. \tag{A.14}$$

5. Polarisation vector of a spin 1 particle

A spin 1 particle of mass m at rest has the polarisation vector

$$\epsilon^\mu(\vec{0}, \lambda = \pm 1) = \frac{1}{\sqrt{2}} \begin{pmatrix} 0 \\ \mp 1 \\ -i \\ 0 \end{pmatrix}\,, \qquad \epsilon^\mu(\vec{0}, \lambda = 0) = \begin{pmatrix} 0 \\ 0 \\ 0 \\ 1 \end{pmatrix}\,. \tag{A.15}$$

The sum over helicities gives (for arbitrary momentum)

$$\sum_{\lambda=1}^{3} \epsilon^*_\mu(\vec{k}, \lambda)\epsilon_\nu(\vec{k}, \lambda) = -g_{\mu\nu} + \frac{k_\mu k_\nu}{m^2}\,. \tag{A.16}$$

The propagator of the ρ meson is then given by

$$D_{\mu\nu}(k) = \frac{-g_{\mu\nu} + \frac{k_\mu k_\nu}{m_\rho^2}}{k^2 - m_\rho^2}\,. \tag{A.17}$$

As we only deal with on-shell pions, the second term in the numerator vanishes when the ρ is coupled to a pair of pions. This is because the ρ momentum is given by the sum of the pion momenta and the vertex contains the difference of the pion momenta (or vice versa). For $k = k_1 + k_2$, for example, the contraction of the second term in the numerator with the pion vertex leads to $(k_1 + k_2) \cdot (k_1 - k_2) = k_1^2 - k_2^2$ which vanishes for two on-shell pions. So we will work with

$$D_{\mu\nu}(k) = \frac{-g_{\mu\nu}}{k^2 - m_\rho^2}\,. \tag{A.18}$$

$\rho_{\mu\nu}$ is defined via

$$\rho_{\mu\nu} = \partial_\mu \vec{\rho}_\nu - \partial_\nu \vec{\rho}_\mu\,. \tag{A.19}$$

Appendix B

Partial Wave Decomposition and Transformation from Helicity Basis to JLS Basis

An adequate way of solving the $2 \to 2$ scattering equation is to make use of a partial wave decomposition. Because of the rotational invariance of the strong interaction, we can decompose the potential V and the T-matrix into submatrices of definite angular momentum J. As we shall see in the following, this reduces a coupled three-dimensional scattering equation of the form

$$\begin{aligned} \langle \vec{k}\,'\lambda_3\lambda_4 \,|T|\, \vec{k}\,\lambda_1\lambda_2 \rangle &= \langle \vec{k}\,'\lambda_3\lambda_4 \,|V|\, \vec{k}\,\lambda_1\lambda_2 \rangle \\ &+ \sum_{\kappa_1\kappa_2} \int d^3q \, \langle \vec{k}\,'\lambda_3\lambda_4 \,|V|\, \vec{q}\,\kappa_1\kappa_2 \rangle G(q) \langle \vec{q}\,\kappa_1\kappa_2 \,|T|\, \vec{k}\,\lambda_1\lambda_2 \rangle \end{aligned} \quad \text{(B.1)}$$

to a set of coupled one-dimensional integral equations.
Furthermore, in the K-matrix approximation, the momentum of the intermediate state is set equal to the on-shell momentum. As a consequence, also the integration over the modulus of the momentum q vanishes, and we are left with an algebraic equation.

Equation (B.1) is given in the helicity basis. Dealing with the scattering problem in the JLS basis has the advantage that certain transitions $\langle L'S' \,|\, V^J \,|LS\rangle$ vanish because of parity and angular momentum conservation. Furthermore, experimental data are often subjected to a partial wave analysis and the results are given in JLS basis. So the second part of this appendix deals with the transformation from helicity basis to JLS basis.

B.1 Partial Wave Decomposition

We start by expanding the two particle plane wave scattering states in eigenstates of the angular momentum operator [82]

$$|k\,\theta\,\phi\,\lambda_1\lambda_2\rangle = \sum_{JM}\left(\frac{2J+1}{4\pi}\right)^{\frac{1}{2}} D^J_{M\lambda}(\phi,\theta,0)\,|k\,JM\,\lambda_1\lambda_2\rangle\,. \tag{B.2}$$

λ_1 and λ_2 are the helicities of the two particles and $\lambda := \lambda_1 - \lambda_2$. $D^J_{MM'}(\alpha,\beta,\gamma)$ is the matrix element of the operator of a finite rotation

$$\mathcal{D}^J(\alpha,\beta,\gamma) = e^{-i\alpha J_z}e^{-i\beta J_y}e^{-i\gamma J_z}\,.$$

$\mathcal{D}^J(\alpha,\beta,\gamma)$ describes a change of reference frame; α,β and γ are the three Euler angles. The matrix elements can be written in the form

$$D^J_{MM'}(\alpha,\beta,\gamma) = \langle\, JM' \,|\, \mathcal{D}^J(\alpha,\beta,\gamma)\,|JM\rangle = e^{-i\alpha M'}d^J_{MM'}(\beta)e^{-i\gamma M} \tag{B.3}$$

where the $d^J_{MM'}(\beta)$ are the reduced rotation matrices [83].[1] We only need the rotation to map two vectors — the relative momenta of the final and initial state — onto each other. Two angles are sufficient to describe this transformation, and we can set $\gamma = 0$.

If we consider the scattering of two spin-0 particles, the matrix elements of the rotation reduce to the familiar Legendre Functions

$$D^J_{00}(\alpha,\beta,\gamma) = P_J(\cos\beta)\,. \tag{B.4}$$

With the expansion (B.2) the matrix elements of the potential V and the transition matrix T can be decomposed into submatrices of definite angular momentum.

$$\langle\, k'\,\theta\,\phi\,\lambda_3\lambda_4\,|\,V\,|k\,0\,0\,\lambda_1\lambda_2\rangle = \sum_J\left(\frac{2J+1}{4\pi}\right) D^{*J}_{\lambda\lambda'}(\Omega_{k'k},0)\,\langle\, k'\,\lambda_3\lambda_4\,|\,V^J\,|k\,\lambda_1\lambda_2\rangle \tag{B.5}$$

In this equation we assume that the relative momentum of the initial state is oriented parallel to the z-axis of the reference frame. $\Omega_{k'k}$ is the solid angle of $\vec{k}'$ with respect to $\vec{k}$. Exploiting the orthogonality of the rotation matrices

$$\int d\Omega D^{*J}_{\lambda\lambda'}(\Omega,0)D^{J'}_{\kappa\kappa'}(\Omega,0) = \frac{4\pi}{2J+1}\delta_{JJ'}\delta_{\lambda\kappa}\delta_{\lambda'\kappa'} \tag{B.6}$$

we arrive at the following expression for V^J,

$$\langle\, k'\,\lambda_3\lambda_4\,|\,V^J\,|k\,\lambda_1\lambda_2\rangle = \int d\Omega_{k'k}D^J_{\lambda\lambda'}(\Omega_{k'k},0)\langle\,\vec{k}'\lambda_3\lambda_4\,|V|\,\vec{k}\,\lambda_1\lambda_2\,\rangle\,. \tag{B.7}$$

[1] We use the conventions of Jacob and Wick. Note that the $d^J_{MM'}(\beta)$ in Edmonds' convention would correspond to $d^J_{MM'}(-\beta) = d^J_{M'M}(\beta)$ in our convention.

Insertion of (B.5) into the scattering equation (B.1) leads to

$$\sum_J \left(\frac{2J+1}{4\pi}\right) D^{*J}_{\lambda\lambda'}(\Omega_{k'k},0)\ \left(\langle\, k'\,\lambda_3\lambda_4\,|\,T^J\,|k\,\lambda_1\lambda_2\rangle - \langle\, k'\,\lambda_3\lambda_4\,|\,V^J\,|k\,\lambda_1\lambda_2\rangle\right)$$
$$= \sum_{\kappa_1\kappa_2 J' J''} \frac{(2J'+1)(2J''+1)}{(4\pi)^2} \int dq\, q^2 \int d\Omega_{qk} D^{*J'}_{\kappa\lambda'}(\Omega_{k'q},0) D^{*J''}_{\lambda\kappa}(\Omega_{qk},0)$$
$$\cdot\langle\, k'\,\lambda_3\lambda_4\,|\,V^{J'}\,|q\,\kappa_1\kappa_2\rangle\, G(q)\,\langle\, q\,\kappa_1\kappa_2\,|\,T^{J''}\,|k\,\lambda_1\lambda_2\rangle\,. \quad \text{(B.8)}$$

The angular integration amounts to

$$\int d\Omega_{qk} D^{*J'}_{\kappa\lambda'}(\Omega_{k'q},0) D^{*J''}_{\lambda\kappa}(\Omega_{qk},0) = \frac{4\pi}{2J'+1}\,\delta_{J'J''} D^{*J'}_{\lambda\lambda'}(\Omega_{k'k},0) \quad \text{(B.9)}$$

with the help of (B.6) and the following relations [83]

$$D^{*J'}_{\kappa\lambda'}(\Omega_{k'q},0) = D^{J'}_{\lambda'\kappa}(\Omega_{qk'},0)\,, \quad \text{(B.10)}$$
$$D^{J'}_{\lambda'\kappa}(\Omega_{qk'},0) = D^{J'}_{\lambda'\kappa}(\Omega_{qk}\Omega_{kk'},0) = \sum_\mu D^{J'}_{\lambda'\mu}(\Omega_{kk'},0)\, D^{J'}_{\mu\kappa}(\Omega_{qk},0)\,. \quad \text{(B.11)}$$

Comparing the coefficients of $D^{*J}_{\lambda\lambda'}(\Omega_{k'k},0)$ in the resulting equation, one arrives at a one-dimensional scattering equation for each value of the angular momentum J:

$$\langle\, k'\,\lambda_3\lambda_4\,|\,T^J\,|k\,\lambda_1\lambda_2\rangle = \langle\, k'\,\lambda_3\lambda_4\,|\,V^J\,|k\,\lambda_1\lambda_2\rangle$$
$$+\sum_{\kappa_1\kappa_2}\int dq\, q^2\,\langle\, k'\,\lambda_3\lambda_4\,|\,V^J\,|q\,\kappa_1\kappa_2\rangle\, G(q)\,\langle\, q\,\kappa_1\kappa_2\,|\,T^J\,|k\,\lambda_1\lambda_2\rangle\,. \quad \text{(B.12)}$$

B.2 Transformation between Helicity Basis and JLS Basis

In the helicity basis, a two particle state is characterised by its total angular momentum J and its projection M, the modulus of the relative momentum k, and the two particles' helicities λ_1 and λ_2. In the JLS basis the helicities of the particles are replaced by the orbital angular momentum L and the total spin S. From this it should be clear that it makes no sense to distinguish between helicity and JLS basis as long as only spin-0 particles are involved.
Helicity basis and JLS basis are related to each other via a linear transformation[2]:

$$|\,JM\,\lambda_1\lambda_2\rangle = \sum_{LS}\langle\, JM\,LS\,|\,JM\lambda_1\lambda_2\,\rangle\,|\,JM\,LS\rangle\,. \quad \text{(B.13)}$$

[2]In the following the dependence of the state vectors on the modulus of the momentum k will be suppressed.

The matrix elements of the transformation matrix can be obtained from

$$|JM\,LS\rangle = \sum_{m_1 m_2} \langle\, JM \,|\, LM_L\, SM_S \,\rangle\langle\, SM_S \,|\, S_1 m_1\, S_2 m_2 \,\rangle Y_{LM_L}\, \chi_{S_1 m_1}\, \zeta_{S_2 m_2} \quad \text{(B.14)}$$

$$|JM\,\lambda_1\lambda_2\rangle = \left(\frac{2J+1}{4\pi}\right)^{\frac{1}{2}} \int d\Omega D^{*J}_{M\lambda}(\Omega,0)\mathcal{D}^J(\Omega,0)\,\chi_{S_1\lambda_1}\,\zeta_{S_2-\lambda_2} \quad \text{(B.15)}$$

where $\chi_{S_1 m_1}$ and $\zeta_{S_2 m_2}$ are the spinors of the two particles. $|JM\,LS\rangle$ can then be expanded in terms of $|JM\,\lambda_1\lambda_2\rangle$ [82]. We obtain the result

$$\langle\, JM\,LS \,|\, JM\lambda_1\lambda_2 \,\rangle = \left(\frac{2L+1}{2J+1}\right)^{\frac{1}{2}} \langle\, JM \,|\, L0\, S\lambda \,\rangle\langle\, S\lambda \,|\, S_1\lambda_1\, S_2 - \lambda_2 \,\rangle\,. \quad \text{(B.16)}$$

The transformation of the potential V and the T-matrix, respectively, is given by

$$\langle\, L'S'|\, V^J |LS\rangle = \sum_{\lambda_1\lambda_2,\lambda_3\lambda_4} \langle\, JM\, L'S' \,|\, JM\,\lambda_3\lambda_4 \,\rangle \cdot\langle\, \lambda_3\lambda_4\,|V^J|\lambda_1\lambda_2\rangle\, \langle\, JM\,\lambda_1\lambda_2 \,|\, JM\,LS \,\rangle\,. \quad \text{(B.17)}$$

The partial wave decomposed scattering equation in JLS basis then reads as follows:

$$\begin{aligned}\langle\, k'\,L'S'\,|T^J|k\,LS\rangle &= \langle\, k'\,L'S'\,|V^J|k\,LS\rangle \quad \text{(B.18)}\\ &+ \sum_{L''S''} \int dq q^2 \langle\, k'\,L'S'\,|V^J|q\,L''S''\rangle\, G(q)\, \langle\, q\,L''S''\,|T^J|k\,LS\rangle\,.\end{aligned}$$

Because of the invariance of the strong interactions under parity transformations, some of the matrix elements of the potential in the JLS basis vanish. The parity

$$\eta = \eta_1\eta_2(-1)^L \quad \text{(B.19)}$$

with η_i the intrinsic parity of particle i, has to be the same for the initial and the final state. This means that for initial and final states with the same intrinsic parity only transitions with even ΔL are allowed. For initial and final states with total spin $S = \frac{1}{2}$ the only allowed transition occurs for $\Delta L = 0$. This follows from the condition

$$|J - S| \leq L \leq J + S\,. \quad \text{(B.20)}$$

On the other hand, if initial and final state have different intrinsic parity, ΔL has to be odd. Equation (B.20) reduces this further to $\Delta L = 1$ for all reaction channels we are interested in.

Parity conservation also reduces the number of independent matrix elements in the helicity basis and thus simplifies the transformation from helicity to JLS basis. A parity transformation connects helicity states of positive and negative helicity in the following way:

$$\langle\, -\lambda_3 - \lambda_4 \,|\, V \,|-\lambda_1 - \lambda_2\rangle = (-1)^{S_3+S_4-S_1-S_2}\, \frac{\eta_3\eta_4}{\eta_1\eta_2}\, \langle\, \lambda_3\lambda_4 \,|\, V \,|\lambda_1\lambda_2\rangle\,. \quad \text{(B.21)}$$

B.2.1 Explicit Expressions for the Transformation Matrices

In this section the matrix elements for the transformation between helicity basis and JLS basis are given explicitely for the case of a spin-$\frac{1}{2}$ and spin-0 product state and a spin-$\frac{3}{2}$ and spin-0 product state.

From equation (B.13) we obtain the following expression for the transformation matrix of $\frac{1}{2} \times 0$ states:

$$\begin{pmatrix} \left|JM; L = J + \frac{1}{2},\, S = \frac{1}{2}\right\rangle \\ \left|JM; L = J - \frac{1}{2},\, S = \frac{1}{2}\right\rangle \end{pmatrix} = \frac{1}{\sqrt{2}} \begin{pmatrix} -1 & 1 \\ 1 & 1 \end{pmatrix} \begin{pmatrix} \left|JM; \lambda_1 = \frac{1}{2},\, \lambda_2 = 0\right\rangle \\ \left|JM; \lambda_1 = -\frac{1}{2},\, \lambda_2 = 0\right\rangle \end{pmatrix} \tag{B.22}$$

With the help of expression (B.21), the πN, σN, ηN and $\pi N \to \eta N$ potentials in JLS basis can then be expressed as a linear combination of two matrix elements in helicity basis.

$$\begin{aligned} &\left\langle L', S' = \tfrac{1}{2} \right| V^J \left| L, S = \tfrac{1}{2} \right\rangle \\ &= \begin{cases} \left\langle \lambda_3 = \frac{1}{2} \right| V^J \left| \lambda_1 = \frac{1}{2} \right\rangle - \left\langle \lambda_3 = -\frac{1}{2} \right| V^J \left| \lambda_1 = \frac{1}{2} \right\rangle & \text{if } L' = L = J + \frac{1}{2} \\ \left\langle \lambda_3 = \frac{1}{2} \right| V^J \left| \lambda_1 = \frac{1}{2} \right\rangle + \left\langle \lambda_3 = -\frac{1}{2} \right| V^J \left| \lambda_1 = \frac{1}{2} \right\rangle & \text{if } L' = L = J - \frac{1}{2}\,. \end{cases} \end{aligned} \tag{B.23}$$

The $\pi N \to \sigma N$ transition demands for $\Delta L = 1$ because the σ has positive intrinsic parity and the π has negative intrinsic parity.

$$\begin{aligned} &\left\langle L', S' = \tfrac{1}{2} \right| V^J \left| L, S = \tfrac{1}{2} \right\rangle \\ &= \begin{cases} -\left\langle \lambda_3 = \frac{1}{2} \right| V^J \left| \lambda_1 = \frac{1}{2} \right\rangle - \left\langle \lambda_3 = -\frac{1}{2} \right| V^J \left| \lambda_1 = \frac{1}{2} \right\rangle & \text{if } L' = L - 1 = J - \frac{1}{2} \\ -\left\langle \lambda_3 = \frac{1}{2} \right| V^J \left| \lambda_1 = \frac{1}{2} \right\rangle + \left\langle \lambda_3 = -\frac{1}{2} \right| V^J \left| \lambda_1 = \frac{1}{2} \right\rangle & \text{if } L' = L + 1 = J + \frac{1}{2}\,. \end{cases} \end{aligned} \tag{B.24}$$

For $\frac{3}{2} \times 0$ states the transformation reads as follows:

$$\begin{pmatrix} \left|JM; L = J + \frac{1}{2},\, S = \frac{3}{2}\right\rangle \\ \left|JM; L = J - \frac{1}{2},\, S = \frac{3}{2}\right\rangle \\ \left|JM; L = J + \frac{3}{2},\, S = \frac{3}{2}\right\rangle \\ \left|JM; L = J - \frac{3}{2},\, S = \frac{3}{2}\right\rangle \end{pmatrix}$$

$$= \begin{pmatrix} a^1_+ & a^1_+ & a^2_+ & a^2_+ \\ a^1_- & -a^1_- & a^2_- & -a^2_- \\ b^1_+ & -b^1_+ & b^2_+ & -b^2_+ \\ b^1_- & b^1_- & b^2_- & b^2_- \end{pmatrix} \begin{pmatrix} \left|JM; \lambda_1 = \frac{1}{2}, \lambda_2 = 0\right\rangle \\ \left|JM; \lambda_1 = -\frac{1}{2}, \lambda_2 = 0\right\rangle \\ \left|JM; \lambda_1 = \frac{3}{2}, \lambda_2 = 0\right\rangle \\ \left|JM; \lambda_1 = -\frac{3}{2}, \lambda_2 = 0\right\rangle \end{pmatrix}. \tag{B.25}$$

The elements of the transformation matrix are given by

matrix element	$+$	$-$
a^1	$-\frac{1}{2\sqrt{2}}\sqrt{\frac{2J+3}{2J}}$	$-\frac{1}{2\sqrt{2}}\sqrt{\frac{2J-1}{2J+2}}$
a^2	$\sqrt{\frac{3}{8}}\sqrt{\frac{2J-1}{2J}}$	$-\sqrt{\frac{3}{8}}\sqrt{\frac{2J+3}{2J+2}}$
b^1	$\sqrt{\frac{3}{8}}\sqrt{\frac{2J+3}{2J+2}}$	$\sqrt{\frac{3}{8}}\sqrt{\frac{2J-1}{2J}}$
b^2	$-\frac{1}{2\sqrt{2}}\sqrt{\frac{2J-1}{2J+2}}$	$\frac{1}{2\sqrt{2}}\sqrt{\frac{2J+3}{2J}}$

One should note that for $J = \frac{1}{2}$ the states with $L = J + \frac{3}{2}$ and $L = J - \frac{3}{2}$ are forbidden because of (B.20). Tensor transitions ($\Delta L = 2$) in the $\pi\Delta$ and $\pi N \to \pi\Delta$ potentials thus only occur for $J \geq \frac{3}{2}$.

Appendix C

Separation of the T-matrix into Pole and Non-Pole Contributions

We start from a scattering equation of the Lippmann-Schwinger type,

$$T = V + VGT\,. \tag{C.1}$$

If the potential can be split into a separable pole potential and a non-pole potential containing the non-separable part of the interaction,

$$V = V^P + V^{NP} = f_0 g_0 f_0^\dagger + V^{NP}\,, \tag{C.2}$$

the T-matrix can also be separated into a pole and a non-pole part,

$$T = T^P + T^{NP} = T^P + V^{NP} + V^{NP} G T^{NP}\,, \tag{C.3}$$

with the non-pole T-matrix obeying the usual scattering equation. Our task is now to derive an expression for T^P. In this we will closely follow [84, 85].

From (C.1) and (C.2), we obtain

$$T = T^{NP} + V^P + V^P GT + V^{NP} GT^P\,. \tag{C.4}$$

The last term in the above expression can be rewritten applying the scattering equation (C.1) to T^{NP},

$$\begin{aligned} V^{NP} G T^P &= \left(T^{NP} - T^{NP} G V^{NP}\right) G T^P \\ &= T^{NP} GT - T^{NP} G T^{NP} - T^{NP} G V^{NP} G T^P \\ &= T^{NP} GV\,(1 + GT) - T^{NP} G V^{NP}\,(1 + GT) \\ &= T^{NP} G V^P (1 + GT)\,. \end{aligned}$$

Equation (C.4) then becomes

$$T = T^{NP} + (1 + T^{NP}G)V^P(1 + GT)\,. \tag{C.5}$$

We define the dressed vertex function

$$f = (1 + T^{NP}G)V^P(1 + GT)\,, \tag{C.6}$$

multiply (C.5) from the left with $f_0^\dagger G$ and solve for $f_0^\dagger GT$:

$$\begin{aligned} f_0^\dagger GT &= f_0^\dagger GT^{NP} f g_0 f_0^\dagger (1 + GT) \\ \Leftrightarrow f_0^\dagger GT &= \left(1 - f_0^\dagger G f g_0\right)^{-1} f_0^\dagger G \left(T^{NP} + f g_0 f_0^\dagger\right)\,. \end{aligned} \tag{C.7}$$

Reinserting this into (C.5) together with the definition of the dressed vertex (C.6) one gets

$$\begin{aligned} T &= T^{NP} + f g_0 f_0^\dagger\,(1 + GT) \\ &= T^{NP} + f g_0 \left\{ f_0^\dagger + \left(1 - f_0^\dagger G f g_0\right)^{-1} f_0^\dagger G \left(T^{NP} + f g_0 f_0^\dagger\right) \right\} \\ &= T^{NP} + f g_0 \left(1 - f_0^\dagger G f g_0\right)^{-1} \left\{ f_0^\dagger + f_0^\dagger G T^{NP} \right\} \\ &= T^{NP} + f \left(g_0^{-1} - f_0^\dagger G f\right)^{-1} f^\dagger\,. \end{aligned}$$

So the T^P can be written as

$$T^P = f g f^\dagger \tag{C.8}$$

with the dressed propagator

$$g = \frac{1}{g_0^{-1} - \Sigma} \tag{C.9}$$

and the self-energy

$$\Sigma = f_0^\dagger G f\,. \tag{C.10}$$

Appendix D

Amplitudes

The transition amplitudes are obtained from the interaction Lagrangians by applying the usual Feynman rules.

The explicit expressions for the γ-matrices, spinors and spin-3/2 projectors can be found in Appendix A.

D.1 Amplitudes for πN Scattering

Listed are the expressions for the potentials contributing to πN scattering without isospin factors. These will be given in subsection D.3.2.

πN potential:

- Nucleon pole

$$\frac{f^2_{\pi NN}}{m^2_\pi}\bar{u}(\vec{p_f},s_f)\gamma_5 \not{k}_f \frac{\not{p}_i + \not{k}_i + M_N}{s-M_N^2}\gamma_5 \not{k}_i u(\vec{p_i},s_i) \tag{D.1}$$

- Nucleon u-exchange

$$\frac{f^2_{\pi NN}}{m^2_\pi}\bar{u}(\vec{p_f},s_f)\gamma_5 \not{k}_i \frac{\not{p}_i - \not{k}_f + M_N}{u-M_N^2}\gamma_5 \not{k}_f u(\vec{p_i},s_i) \tag{D.2}$$

- σ exchange

$$g_{\sigma NN}\bar{u}(\vec{p_f},s_f)u(\vec{p_i},s_i)\,\frac{1}{t-m_\sigma^2}\,\left[g_1 m_\pi^2 - g_2 k_i\cdot k_f\right] \tag{D.3}$$

- ρ exchange

$$g_{\rho NN} g_{\rho\pi\pi} \bar{u}(\vec{p_f}, s_f) \left[\gamma^\mu + i \frac{\kappa}{2M_N} \sigma^{\mu\nu} (k_i - k_f)_\nu \right] u(\vec{p_i}, s_i) \, \frac{-g_{\mu\alpha}}{t - m_\rho^2} \, (k_i + k_f)^\alpha \tag{D.4}$$

- Δ pole

$$\frac{f_{\pi N\Delta}^2}{m_\pi^2} \bar{u}(\vec{p_f}, s_f) k_f^\mu \frac{(\not{p}_i + \not{k}_i + M_\Delta) P_{\mu\nu}(p_i + k_i, M_\Delta)}{s - M_\Delta^2} \, k_i^\nu u(\vec{p_i}, s_i) \tag{D.5}$$

- Δ u-exchange

$$\frac{f_{\pi N\Delta}^2}{m_\pi^2} \bar{u}(\vec{p_f}, s_f) k_f^\mu \frac{(\not{p}_i - \not{k}_f + M_\Delta) P_{\mu\nu}(p_i - k_f, M_\Delta)}{u - M_\Delta^2} \, k_i^\nu u(\vec{p_i}, s_i) \tag{D.6}$$

- Roper pole

$$\frac{f_{P_{11}\pi N}^2}{m_\pi^2} \bar{u}(\vec{p_f}, s_f) \gamma_5 \not{k}_f \frac{\not{p}_i + \not{k}_i + M_{P_{11}}}{s - M_{P_{11}}^2} \, \gamma_5 \not{k}_i u(\vec{p_i}, s_i) \tag{D.7}$$

- D_{13} pole

$$\left(\frac{f_{D_{13}\pi N}}{m_\pi^2} \right)^2 \bar{u}(\vec{p_f}, s_f) \gamma_5 \not{k}_f k_f^\mu \cdot \frac{(\not{p}_i + \not{k}_i + M_{D_{13}}) P_{\mu\nu}(p_i + k_i, M_{D_{13}})}{s - M_{D_{13}}^2} \, \gamma_5 \not{k}_i k_i^\nu u(\vec{p_i}, s_i) \tag{D.8}$$

- S_{11} pole

$$\frac{f_{S_{11}\pi N}^2}{m_\pi^2} \bar{u}(\vec{p_f}, s_f) \not{k}_f \frac{\not{p}_i + \not{k}_i + M_{S_{11}}}{s - M_{S_{11}}^2} \, \not{k}_i u(\vec{p_i}, s_i) \tag{D.9}$$

<u>$\pi N \to \sigma N$ potential:</u>

- Nucleon pole

$$-i \frac{f_{\pi NN}}{m_\pi} g_{\sigma NN} \bar{u}(\vec{p_f}, s_f) \frac{\not{p}_i + \not{k}_i + M_N}{s - M_N^2} \, \gamma_5 \not{k}_i u(\vec{p_i}, s_i) \tag{D.10}$$

- Nucleon u-exchange

$$-i \frac{f_{\pi NN}}{m_\pi} g_{\sigma NN} \bar{u}(\vec{p_f}, s_f) \gamma_5 \not{k}_f \frac{\not{p}_f - \not{k}_i + M_N}{u - M_N^2} \, u(\vec{p_i}, s_i) \tag{D.11}$$

- π exchange

$$-i\frac{f_{\pi NN}}{m_\pi}(-2M_N)\bar{u}(\vec{p_f},s_f)\gamma_5 u(\vec{p_i},s_i)\,\frac{1}{t-m_\pi^2}\left[g_1 m_\pi^2 - g_2 k_i\cdot k_f\right] \tag{D.12}$$

- Roper pole

$$-i\frac{f_{P_{11}\pi N}}{m_\pi}g_{P_{11}\sigma N}\bar{u}(\vec{p_f},s_f)\frac{\not{p}_i+\not{k}_i+M_{P_{11}}}{s-M_{P_{11}}^2}\,\gamma_5\not{k}_i u(\vec{p_i},s_i) \tag{D.13}$$

<u>σN potential:</u>

- Nucleon pole

$$g_{\sigma NN}^2\bar{u}(\vec{p_f},s_f)\frac{\not{p}_i+\not{k}_i+M_N}{s-M_N^2}\,u(\vec{p_i},s_i) \tag{D.14}$$

- Nucleon u-exchange

$$g_{\sigma NN}^2\bar{u}(\vec{p_f},s_f)\frac{\not{p}_i-\not{k}_f+M_N}{u-M_N^2}\,u(\vec{p_i},s_i) \tag{D.15}$$

- σ exchange

$$g_{\sigma NN}g_{\sigma\sigma\sigma}m_\sigma\bar{u}(\vec{p_f},s_f)u(\vec{p_i},s_i)\,\frac{1}{t-m_\sigma^2} \tag{D.16}$$

- Roper pole

$$g_{P_{11}\sigma N}^2\bar{u}(\vec{p_f},s_f)\frac{\not{p}_i+\not{k}_i+M_{P_{11}}}{s-M_{P_{11}}^2}\,u(\vec{p_i},s_i) \tag{D.17}$$

<u>$\pi N\to\pi\Delta$ potential:</u>

- Nucleon pole

$$-\frac{f_{\pi NN}f_{\pi N\Delta}}{m_\pi^2}\bar{u}_\mu(\vec{p_f},s_f)k_f^\mu\frac{\not{p}_i+\not{k}_i+M_N}{s-M_N^2}\,\gamma_5\not{k}_i u(\vec{p_i},s_i) \tag{D.18}$$

- Nucleon u-exchange

$$-\frac{f_{\pi NN}f_{\pi N\Delta}}{m_\pi^2}\bar{u}_\mu(\vec{p_f},s_f)k_i^\mu\frac{\not{p}_i-\not{k}_f+M_N}{u-M_N^2}\,\gamma_5\not{k}_f u(\vec{p_i},s_i) \tag{D.19}$$

- ρ exchange

$$\frac{f_{\rho N\Delta}}{m_\rho} g_{\rho\pi\pi} \bar{u}_\mu(\vec{p_f}, s_f)\gamma_5\gamma_\alpha \cdot \left[\frac{(p_f - p_i)^\mu (k_f + k_i)^\alpha}{t - m_\rho^2} - \frac{(p_f - p_i)^\alpha (k_f + k_i)^\mu}{t - m_\rho^2}\right] u(\vec{p_i}, s_i) \tag{D.20}$$

- Δ pole

$$\frac{f_{\pi\Delta\Delta} f_{\pi N\Delta}}{m_\pi^2} \bar{u}_\mu(\vec{p_f}, s_f)\gamma_5 \not{k}_f \frac{(\not{p}_i + \not{k}_i + M_\Delta) P^{\mu\nu}(p_i + k_i, M_\Delta)}{s - M_\Delta^2} k_{i\nu} u(\vec{p_i}, s_i) \tag{D.21}$$

- Δ u-exchange

$$\frac{f_{\pi\Delta\Delta} f_{\pi N\Delta}}{m_\pi^2} \bar{u}_\mu(\vec{p_f}, s_f)\gamma_5 \not{k}_i \frac{(\not{p}_i - \not{k}_f + M_\Delta) P^{\mu\nu}(p_i - k_f, M_\Delta)}{u - M_\Delta^2} k_{f\nu} u(\vec{p_i}, s_i) \tag{D.22}$$

- Roper pole

$$-\frac{f_{P_{11}\pi N} f_{P_{11}\pi\Delta}}{m_\pi^2} \bar{u}_\mu(\vec{p_f}, s_f) k_f^\mu \frac{\not{p}_i + \not{k}_i + M_{P_{11}}}{s - M_{P_{11}}^2} \gamma_5 \not{k}_i u(\vec{p_i}, s_i) \tag{D.23}$$

- D_{13} pole

$$\frac{f_{D_{13}\pi\Delta} f_{D_{13}\pi N}}{m_\pi^3} \bar{u}_\mu(\vec{p_f}, s_f) \not{k}_f \cdot \frac{(\not{p}_i + \not{k}_i + M_{D_{13}}) P^{\mu\nu}(p_i + k_i, M_{D_{13}})}{s - M_{D_{13}}^2} \gamma_5 \not{k}_i k_{i\nu} u(\vec{p_i}, s_i) \tag{D.24}$$

<u>$\pi\Delta$ potential:</u>

- Nucleon pole

$$\frac{f_{\pi N\Delta}^2}{m_\pi^2} \bar{u}_\mu(\vec{p_f}, s_f) k_f^\mu \frac{\not{p}_i + \not{k}_i + M_N}{s - M_N^2} k_i^\nu u_\nu(\vec{p_i}, s_i) \tag{D.25}$$

- ρ exchange

$$-g_{\rho\Delta\Delta} g_{\rho\pi\pi} \bar{u}_\alpha(\vec{p_f}, s_f) \left[\gamma^\mu + i\frac{\kappa_{\rho\Delta\Delta}}{2M_N}\sigma^{\mu\nu}(k_i - k_f)_\nu\right] u^\alpha(\vec{p_i}, s_i) \frac{(k_i + k_f)_\mu}{t - m_\rho^2} \tag{D.26}$$

- Δ pole

$$\frac{f_{\pi\Delta\Delta}^2}{m_\pi^2} \bar{u}_\mu(\vec{p_f}, s_f)\gamma_5 \not{k}_f \frac{(\not{p}_i + \not{k}_i + M_\Delta) P^{\mu\nu}(p_i + k_i, M_\Delta)}{s - M_\Delta^2} \gamma_5 \not{k}_i u_\nu(\vec{p_i}, s_i) \tag{D.27}$$

- Roper pole

$$\frac{f^2_{P_{11}\pi\Delta}}{m^2_\pi}\bar{u}_\mu(\vec{p_f},s_f)k_f^\mu\frac{\not{p}_i+\not{k}_i+M_{P_{11}}}{s-M^2_{P_{11}}}\,k_i^\nu u_\nu(\vec{p_i},s_i) \tag{D.28}$$

- D_{13} pole

$$\frac{f^2_{D_{13}\pi\Delta}}{m^2_\pi}\bar{u}_\mu(\vec{p_f},s_f)\,\not{k}_f\frac{(\not{p}_i+\not{k}_i+M_{D_{13}})P^{\mu\nu}(p_i+k_i,M_{D_{13}})}{s-M^2_{D_{13}}}\,\not{k}_i u_\nu(\vec{p_i},s_i) \tag{D.29}$$

<u>$\sigma N \to \pi\Delta$ potential:</u>

- Nucleon pole

$$-ig_{\sigma NN}\frac{f_{\pi N\Delta}}{m_\pi}\bar{u}_\mu(\vec{p_f},s_f)k_f^\mu\frac{\not{p}_i+\not{k}_i+M_N}{s-M^2_N}\,u(\vec{p_i},s_i) \tag{D.30}$$

- Roper pole

$$-ig_{P_{11}\sigma N}\frac{f_{P_{11}\pi\Delta}}{m_\pi}\bar{u}_\mu(\vec{p_f},s_f)k_f^\mu\frac{\not{p}_i+\not{k}_i+M_{P_{11}}}{s-M^2_{P_{11}}}\,u(\vec{p_i},s_i) \tag{D.31}$$

<u>$\pi N \to \eta N$ potential:</u>

- S_{11} pole

$$\frac{f_{S_{11}\pi N}f_{S_{11}\eta N}}{m_\pi m_\eta}\bar{u}(\vec{p_f},s_f)\,\not{k}_f\frac{\not{p}_i+\not{k}_i+M_{S_{11}}}{s-M^2_{S_{11}}}\,\not{k}_i u(\vec{p_i},s_i) \tag{D.32}$$

<u>ηN potential:</u>

- S_{11} pole

$$\frac{f^2_{S_{11}\eta N}}{m^2_\eta}\bar{u}(\vec{p_f},s_f)\,\not{k}_f\frac{\not{p}_i+\not{k}_i+M_{S_{11}}}{s-M^2_{S_{11}}}\,\not{k}_i u(\vec{p_i},s_i) \tag{D.33}$$

D.2 $\pi N \to \pi\pi N$ Amplitudes

This section contains the invariant matrix elements $-i\,\mathcal{M}$ for pion-induced two-pion production

$$\pi(k_a)N(p_b, s_b) \to \pi(k_1)\pi(k_2)N(p_3, s_3)$$

without isospin factors. The isospin factors are given in subsection D.3.2. We introduce the following Lorentz-invariant quantities:

$$\begin{aligned} s &= (k_a + p_b)^2\,, & t &= (p_b - p_3)^2\,,\\ s_{12} &= (k_1 + k_2)^2\,, & t_1 &= (k_1 - k_a)^2\,,\\ s_{13} &= (k_1 + p_3)^2\,, & t_2 &= (k_2 - k_a)^2\,,\\ s_{23} &= (k_2 + p_3)^2\,. \end{aligned}$$

The labels in front of the expressions for the amplitudes refer to the Feynman diagrams displayed in Figs. 2.1–2.3.
The contributions of diagrams (B.1) and (C.1) each contain three parts that have different isospin factors.

(A.1) $$\left(\frac{f_{NN\pi}}{m_\pi}\right)^3 \bar{u}(\vec{p}_3, s_3)\gamma_5 \not{k}_2 \frac{\not{p}_3 + \not{k}_2 + M_N}{s_{23} - M_N^2 - \Sigma_N}\gamma_5 \not{k}_1 \frac{\not{p}_b + \not{k}_a + M_N}{s - M_N^2 - \Sigma_N}\gamma_5 \not{k}_a u(\vec{p}_b, s_b)$$

(A.2) can be derived from expression (A.1) by interchanging the pions $(k_1 \leftrightarrow k_2)$.

(A.3) $$\left(\frac{f_{NN\pi}}{m_\pi}\right)^3 \bar{u}(\vec{p}_3, s_3)\gamma_5 \not{k}_2 \frac{\not{p}_3 + \not{k}_2 + M_N}{s_{23} - M_N^2 - \Sigma_N}\gamma_5 \not{k}_a \cdot \frac{\not{p}_b - \not{k}_1 + M_N}{(p_b - k_1)^2 - M_N^2}\gamma_5 \not{k}_1 u(\vec{p}_b, s_b)$$

(A.4) $(k_1 \leftrightarrow k_2)$

(A.5) $$\left(\frac{f_{NN\pi}}{m_\pi}\right)^3 \bar{u}(\vec{p}_3, s_3)\gamma_5 \not{k}_a \frac{\not{p}_3 - \not{k}_a + M_N}{(p_3 - k_a)^2 - M_N^2}\gamma_5 \not{k}_2 \cdot \frac{\not{p}_b - \not{k}_1 + M_N}{(p_b - k_1)^2 - M_N^2}\gamma_5 \not{k}_1 u(\vec{p}_b, s_b)$$

(A.6) $(k_1 \leftrightarrow k_2)$

(B.1) $$(a)\ \frac{g_A}{4F_\pi^3}\bar{u}(\vec{p}_3, s_3)\gamma_5(\not{k}_1 + \not{k}_2)u(\vec{p}_b, s_b)$$

$$(b)\ \frac{g_A}{4F_\pi^3}\bar{u}(\vec{p}_3,s_3)\gamma_5(\not{k}_1-\not{k}_a)u(\vec{p}_b,s_b)$$
$$(c)\ \frac{g_A}{4F_\pi^3}\bar{u}(\vec{p}_3,s_3)\gamma_5(\not{k}_2-\not{k}_a)u(\vec{p}_b,s_b)$$

Diagrams involving π exchange:

(C.1) $$(a)\ -\frac{f_{NN\pi}}{m_\pi}\frac{1}{F_\pi^2}\,\bar{u}(\vec{p}_3,s_3)\gamma_5(\not{p}_b-\not{p}_3)u(\vec{p}_b,s_b)\cdot\frac{1}{t-m_\pi^2}\left(s_{12}-m_\pi^2\right)$$
$$(b)\ -\frac{f_{NN\pi}}{m_\pi}\frac{1}{F_\pi^2}\,\bar{u}(\vec{p}_3,s_3)\gamma_5(\not{p}_b-\not{p}_3)u(\vec{p}_b,s_b)\cdot\frac{1}{t-m_\pi^2}\left(t_1-m_\pi^2\right)$$
$$(c)\ -\frac{f_{NN\pi}}{m_\pi}\frac{1}{F_\pi^2}\,\bar{u}(\vec{p}_3,s_3)\gamma_5(\not{p}_b-\not{p}_3)u(\vec{p}_b,s_b)\cdot\frac{1}{t-m_\pi^2}\left(t_2-m_\pi^2\right)$$

(C.2) $$\frac{f_{NN\pi}}{m_\pi}\,\bar{u}(\vec{p}_3,s_3)\gamma_5(\not{p}_b-\not{p}_3)u(\vec{p}_b,s_b)\cdot\frac{1}{t-m_\pi^2}$$
$$\cdot\left[2g_1m_\pi^2+g_2\,k_1\cdot k_2\right]\frac{1}{s_{12}-m_\sigma^2-\Sigma_\sigma}\left[2g_1m_\pi^2+g_2\,k_a\cdot(p_b-p_3)\right]$$

(C.3) $$-\frac{f_{NN\pi}}{m_\pi}g_{\rho\pi\pi}^2\bar{u}(\vec{p}_3,s_3)\gamma_5(\not{p}_b-\not{p}_3)u(\vec{p}_b,s_b)\cdot\frac{1}{t-m_\pi^2}$$
$$\cdot((p_b-p_3)-k_a)^\mu\,\frac{-g_{\mu\nu}}{s_{12}-m_\rho^2-\Sigma_\rho}(k_1-k_2)^\nu$$

(C.4) $$\frac{f_{NN\pi}}{m_\pi}\frac{g_{\rho\pi\pi}^2}{m_\rho^2}\,\bar{u}(\vec{p}_3,s_3)\gamma_5(\not{p}_b-\not{p}_3)u(\vec{p}_b,s_b)\cdot\frac{1}{t-m_\pi^2}$$
$$\cdot((p_b-p_3)-k_a)\cdot(k_1-k_2)$$

Diagrams involving ρ exchange:

(D.1) $$-\frac{f_{NN\pi}}{m_\pi}g_{NN\rho}\,g_{\rho\pi\pi}\bar{u}(\vec{p}_3,s_3)\left(\gamma^\mu-\frac{i\kappa}{2M_N}\sigma^{\mu\alpha}(k_1+k_2)_\alpha\right)$$
$$\cdot\frac{\not{p}_b+\not{k}_a+M_N}{s-M_N^2-\Sigma_N}\gamma_5\not{k}_a u(\vec{p}_b,s_b)\cdot\frac{-g_{\mu\nu}}{s_{12}-m_\rho^2-\Sigma_\rho}(k_1-k_2)^\nu$$

(D.2) $$-\frac{f_{NN\pi}}{m_\pi}g_{NN\rho}\,g_{\rho\pi\pi}\bar{u}(\vec{p}_3,s_3)\gamma_5\not{k}_a\frac{\not{p}_3-\not{k}_a+M_N}{(p_3-k_a)^2-M_N^2}$$
$$\cdot\left(\gamma^\mu-\frac{i\kappa}{2M_N}\sigma^{\mu\alpha}(k_1+k_2)_\alpha\right)u(\vec{p}_b,s_b)\cdot\frac{-g_{\mu\nu}}{s_{12}-m_\rho^2-\Sigma_\rho}(k_1-k_2)^\nu$$

(D.3) $$\frac{f_{NN\pi}}{m_\pi}g_{NN\rho}\,g_{\rho\pi\pi}\bar{u}(\vec{p}_3,s_3)\gamma_5\not{k}_2\frac{\not{p}_3+\not{k}_2+M_N}{s_{23}-M_N^2-\Sigma_N}$$
$$\cdot\left(\gamma^\mu-\frac{i\kappa}{2M_N}\sigma^{\mu\alpha}(k_1-k_a)_\alpha\right)u(\vec{p}_b,s_b)\cdot\frac{-g_{\mu\nu}}{t_1-m_\rho^2}(k_1+k_a)^\nu$$

(D.4) $$(k_1\leftrightarrow k_2)$$

(D.5) $$\frac{f_{NN\pi}}{m_\pi} g_{NN\rho}\, g_{\rho\pi\pi} \bar{u}(\vec{p}_3, s_3) \frac{\not{p}_b - \not{k}_2 + M_N}{(p_b - k_2)^2 - M_N^2} \gamma_5 \not{k}_2 \cdot \left(\gamma^\mu - \frac{i\kappa}{2M_N} \sigma^{\mu\alpha} (k_1 - k_a)_\alpha \right) u(\vec{p}_b, s_b) \cdot \frac{-g_{\mu\nu}}{t_1 - m_\rho^2} (k_1 + k_a)^\nu$$

(D.6) $(k_1 \leftrightarrow k_2)$

Diagrams involving σ exchange:

(E.1) $$-g_{NN\sigma} \frac{f_{NN\pi}}{m_\pi} \bar{u}(\vec{p}_3, s_3) \frac{\not{p}_b + \not{k}_a + M_N}{s - M_N^2 - \Sigma_N} \gamma_5 \not{k}_a u(\vec{p}_b, s_b) \cdot \frac{1}{s_{12} - m_\sigma^2 - \Sigma_\sigma} \left[2g_1 m_\pi^2 + g_2 k_1 \cdot k_2 \right]$$

(E.2) $$-g_{NN\sigma} \frac{f_{NN\pi}}{m_\pi} \bar{u}(\vec{p}_3, s_3)\, \gamma_5 \not{k}_a \frac{\not{p}_3 - \not{k}_a + M_N}{(p_3 - k_a)^2 - M_N^2} \cdot \frac{1}{s_{12} - m_\sigma^2 - \Sigma_\sigma} \left[2g_1 m_\pi^2 + g_2 k_1 \cdot k_2 \right]$$

(E.3) $$-g_{NN\sigma} \frac{f_{NN\pi}}{m_\pi} \bar{u}(\vec{p}_3, s_3)\, \gamma_5 \not{k}_2 \frac{\not{p}_3 + \not{k}_2 + M_N}{s_{23} - M_N^2 - \Sigma_N} \cdot \frac{1}{t_1 - m_\sigma^2} \left[2g_1 m_\pi^2 - g_2 k_1 \cdot k_a \right]$$

(E.4) $(k_1 \leftrightarrow k_2)$

(E.5) $$-g_{NN\sigma} \frac{f_{NN\pi}}{m_\pi} \bar{u}(\vec{p}_3, s_3) \frac{\not{p}_b - \not{k}_2 + M_N}{(p_b - k_2)^2 - M_N^2} \gamma_5 \not{k}_2 u(\vec{p}_b, s_b) \cdot \frac{1}{t_1 - m_\sigma^2} \left[2g_1 m_\pi^2 - g_2 k_1 \cdot k_a \right]$$

(E.6) $(k_1 \leftrightarrow k_2)$

Diagrams with Δ excitation:

(F.1) $$\frac{f_{NN\pi}}{m_\pi} \left(\frac{f_{N\Delta\pi}}{m_\pi} \right)^2 \bar{u}(\vec{p}_3, s_3) \gamma_5 \not{k}_2 \frac{\not{p}_3 + \not{k}_2 + M_N}{s_{23} - M_N^2 - \Sigma_N} k_1^\mu \cdot D_{\mu\nu}(p_b + k_a, M_\Delta) k_a^\nu u(\vec{p}_b, s_b)$$

(F.2) $(k_1 \leftrightarrow k_2)$

(F.3) $$\frac{f_{NN\pi}}{m_\pi} \left(\frac{f_{N\Delta\pi}}{m_\pi} \right)^2 \bar{u}(\vec{p}_3, s_3) \gamma_5 \not{k}_2 \frac{\not{p}_3 + \not{k}_2 + M_N}{s_{23} - M_N^2 - \Sigma_N} k_a^\mu \cdot D_{\mu\nu}(p_b - k_1, M_\Delta) k_1^\nu u(\vec{p}_b, s_b)$$

(F.4) $(k_1 \leftrightarrow k_2)$

(F.5) $$\frac{f_{NN\pi}}{m_\pi}\left(\frac{f_{N\Delta\pi}}{m_\pi}\right)^2 \bar{u}(\vec{p}_3,s_3)\gamma_5 \not{k}_a \frac{\not{p}_3 - \not{k}_a + M_N}{(p_3-k_a)^2 - M_N^2} k_2^\mu \cdot D_{\mu\nu}(p_b-k_1,M_\Delta)k_1^\nu u(\vec{p}_b,s_b)$$

(F.6) $(k_1 \leftrightarrow k_2)$

(F.7) $$\frac{f_{NN\pi}}{m_\pi}\left(\frac{f_{N\Delta\pi}}{m_\pi}\right)^2 \bar{u}(\vec{p}_3,s_3)k_2^\mu D_{\mu\nu}(p_3+k_2,M_\Delta)k_1^\nu \cdot \frac{\not{p}_b + \not{k}_a + M_N}{s - M_N^2 - \Sigma_N}\gamma_5 \not{k}_a u(\vec{p}_b,s_b)$$

(F.8) $(k_1 \leftrightarrow k_2)$

(F.9) $$\frac{f_{NN\pi}}{m_\pi}\left(\frac{f_{N\Delta\pi}}{m_\pi}\right)^2 \bar{u}(\vec{p}_3,s_3)k_2^\mu D_{\mu\nu}(p_3+k_2,M_\Delta)k_a^\nu \cdot \frac{\not{p}_b - \not{k}_1 + M_N}{(p_b-k_1)^2 - M_N^2}\gamma_5 \not{k}_1 u(\vec{p}_b,s_b)$$

(F.10) $(k_1 \leftrightarrow k_2)$

(F.11) $$\frac{f_{NN\pi}}{m_\pi}\left(\frac{f_{N\Delta\pi}}{m_\pi}\right)^2 \bar{u}(\vec{p}_3,s_3)k_a^\mu D_{\mu\nu}(p_3-k_a,M_\Delta)k_2^\nu \cdot \frac{\not{p}_b - \not{k}_1 + M_N}{(p_b-k_1)^2 - M_N^2}\gamma_5 \not{k}_1 u(\vec{p}_b,s_b)$$

(F.12) $(k_1 \leftrightarrow k_2)$

Diagrams with double Δ excitation:

(G.1) $$-\frac{f_{\Delta\Delta\pi}}{m_\pi}\left(\frac{f_{N\Delta\pi}}{m_\pi}\right)^2 \bar{u}(\vec{p}_3,s_3)k_2^\mu D_{\mu\nu}(p_3+k_2,M_\Delta)\gamma_5 \not{k}_1 \cdot D^{\nu\lambda}(p_b+k_a,M_\Delta)(k_a)_\lambda u(\vec{p}_b,s_b)$$

(G.2) $(k_1 \leftrightarrow k_2)$

(G.3) $$-\frac{f_{\Delta\Delta\pi}}{m_\pi}\left(\frac{f_{N\Delta\pi}}{m_\pi}\right)^2 \bar{u}(\vec{p}_3,s_3)k_2^\mu D_{\mu\nu}(p_3+k_2,M_\Delta)\gamma_5 \not{k}_a \cdot D^{\nu\lambda}(p_b-k_1,M_\Delta)(k_1)_\lambda u(\vec{p}_b,s_b)$$

(G.4) $(k_1 \leftrightarrow k_2)$

(G.5) $$-\frac{f_{\Delta\Delta\pi}}{m_\pi}\left(\frac{f_{N\Delta\pi}}{m_\pi}\right)^2 \bar{u}(\vec{p}_3,s_3)k_a^\mu D_{\mu\nu}(p_3-k_a,M_\Delta)\gamma_5 \not{k}_2 \cdot D^{\nu\lambda}(p_b-k_1,M_\Delta)(k_1)_\lambda u(\vec{p}_b,s_b)$$

(G.6) $(k_1 \leftrightarrow k_2)$

Diagrams with Δ and ρ excitation:

(H.1) $$\frac{f_{N\Delta\rho} f_{N\Delta\pi} g_{\rho\pi\pi}}{m_\rho m_\pi}\, \bar{u}(\vec{p}_3, s_3)\gamma_5 \left[-(k_1+k_2)^\mu \gamma^\alpha + g^{\mu\alpha}(\not{k}_1 + \not{k}_2)\right] D_{\mu\nu}(p_b + k_a, M_\Delta) \cdot k_a^\nu u(\vec{p}_b, s_b) \frac{-g_{\alpha\beta}}{s_{12} - m_\rho^2 - \Sigma_\rho}(k_1 - k_2)^\beta$$

(H.2) $$\frac{f_{N\Delta\rho} f_{N\Delta\pi} g_{\rho\pi\pi}}{m_\rho m_\pi} \bar{u}(\vec{p}_3, s_3) k_a^\mu D_{\mu\nu}(p_3 - k_a, M_\Delta) \cdot \gamma_5 [-(k_1+k_2)^\nu \gamma^\alpha + g^{\nu\alpha}(\not{k}_1 + \not{k}_2)] u(\vec{p}_b, s_b) \frac{-g_{\alpha\beta}}{s_{12} - m_\rho^2 - \Sigma_\rho}(k_1 - k_2)^\beta$$

(H.3) $$-\frac{f_{N\Delta\rho} f_{N\Delta\pi} g_{\rho\pi\pi}}{m_\rho m_\pi} \bar{u}(\vec{p}_3, s_3) k_2^\mu D_{\mu\nu}(p_3 + k_2, M_\Delta) \cdot \gamma_5 [(k_a - k_1)^\nu \gamma^\alpha + g^{\nu\alpha}(\not{k}_a - \not{k}_1)] u(\vec{p}_b, s_b) \frac{-g_{\alpha\beta}}{t_1 - m_\rho^2}(k_a + k_1)^\beta$$

(H.4) $(k_1 \leftrightarrow k_2)$

(H.5) $$-\frac{f_{N\Delta\rho} f_{N\Delta\pi} g_{\rho\pi\pi}}{m_\rho m_\pi} \bar{u}(\vec{p}_3, s_3)\gamma_5 [(k_a - k_1)^\mu \gamma^\alpha + g^{\mu\alpha}(\not{k}_a - \not{k}_1)] D_{\mu\nu}(p_b - k_2, M_\Delta) \cdot k_2^\nu u(\vec{p}_b, s_b) \frac{-g_{\alpha\beta}}{t_1 - m_\rho^2}(k_a + k_1)^\beta$$

(H.6) $(k_1 \leftrightarrow k_2)$

Diagrams with $N^\star(1440)$ excitation:

(I.1) $$\frac{f_{NN\pi}}{m_\pi}\left(\frac{f_{P_{11}N\pi}}{m_\pi}\right)^2 \bar{u}(\vec{p}_3, s_3)\gamma_5 \not{k}_2 \frac{\not{p}_3 + \not{k}_2 + M_N}{s_{23} - M_N^2 - \Sigma_N}\gamma_5 \not{k}_1 \frac{\not{p}_b + \not{k}_a + M_{P_{11}}}{s - M_{P_{11}}^2 - \Sigma_{P_{11}}}\gamma_5 \not{k}_a u(\vec{p}_b, s_b)$$

(I.2) $(k_1 \leftrightarrow k_2)$

(J.1) $$\frac{f_{P_{11}N\pi} f_{P_{11}\Delta\pi} f_{N\Delta\pi}}{m_\pi^3} \bar{u}(\vec{p}_3, s_3) k_2^\mu D_{\mu\nu}(p_3 + k_2, M_\Delta) k_1^\nu \cdot \frac{\not{p}_b + \not{k}_a + M_{P_{11}}}{s - M_{P_{11}}^2 - \Sigma_{P_{11}}}\gamma_5 \not{k}_a u(\vec{p}_b, s_b)$$

(J.2) $(k_1 \leftrightarrow k_2)$

(K.1) $$-g_{P_{11}\sigma N}\frac{f_{P_{11}N\pi}}{m_\pi}\, \bar{u}(\vec{p}_3, s_3)\frac{\not{p}_b + \not{k}_a + M_{P_{11}}}{s - M_{P_{11}}^2 - \Sigma_{P_{11}}}\gamma_5 \not{k}_a u(\vec{p}_b, s_b) \cdot \frac{1}{s_{12} - m_\sigma^2 - \Sigma_\sigma}\left[2g_1 m_\pi^2 + g_2 k_1 \cdot k_2\right]$$

(K.2) $$-g_{P_{11}\sigma N}\frac{f_{P_{11}N\pi}}{m_\pi}\,\bar{u}(\vec{p}_3,s_3)\,\gamma_5\,\not{k}_a\frac{\not{p}_3-\not{k}_a+M_{P_{11}}}{(p_3-k_a)^2-M_{P_{11}}^2}\cdot\frac{1}{s_{12}-m_\sigma^2-\Sigma_\sigma}\,\left[2g_1m_\pi^2+g_2k_1\cdot k_2\right]$$

(K.3) $$-g_{P_{11}\sigma N}\frac{f_{P_{11}N\pi}}{m_\pi}\,\bar{u}(\vec{p}_3,s_3)\,\gamma_5\,\not{k}_2\frac{\not{p}_3+\not{k}_2+M_{P_{11}}}{s_{23}-M_{P_{11}}^2-\Sigma_{P_{11}}}\cdot\frac{1}{t_1-m_\sigma^2}\left[2g_1m_\pi^2-g_2k_1\cdot k_a\right]$$

(K.4) $$(k_1\leftrightarrow k_2)$$

(K.5) $$-g_{P_{11}\sigma N}\frac{f_{P_{11}N\pi}}{m_\pi}\,\bar{u}(\vec{p}_3,s_3)\frac{\not{p}_b-\not{k}_2+M_{P_{11}}}{(p_b-k_2)^2-M_{P_{11}}^2}\,\gamma_5\,\not{k}_2u(\vec{p}_b,s_b)\cdot\frac{1}{t_1-m_\sigma^2}\left[2g_1m_\pi^2-g_2k_1\cdot k_a\right]$$

(K.6) $$(k_1\leftrightarrow k_2)$$

Diagrams with $N^\star(1520)$ excitation:

(L.1) $$\frac{f_{NN\pi}}{m_\pi}\left(\frac{f_{D_{13}N\pi}}{m_\pi^2}\right)^2\bar{u}(\vec{p}_3,s_3)\gamma_5\,\not{k}_2\frac{\not{p}_3+\not{k}_2+M_N}{s_{23}-M_N^2-\Sigma_N}\gamma_5\,\not{k}_1k_1^\mu\cdot D_{\mu\nu}(p_b+k_a,M_{D_{13}})\gamma_5\,\not{k}_ak_a^\nu u(\vec{p}_b,s_b)$$

(L.2) $$(k_1\leftrightarrow k_2)$$

(M.1) $$-\frac{f_{D_{13}\Delta\pi}f_{D_{13}N\pi}f_{N\Delta\pi}}{m_\pi^4}\bar{u}(\vec{p}_3,s_3)k_2^\mu D_{\mu\nu}(p_3+k_2,M_\Delta)\,\not{k}_1\cdot D^{\nu\lambda}(p_b+k_a,M_{D_{13}})\gamma_5\,\not{k}_a(k_a)_\lambda u(\vec{p}_b,s_b)$$

(M.2) $$(k_1\leftrightarrow k_2)$$

Diagrams with $N^\star(1535)$ excitation:

(N.1) $$\frac{f_{NN\pi}}{m_\pi}\left(\frac{f_{S_{11}N\pi}}{m_\pi}\right)^2\bar{u}(\vec{p}_3,s_3)\gamma_5\,\not{k}_2\,\frac{\not{p}_3+\not{k}_2+M_N}{s_{23}-M_N^2-\Sigma_N}\,\not{k}_1\frac{\not{p}_b+\not{k}_a+M_{S_{11}}}{s-M_{S_{11}}^2-\Sigma_{S_{11}}}\,\not{k}_au(\vec{p}_b,s_b)$$

(N.2) $$(k_1\leftrightarrow k_2)$$

D.3 The Isospin Part of the Potential

In this section we deal with the isospin part of the interaction. We use the 'baryon first' convention. This means that in any Clebsch-Gordan coefficient the baryon stands in the first position.

The isospin part of the wavefunction of an isospin-$\frac{1}{2}$ particle is given by a two-component spinor $\chi_{\pm\frac{1}{2}}$ obeying

$$\chi^\dagger_m \chi_{m'} \;=\; \delta_{m,m'} \;.$$

This relation also holds for an isospin-$\frac{3}{2}$ particle described by a four-component isospinor $\varphi_{\pm\frac{1}{2},\pm\frac{3}{2}}$.

For the description of isospin-1 particles we use the spherical basis vectors $\phi_{0,\pm1}$. These fulfil the relations [83]

$$\begin{aligned} \phi^*_m &= (-1)^m \phi_{-m} \;, \\ \phi^*_m \phi_{m'} &= \delta_{m,m'} \;, \\ (\phi_m \times \phi_{m'}) &= \sum_{m''=0,\pm1} i\sqrt{2}\,\langle\, 1\, m\, 1\, m' \,|\, 1\, m''\,\rangle\, \phi_{m''} \;. \end{aligned} \tag{D.34}$$

For a πNN vertex we get from the interaction lagrangian an isospin part of

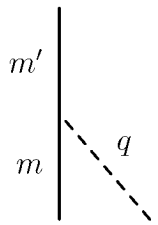

$$\chi^\dagger_{m'} \tau \phi_q \chi_m = \sqrt{3} \langle \frac{1}{2}\, m\, 1\, q | \frac{1}{2}\, m' \rangle \,. \tag{D.35}$$

The $\pi N\Delta$ and $\pi\Delta\Delta$ vertices get the isospin factors

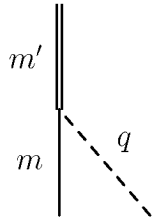

$$\varphi^{\dagger}_{m'} T \phi_q \chi_m = \langle \frac{1}{2}\, m\, 1\, q | \frac{3}{2}\, m' \rangle \qquad \text{(D.36)}$$

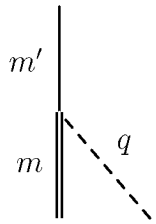

$$\chi^{\dagger}_{m'} T^{\dagger} \phi_q \varphi_m = -\sqrt{2}\, \langle \frac{3}{2}\, m\, 1\, q | \frac{1}{2}\, m' \rangle \qquad \text{(D.37)}$$

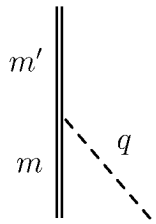

$$\varphi^{\dagger}_{m'} T \phi_q \varphi_m = \sqrt{\frac{5}{3}} \langle \frac{3}{2}\, m\, 1\, q | \frac{3}{2}\, m' \rangle\ . \qquad \text{(D.38)}$$

D.3.1 Isospin Factors for πN scattering

In Table D.2 the isospin factors for πN scattering are given in the isospin basis. It is convenient to work in the isospin basis because the scattering equations for different isospin decouple.
The total cross sections for πN scattering are given in the particle basis. The particle basis is related to the isospin basis via the relation

$$\left| t^a t^a_3, t^b t^b_3 \right\rangle = \sum_{I, I_3} \left\langle\, I I_3 \,|\, t^a t^a_3, t^b t^b_3 \,\right\rangle\ |I I_3\rangle\,, \qquad \text{(D.39)}$$

where $t^a 4$ (t^b) is the isospin of particle a (b) and t^a_3 (t^b_3) its third component. So for the πN states that are accessible in πN scattering experiments we get

$$\begin{aligned} |\pi^+ p\rangle &= \left| \tfrac{3}{2}\, \tfrac{3}{2} \right\rangle \\ |\pi^- p\rangle &= \sqrt{\frac{1}{3}}\, \left| \tfrac{3}{2}\, -\tfrac{1}{2} \right\rangle + \sqrt{\frac{2}{3}}\, \left| \tfrac{1}{2}\, -\tfrac{1}{2} \right\rangle \\ |\pi^0 n\rangle &= \sqrt{\frac{2}{3}}\, \left| \tfrac{3}{2}\, -\tfrac{1}{2} \right\rangle - \sqrt{\frac{1}{3}}\, \left| \tfrac{1}{2}\, -\tfrac{1}{2} \right\rangle \end{aligned} \qquad \text{(D.40)}$$

Potential	Diagram	$IF(I=\frac{1}{2})$	$IF(I=\frac{3}{2})$
πN	$N, N^\star$ pole	3	0
	N u-exchange	-1	2
	σ exchange	1	1
	ρ exchange	-2	1
	Δ pole	0	1
	Δ u-exchange	$\frac{4}{3}$	$\frac{1}{3}$
$\pi N \to \sigma N$	$N, N^\star$ pole	$\sqrt{3}$	0
	N u-exchange	$\sqrt{3}$	0
	π exchange	$\sqrt{3}$	0
σN	$N, N^\star$ pole	1	0
	N u-exchange	1	0
	σ exchange	1	0
$\pi N \to \pi\Delta$	$N, N^\star$ pole	$-\sqrt{6}$	0
	N u-exchange	$-\sqrt{\frac{8}{3}}$	$\sqrt{\frac{5}{3}}$
	ρ exchange	$\sqrt{\frac{2}{3}}$	$\sqrt{\frac{5}{3}}$
	Δ pole	0	$\sqrt{\frac{5}{3}}$
	Δ u-exchange	$-\frac{5}{3}\sqrt{\frac{2}{3}}$	$-\frac{10}{3\sqrt{15}}$
$\pi\Delta$	$N, N^\star$ pole	2	0
	ρ exchange	$\frac{5}{3}$	$\frac{2}{3}$
	Δ pole	0	$\frac{5}{3}$
	Δ u-exchange	$-\frac{10}{9}$	$\frac{11}{9}$
$\sigma N \to \pi\Delta$	$N, N^\star$ pole	$-\sqrt{2}$	0
$\pi N \to \eta N$	$N^\star$ pole	$\sqrt{3}$	0
ηN	$N^\star$ pole	1	0

Table D.2: Isospin Factors for Pion-Nucleon scattering.

D.3.2 Isospin Factors for $\pi N \to \pi\pi N$

Pion-induced two-pion production on the nucleon is experimentally accessible in the five reaction channels

$$\begin{aligned}
(1) &: \pi^-(k_a)p(p_b) \to \pi^-(k_1)\pi^+(k_2)n(p_3) \\
(2) &: \pi^-(k_a)p(p_b) \to \pi^0(k_1)\pi^0(k_2)n(p_3) \\
(3) &: \pi^-(k_a)p(p_b) \to \pi^0(k_1)\pi^-(k_2)p(p_3) \\
(4) &: \pi^+(k_a)p(p_b) \to \pi^+(k_1)\pi^+(k_2)n(p_3) \\
(5) &: \pi^+(k_a)p(p_b) \to \pi^0(k_1)\pi^+(k_2)p(p_3)
\end{aligned}$$

The amplitudes from Section D.2 have to be multiplied with an isospin factor for each of these reaction channels. The isospin factors for each amplitude are listed in Table D.3.

	$\pi^-p \to$			$\pi^+p \to$	
	$\pi^+\pi^-n$	$\pi^0\pi^0n$	$\pi^0\pi^-p$	$\pi^+\pi^+n$	$\pi^+\pi^0p$
(A.1)	$-2\sqrt{2}$	$\sqrt{2}$	-2	0	0
(A.2)	0	$\sqrt{2}$	2	0	0
(A.3)	0	$-\sqrt{2}$	2	$-2\sqrt{2}$	0
(A.4)	0	$-\sqrt{2}$	0	$-2\sqrt{2}$	2
(A.5)	0	$\sqrt{2}$	0	0	2
(A.6)	$-2\sqrt{2}$	$\sqrt{2}$	0	0	-2
(B.1)(a)	$-\sqrt{2}$	$\sqrt{2}$	0	0	0
(B.1)(b)	$-\sqrt{2}$	0	0	$-\sqrt{2}$	0
(B.1)(c)	0	0	1	$-\sqrt{2}$	1
(C.1)(a)	$-\sqrt{2}$	$\sqrt{2}$	0	0	0
(C.1)(b)	$-\sqrt{2}$	0	0	$-\sqrt{2}$	0
(C.1)(c)	0	0	1	$-\sqrt{2}$	1

Table D.3: Isospin Factors for Pion-induced two-Pion Production.

	$\pi^- p \to$			$\pi^+ p \to$	
	$\pi^+\pi^- n$	$\pi^0\pi^0 n$	$\pi^0\pi^- p$	$\pi^+\pi^+ n$	$\pi^+\pi^0 p$
(C.2)	$-\sqrt{2}$	$\sqrt{2}$	0	0	0
(C.3)	$-\sqrt{2}$	0	-1	0	-1
(C.4)	$-\sqrt{2}$	0	-1	0	-1
(D.1)	$-\sqrt{2}$	0	-2	0	0
(D.2)	$\sqrt{2}$	0	0	0	2
(D.3)	$\sqrt{2}$	$-\sqrt{2}$	2	$-\sqrt{2}$	0
(D.4)	0	$-\sqrt{2}$	-1	$-\sqrt{2}$	1
(D.5)	$-\sqrt{2}$	$\sqrt{2}$	0	$\sqrt{2}$	-2
(D.6)	0	$\sqrt{2}$	-1	$\sqrt{2}$	1
(E.1)	$-\sqrt{2}$	$\sqrt{2}$	0	0	0
(E.2)	$-\sqrt{2}$	$\sqrt{2}$	0	0	0
(E.3)	$-\sqrt{2}$	0	0	$-\sqrt{2}$	0
(E.4)	0	0	1	$-\sqrt{2}$	1
(E.5)	$-\sqrt{2}$	0	0	$-\sqrt{2}$	0
(E.6)	0	0	1	$-\sqrt{2}$	1
(F.1)	$-\frac{\sqrt{2}}{3}$	$-\frac{\sqrt{2}}{3}$	$\frac{2}{3}$	$-\sqrt{2}$	0
(F.2)	0	$-\frac{\sqrt{2}}{3}$	$\frac{1}{3}$	$-\sqrt{2}$	1
(F.3)	$-\sqrt{2}$	$\frac{\sqrt{2}}{3}$	$-\frac{2}{3}$	$-\frac{\sqrt{2}}{3}$	0
(F.4)	0	$\frac{\sqrt{2}}{3}$	1	$-\frac{\sqrt{2}}{3}$	$\frac{1}{3}$
(F.5)	$-\sqrt{2}$	$\frac{\sqrt{8}}{3}$	0	0	$-\frac{2}{3}$
(F.6)	$-\frac{\sqrt{2}}{3}$	$\frac{\sqrt{8}}{3}$	0	0	$\frac{2}{3}$
(F.7)	$-\frac{\sqrt{2}}{3}$	$\frac{\sqrt{8}}{3}$	$\frac{2}{3}$	0	0
(F.8)	$-\sqrt{2}$	$\frac{\sqrt{8}}{3}$	$-\frac{2}{3}$	0	0
(F.9)	0	$\frac{\sqrt{2}}{3}$	$\frac{1}{3}$	$-\frac{\sqrt{2}}{3}$	1

Table D.3: Isospin Factors for Pion-induced two-Pion Production.

	$\pi^- p \to$			$\pi^+ p \to$	
	$\pi^+\pi^- n$	$\pi^0\pi^0 n$	$\pi^0\pi^- p$	$\pi^+\pi^+ n$	$\pi^+\pi^0 p$
(F.10)	$-\sqrt{2}$	$\frac{\sqrt{2}}{3}$	0	$-\frac{\sqrt{2}}{3}$	$-\frac{2}{3}$
(F.11)	0	$-\frac{\sqrt{2}}{3}$	1	$-\sqrt{2}$	$\frac{1}{3}$
(F.12)	$-\frac{\sqrt{2}}{3}$	$-\frac{\sqrt{2}}{3}$	0	$-\sqrt{2}$	$\frac{2}{3}$
(G.1)	$\frac{\sqrt{8}}{9}$	$-\frac{\sqrt{2}}{9}$	$-\frac{1}{9}$	$-\frac{\sqrt{2}}{3}$	1
(G.2)	$-\frac{\sqrt{2}}{3}$	$-\frac{\sqrt{2}}{9}$	$\frac{4}{9}$	$-\frac{\sqrt{2}}{3}$	$-\frac{2}{3}$
(G.3)	$-\frac{\sqrt{2}}{3}$	$\frac{4\sqrt{2}}{9}$	$\frac{4}{9}$	$\frac{\sqrt{8}}{9}$	$-\frac{2}{3}$
(G.4)	$-\frac{\sqrt{2}}{3}$	$\frac{4\sqrt{2}}{9}$	$-\frac{2}{3}$	$\frac{\sqrt{8}}{9}$	$\frac{4}{9}$
(G.5)	$-\frac{\sqrt{2}}{3}$	$-\frac{\sqrt{2}}{9}$	$-\frac{2}{3}$	$-\frac{\sqrt{2}}{3}$	$\frac{4}{9}$
(G.6)	$\frac{\sqrt{8}}{9}$	$-\frac{\sqrt{2}}{9}$	1	$-\frac{\sqrt{2}}{3}$	$-\frac{1}{9}$
(H.1)	$\frac{\sqrt{2}}{3}$	0	$-\frac{1}{3}$	0	1
(H.2)	$-\frac{\sqrt{2}}{3}$	0	-1	0	$-\frac{1}{3}$
(H.3)	$-\frac{\sqrt{2}}{3}$	$\frac{\sqrt{2}}{3}$	$\frac{1}{3}$	$\frac{\sqrt{2}}{3}$	-1
(H.4)	0	$\frac{\sqrt{2}}{3}$	$-\frac{2}{3}$	$\frac{\sqrt{2}}{3}$	$\frac{2}{3}$
(H.5)	$\frac{\sqrt{2}}{3}$	$-\frac{\sqrt{2}}{3}$	1	$-\frac{\sqrt{2}}{3}$	$-\frac{1}{3}$
(H.6)	0	$-\frac{\sqrt{2}}{3}$	$-\frac{2}{3}$	$-\frac{\sqrt{2}}{3}$	$\frac{2}{3}$
(I.1)	$-2\sqrt{2}$	$\sqrt{2}$	-2	0	0
(I.2)	0	$\sqrt{2}$	2	0	0
(J.1)	$-\frac{\sqrt{2}}{3}$	$\frac{\sqrt{8}}{3}$	$\frac{2}{3}$	0	0
(J.2)	$-\sqrt{2}$	$\frac{\sqrt{8}}{3}$	$-\frac{2}{3}$	0	0
(K.1)	$-\sqrt{2}$	$\sqrt{2}$	0	0	0
(K.2)	$-\sqrt{2}$	$\sqrt{2}$	0	0	0
(K.3)	$-\sqrt{2}$	0	0	$-\sqrt{2}$	0
(K.4)	0	0	1	$-\sqrt{2}$	1
(K.5)	$-\sqrt{2}$	0	0	$-\sqrt{2}$	0

Table D.3: Isospin Factors for Pion-induced two-Pion Production.

	$\pi^- p \to$			$\pi^+ p \to$	
	$\pi^+\pi^- n$	$\pi^0\pi^0 n$	$\pi^0\pi^- p$	$\pi^+\pi^+ n$	$\pi^+\pi^0 p$
(K.6)	0	0	1	$-\sqrt{2}$	1
(L.1)	$-2\sqrt{2}$	$\sqrt{2}$	-2	0	0
(L.2)	0	$\sqrt{2}$	2	0	0
(M.1)	$-\frac{\sqrt{2}}{3}$	$\frac{\sqrt{8}}{3}$	$\frac{2}{3}$	0	0
(M.2)	$-\sqrt{2}$	$\frac{\sqrt{8}}{3}$	$-\frac{2}{3}$	0	0
(N.1)	$-2\sqrt{2}$	$\sqrt{2}$	-2	0	0
(N.2)	0	$\sqrt{2}$	2	0	0

Table D.3: Isospin Factors for Pion-induced two-Pion Production.

Appendix E

Observables

We are interested in the scattering of two particles into three particles:

$$A + B \to 1 + 2 + 3\,.$$

The transition probability from the initial to the final state is given by the matrix element $\langle\, 1,2,3 \,|\, \mathcal{M} \,|A,B\rangle \;= \mathcal{M}(p_A, p_B; p_1, p_2, p_3)$. The explicit expressions for the matrix elements for two–Pion production can be found in Appendix D.
Measurable quantities are calculated by taking the absolute square of the matrix element. The total cross section is defined as the integral of $|\mathcal{M}(p_A, p_B; p_1, p_2, p_3)|^2$ over all possible values of the momenta $\vec{p}_i$ of the outgoing particles - the three-body phase space - normalised by the incoming flux $|\vec{j}_{\rm in}|$:

$$\begin{aligned}
\sigma \;&=\; \frac{\mathcal{B}}{|\vec{j}_{\rm in}|} \int \frac{d^3p_1}{(2\pi)^3 2E_1} \int \frac{d^3p_2}{(2\pi)^3 2E_2} \int \frac{d^3p_3}{(2\pi)^3 2E_3} \\
&\qquad \cdot (2\pi)^4\, \delta^{(4)}(p_A + p_B - p_1 - p_2 - p_3) \cdot \overline{|\mathcal{M}(p_A, p_B; p_1, p_2, p_3)|^2} \\
&=\; \frac{\mathcal{B}}{4|\vec{p}_A^{\,\rm cm}|\sqrt{s}} \frac{1}{(2\pi)^5} \int \frac{d^3p_1}{2E_1} \int \frac{d^3p_2}{2E_2} \int \frac{d^3p_3}{2E_3} \qquad \text{(E.1)} \\
&\qquad \cdot \delta^{(4)}(p_A + p_B - p_1 - p_2 - p_3) \cdot \overline{|\mathcal{M}(p_A, p_B; p_1, p_2, p_3)|^2}.
\end{aligned}$$

Here, E_1, E_2 and E_3 are the on-shell energies of the outgoing particles, $\vec{p}_A^{\,\rm cm}$ is the momentum of particle A in the centre-of-momentum frame of the incoming particles A and B, and $\sqrt{s}$ is the invariant mass, $s = (p_A + p_B)^2$.
$\mathcal{B}$ is a Bose symmetry factor, $\mathcal{B} = 1/n!$, where n is the number of identical particles in the final state. In the case of pion-induced two-pion production, we have $\mathcal{B} = 1/2$ for the $\pi^0\pi^0 n$ and $\pi^+\pi^+ n$ final states and $\mathcal{B} = 1$ for $\pi^+\pi^- n$, $\pi^0\pi^- p$ and $\pi^+\pi^0 p$.

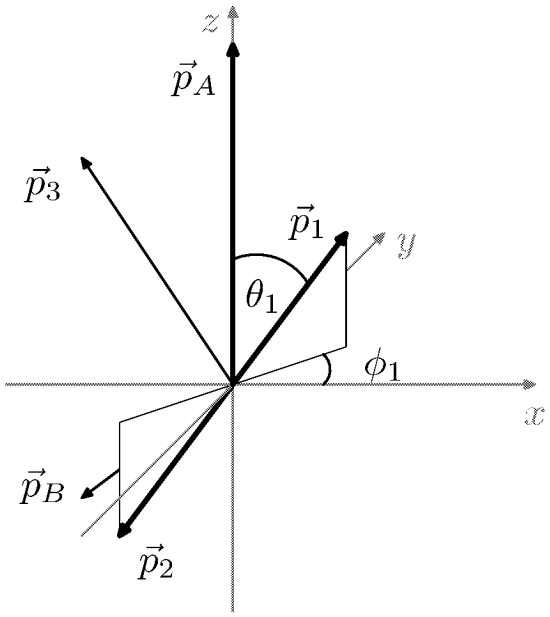

Figure E.1: The scattering of two to three particles in the rest frame of two outgoing particles (here 1 and 2). The scattering plane (xz plane) is defined by the momenta of the incoming particles $\vec{p}_A$ and $\vec{p}_B$ and the outgoing particle $\vec{p}_3$. This reference frame is often referred to as the Gottfried-Jackson frame.

$\overline{|\mathcal{M}|^2}$ is the spin averaged absolute square of the matrix element. If only spinless particles take part in the reaction, then $\overline{|\mathcal{M}|^2} = |\mathcal{M}|^2$. But if particles carrying spin like the nucleon or the photon participate in the reaction and we consider only unpolarised cross sections, one has to average over the spin of particles in the initial state and sum over the spins of the final state particles,

$$\overline{|\mathcal{M}|^2} = \frac{1}{2} \sum_{s_i=\pm\frac{1}{2}} \sum_{s_f=\pm\frac{1}{2}} |\mathcal{M}|^2 \qquad \text{for pion-induced two-pion production}$$

$$\overline{|\mathcal{M}|^2} = \frac{1}{4} \sum_{\lambda=\pm 1} \sum_{s_i=\pm\frac{1}{2}} \sum_{s_f=\pm\frac{1}{2}} |\mathcal{M}|^2 \quad \text{for two-pion photoproduction.}$$

Some of the integrations over the momentum conserving δ-function can be performed. In particular we only deal with unpolarised particles. This leads to a rotational invariance with respect to the beam axis. So we are left with the integration over four kinematical variables. Introducing the invariants $s_{12} = (p_1 + p_2)^2$ and $t = (p_B - p_3)^2$, we arrive at the following expression for the total cross section:

$$\sigma = \frac{\mathcal{B}}{16 s |\vec{p}_A^{\,\mathrm{cm}}|^2} \frac{\pi}{(2\pi)^5} \int_{s_{12}^{\min}}^{s_{12}^{\max}} ds_{12} \int_{t^{\min}}^{t^{\max}} dt \int_0^{2\pi} d\phi_1 \int_{-1}^{1} d\cos\theta_1 \left[\frac{|\vec{p}_1|}{4\sqrt{s_{12}}} \overline{|\mathcal{M}|^2} \right]_{\mathrm{cm12}} . \quad \text{(E.2)}$$

ϕ_1 and θ_1 are the polar and azimuthal angles of particle 1 in the centre-of-momentum frame of particles 1 and 2 (see Fig. E.1). The integrand also has to be taken in the rest frame of particles 1 and 2.
The bounds of the phase space integration are given by

$$\begin{aligned} s_{12}^{\min} &= (m_1+m_2)^2\,, \\ s_{12}^{\max} &= (\sqrt{s}-m_3)^2\,, \\ t^{\min} &= m_B^2+m_3^2-2E_b^{\rm cm}E_3^{\rm cm}-2|\vec{p}_3^{\,\rm cm}||\vec{p}_B^{\,\rm cm}|\,, \\ t^{\max} &= m_B^2+m_3^2-2E_b^{\rm cm}E_3^{\rm cm}+2|\vec{p}_3^{\,\rm cm}||\vec{p}_B^{\,\rm cm}|\,. \end{aligned}$$

The bounds of the t–integration depend on s_{12} via the relation

$$|\vec{p}_3^{\,\rm cm}| = \frac{1}{2\sqrt{s}}\sqrt{(s-(m_3+\sqrt{s_{12}})^2)\,(s-(m_3-\sqrt{s_{12}})^2)}\,.$$

Differential cross sections are obtained by fixing one or more of the kinematical variables.

Single Differential Cross Sections

$$\frac{d\sigma}{ds_{12}} = \frac{\mathcal{B}}{16|\vec{p}_A^{\,\rm cm}|^2 s}\,\frac{\pi}{(2\pi)^5}\int_{t^{\min}}^{t^{\max}}dt\int_0^{2\pi}d\phi_1\int_{-1}^{1}d\cos\theta_1\left[\frac{|\vec{p}_1|}{4\sqrt{s_{12}}}\,\overline{|\mathcal{M}|^2}\right]_{\rm cm12}. \tag{E.3}$$

$$\frac{d\sigma}{dt} = \frac{\mathcal{B}}{16|\vec{p}_A^{\,\rm cm}|^2 s}\,\frac{\pi}{(2\pi)^5}\int_{\tilde{s}_{12}^{\min}}^{\tilde{s}_{12}^{\max}}ds_{12}\int_0^{2\pi}d\phi_1\int_{-1}^{1}d\cos\theta_1\left[\frac{|\vec{p}_1|}{4\sqrt{s_{12}}}\,\overline{|\mathcal{M}|^2}\right]_{\rm cm12}. \tag{E.4}$$

In the expression for $d\sigma/dt$ the bounds of the s_{12}–integration depend on t:

$$\begin{aligned} \tilde{s}_{12}^{\max/\min} = \frac{1}{2m_B^2}\Big[&(m_B^2-m_3^2)(s-m_B^2)+m_A^2(m_B^2+m_3^2)+(s+m_B^2-m_A^2)\,t \\ &\pm 2\sqrt{s}\,|\vec{p}_B^{\,\rm cm}|\sqrt{(t-(m_B+m_3)^2)(t-(m_B-m_3)^2)}\Big]\,, \end{aligned}$$

and $(m_1+m_2)^2 \le s_{12} \le (\sqrt{s}-m_3)^2$.

$$\frac{d\sigma}{d\cos\theta_1} = \frac{\mathcal{B}}{16s|\vec{p}_A^{\,\rm cm}|^2}\,\frac{\pi}{(2\pi)^5}\int_{s_{12}^{\min}}^{s_{12}^{\max}}ds_{12}\int_{t^{\min}}^{t^{\max}}dt\int_0^{2\pi}d\phi_1\left[\frac{|\vec{p}_1|}{4\sqrt{s_{12}}}\,\overline{|\mathcal{M}|^2}\right]_{\rm cm12}. \tag{E.5}$$

$$\frac{d\sigma}{d\phi_1} = \frac{\mathcal{B}}{16s|\vec{p}_A^{\,\rm cm}|^2}\,\frac{\pi}{(2\pi)^5}\int_{s_{12}^{\min}}^{s_{12}^{\max}}ds_{12}\int_{t^{\min}}^{t^{\max}}dt\int_{-1}^{1}d\cos\theta_1\left[\frac{|\vec{p}_1|}{4\sqrt{s_{12}}}\,\overline{|\mathcal{M}|^2}\right]_{\rm cm12}. \tag{E.6}$$

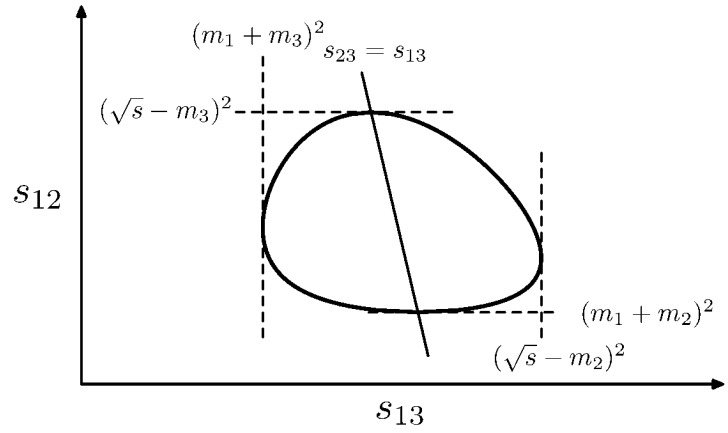

Figure E.2: Dalitz plot with the bounds of the physical region given. In the case of identical particles 1 and 2 the line with $s_{23} = s_{13}$ is a symmetry axis of the Dalitz plot.

Dalitz Plot

A standard representation of the three particle final state is the Dalitz plot. The double differential cross section

$$\frac{d^2\sigma}{ds_{12}\,ds_{13}} = \frac{\mathcal{B}}{64|\vec{p}_A^{\,\mathrm{cm}}|s^{3/2}}\,\frac{\pi}{(2\pi)^5}\int_0^{2\pi} d\phi_1 \int_{-1}^{1} d\cos\theta_1 \left[\overline{|\mathcal{M}|^2}\right]_{\mathrm{cm12}} \tag{E.7}$$

is plotted in a two dimensional plot as a function of s_{12} and s_{13}. For a given value of s_{12}, s_{13} lies between

$$s_{13}^{\mathrm{max/min}} = (E_1^{\mathrm{cm12}} + E_3^{\mathrm{cm12}})^2 - \left(\sqrt{(E_1^{\mathrm{cm12}})^2 - m_1^2} \mp \sqrt{(E_3^{\mathrm{cm12}})^2 - m_3^2}\right)^2$$

with $E_1^{\mathrm{cm12}} = (s_{12} + m_1^2 - m_2^2)/2\sqrt{s_{12}}$ and $E_3^{\mathrm{cm12}} = (s - s_{12} - m_3^2)/2\sqrt{s_{12}}$ the energies of particles 1 and 2 in the centre-of-momentum frame of particles 1 and 2.
Lines with constant $s_{23} = c$ obey the equation $s_{12} = (s + \sum_{i=1}^{3} m_i^2 - c) - s_{13}$. In the case that 1 and 2 are identical particles, the line with $s_{23} = s_{13}$ is a symmetry axis of the Dalitz plot. It obeys the equation $s_{12} = s + \sum_{i=1}^{3} m_i^2 - 2s_{13}$.

Angular Correlation Function

The angular correlation function $W(\theta_1, \phi_1)$ is defined as the ratio

$$W(\theta_1, \phi_1) = 4\pi\,\frac{d^3\sigma/d\Omega_1 d\Omega_2 dT_2}{d^2\sigma/d\Omega_2 dT_2}\,. \tag{E.8}$$

The triple differential cross section is given by the expression

$$\frac{d^3\sigma}{d\Omega_1\,d\Omega_2\,dT_2} = \frac{\mathcal{B}}{32|\vec{p}_a^{\,\mathrm{cm}}|\sqrt{s}}\,\frac{1}{(2\pi)^5}\,\frac{|\vec{p}_1^{\,\mathrm{cm}}||\vec{p}_2^{\,\mathrm{cm}}|}{E_1^{\mathrm{cm}} + E_3^{\mathrm{cm}} + E_1^{\mathrm{cm}}\frac{|\vec{p}_2^{\,\mathrm{cm}}|}{|\vec{p}_1^{\,\mathrm{cm}}|}\cos\theta_{12}^{\mathrm{cm}}}\,\overline{|\mathcal{M}|^2}\,. \tag{E.9}$$

T_2 is the kinetic energy of particle 2 in the centre-of-momentum frame, $\theta_{12}^{\mathrm{cm}}$ is the angle between $\vec{p}_1^{\,\mathrm{cm}}$ and $\vec{p}_2^{\,\mathrm{cm}}$, and $\Omega_{1,2}$ specifies the solid angle of $\vec{p}_{1,2}^{\,\mathrm{cm}}$.

Integrating over the solid angle of particle 1 leads to the double differential cross section

$$\begin{aligned}\frac{d^2\sigma}{d\Omega_2\, dT_2} &= \frac{\mathcal{B}|\vec{p}_2^{\,\mathrm{cm}}|}{32|\vec{p}_a^{\,\mathrm{cm}}|\sqrt{s}}\,\frac{1}{(2\pi)^5} \\ &\quad\cdot \int_0^{2\pi} d\phi_1 \int_{-1}^{1} d\cos\theta_1\, \frac{|\vec{p}_1^{\,\mathrm{cm}}|}{E_1^{\mathrm{cm}} + E_3^{\mathrm{cm}} + E_1^{\mathrm{cm}}\frac{|\vec{p}_2^{\,\mathrm{cm}}|}{|\vec{p}_1^{\,\mathrm{cm}}|}\cos\theta_{12}^{\mathrm{cm}}}\,\overline{|\mathcal{M}|^2}\,.\end{aligned} \tag{E.10}$$

Bibliography

[1] E. Oset and A. Ramos, Nucl. Phys. **A 635**, 99 (1998).

[2] M.F.M. Lutz and E.E. Kolomeitsev, Nucl. Phys. **700**, 193 (2002).

[3] D. Jido et al., Nucl. Phys. **A 725**, 181 (2003).

[4] S. Capstick and W. Roberts, Prog. Part. Nucl. Phys. **45**, S241 (2000).

[5] U. Löring, B.Ch. Metsch, and H.R. Petry, Eur. Phys. J A **10**, 395 (2001).

[6] L.Y. Glozman and D.O. Riska, Phys. Rep. **268**, 263 (1996).

[7] W. Melnitchouk et al., Phys. Rev. D **67**, 114506 (2003).

[8] S.J. Dong et al., LANL preprint hep-ph/0306199 (2003).

[9] C. Schütz, J. Haidenbauer, J. Speth, and J.W. Durso, Phys. Rev. C **57**, 1464 (1998).

[10] O. Krehl, C. Hanhart, S. Krewald, and J. Speth, Phys. Rev. C **62**, 025207 (2000).

[11] A.M. Gasparyan, J. Haidenbauer, C. Hanhart, and J. Speth, Phys. Rev. C **68**, 045207 (2003).

[12] T. Nakano et al., LANL preprint hep-ex/0301020 (2003).

[13] V.V. Barmin et al., LANL preprint hep-ex/0304040 (2003).

[14] S. Stepanyan et al., LANL preprint hep-ex/0307018 (2003).

[15] J. Barth et al., LANL preprint hep-ex/0307083 (2003).

[16] A. Zabrodin et al., Phys. Rev. C **60**, 055201 (1999).

[17] M. Wolf et al., Eur. Phys. J. A **9**, 5 (2000).

[18] W. Langgärtner et al., Phys. Rev. Lett. **87**, 052001 (2001).

[19] J.A. Gomez Tejedor and E. Oset, Nucl. Phys. **A 600**, 413 (1996).

[20] J. Ahrens et al., Phys. Lett. **551**, 49 (2003).

[21] V.D. Burkert, Eur. Phys. J A **17**, 303 (2003).

[22] K. Craig, prl **91**, 102301 (2003).

[23] V. Bernard, N. Kaiser, and U.-G. Meißner, Nucl. Phys. **A 619**, 261 (1997).

[24] E. Oset and M.J. Vicente-Vacas, Nucl. Phys. **A 446**, 584 (1985).

[25] N. Fazel, R.R. Johnson and V. Sossi, πN Newsletter **7**, 53 (1992).

[26] M. Kermani et al., Phys. Rev. C **58**, 3419 (1998).

[27] J. Gasser and H. Leutwyler, Ann. Phys. (N.Y.) **158**, 142 (1984).

[28] G. Ecker, J.Gasser, A. Pich, and E. de Rafael, Nucl. Phys. **B 321**, 311 (1989).

[29] V. Bernard, N. Kaiser, and U.-G. Meißner, Nucl. Phys. **A 615**, 483 (1997).

[30] J. Wess and B. Zumino, Phys. Rev. **163**, 1727 (1967).

[31] K. Hagiwara et al., Phys. Rev. D **66**, 010001 (2002).

[32] D.R. Phillips and S.J. Wallace, Phys. Rev. C **54**, 507 (1996).

[33] E.D. Cooper and B.K. Jennings, Nucl. Phys. **A 500**, 553 (1989).

[34] W. Glöckle, *The Quantum Mechanical Few-Body Problem* (Springer-Verlag, Heidelberg, 1983).

[35] R. Machleidt, K. Holinde and Ch. Elster, Phys. Rep. **149**, 1 (1987).

[36] B.C. Pearce and B.K. Jennings, Nucl. Phys. **A 528**, 655 (1990).

[37] R.E. Cutkosky, J. Math. Phys. **1**, 429 (1960).

[38] S.D. Protopopescu et al., Phys. Rev. D **7**, 1279 (1973).

[39] L. Rosselet et al., Phys. Rev. D **15**, 574 (1977).

[40] S. Weinberg, Phys. Rev. **166**, 1568 (1968).

[41] B. Borasoy and U.-G. Meißner, Int. J. Mod. Phys. A **11**, 5183 (1996).

[42] B. Hyams et al., Nucl. Phys. **B 64**, 134 (1973).

[43] C.D. Froggatt and J.L. Petersen, Nucl. Phys. **B 129**, 89 (1977).

[44] K. Takamatsu, Nucl. Phys. **A 675**, 312c (2000).

[45] B.R. Martin, D. Morgan, and G. Shaw, *Pion Pion Interactions In Particle Physics* (Academic Press, London, 1976).

[46] J. Gasser and H. Leutwyler, Nucl. Phys. **B 250**, 465, 517, 539 (1985).

[47] D. Lohse, J.W. Durso, K. Holinde, and J. Speth, Nucl. Phys. **A 516**, 513 (1990).

[48] G. Höhler and E. Pietarinen, Nucl. Phys. **B 95**, 210 (1975).

[49] P. Mergell, U.-G. Meißner, and D. Drechsel, Nucl. Phys. **596**, 367 (1996).

[50] R. Koch and E. Pietarinen, Nucl. Phys. **A336**, 331 (1980).

[51] R.A. Arndt, I.I. Stratkovsky, R.L. Workman, and M.M. Pavan, Phys. Rev. C **52**, 2120 (1995).

[52] R. Koch, Nucl. Phys. **A 448**, 707 (1986).

[53] V. Bernard, N. Kaiser, and U.-G. Meißner, Int. J. Mod. Phys. E **4**, 193 (1995).

[54] K. Kawarabayashi and M. Suzuki, Phys. Rev. Lett. **16**, 255 (1966).

[55] Fayyazuddin and Riazuddin, Phys. Rev. **147**, 1071 (1966).

[56] V. Sossi, N. Fazel, R.R. Johnson, and M.J. Vicente-Vacas, Phys. Lett. **B287**, 287 (1993).

[57] N. Fettes, V. Bernard, U.-G. Meißner, Nucl. Phys. **A 669**, 269 (2000).

[58] V.V. Vereshagin et al., Nucl. Phys. **A 592**, 413 (1995).

[59] N. Fettes, Berichte des Forschungszentrums Jülich No. 3814 (2000).

[60] S. Schneider, J. Haidenbauer, C. Hanhart, and J.A. Niskanen, Phys. Rev. C **67**, 044003 (2003).

[61] W.O. Lock and D.F. Measday, *Intermediate Energy Physics* (Methuen, London, 1970).

[62] D. Ashery et al., Phys. Rev. Lett. **47**, 895 (1981).

[63] K.A. Aniol et al., Phys. Rev. C **33**, 1714 (1986).

[64] P. Weber et al., Nucl. Phys. **A501**, 765 (1989).

[65] J. Aclander et al., Phys. Lett. **B300**, 19 (1993).

[66] S. MayTal-Beck et al., Phys. Rev. Lett. **68**, 3012 (1992).

[67] J.A. Niskanen and A.W. Thomas, Phys. Lett. **B196**, 299 (1987).

[68] J.A. Niskanen, L. Swift and A.W. Thomas, Phys. Rev. C **40**, 2420 (1989).

[69] V. Baru, J. Haidenbauer, C. Hanhart, and J.A. Niskanen, Eur. Phys. J. A **16**, 437 (2003).

[70] Ch. Hajduk, A.M. Green, and M.E. Sainio, Nucl. Phys. **A 337**, 13 (1980).

[71] R. Machleidt, Phys. Rev. C **63**, 024001 (2001).

[72] M. Lacombe et al., Phys. Rev. C **21**, 861 (1980).

[73] R. Reid, Ann. Phys. (N.Y.) **50**, 411 (1968).

[74] J.A. Niskanen, Phys. Rev. C **49**, 1285 (1994).

[75] H.O. Meyer et al., Nucl. Phys. **A 539**, 633 (1992).

[76] T.-S.H. Lee and D.O. Riska, Phys. Rev. Lett. **70**, 2237 (1993).

[77] C.J. Horowitz, H.O. Meyer, and D.K. Kriegel, Phys. Rev. C **49**, 1337 (1994).

[78] J.A. Niskanen, Phys. Rev. C **53**, 526 (1996).

[79] J.A. Niskanen, Nucl. Phys. **A 298**, 417 (1978).

[80] C.J. Horowitz, Phys. Rev. C **48**, 2920 (1993).

[81] J.L. Friar, B.F. Gibson, and G.L. Payne, Ann. Rev. Nu. Sci. **34**, 403 (1984).

[82] M. Jacob and G.G. Wick, Ann. Phys. (N.Y.) **7**, 404 (1959).

[83] A. Edmonds, *Angular Momentum in Quantum Mechanics* (Princeton University Press, Princeton, 1957).

[84] I.R. Afnan and A.T. Stelbovics, Phys. Rev. C **23**, 1384 (1981).

[85] C. Schütz, Berichte des Forschungszentrums Jülich No. 2733 (1993).

Acknowledgements

First of all I would like to thank my advisor Prof. Krewald for many valuable discussions and suggestions concerning this thesis.

My gratitude goes to Prof. Meißner for his interest in my work and for agreeing to assess my thesis.

I also want to express my thanks to Dr. Christoph Hanhart and Felix Sassen for a careful reading of the manuscript and many constructive suggestions.

I profited very much from the collaborations with Dr. Alexander Sibirtsev, Prof. Charlotte Elster, Dr. Johann Haidenbauer, Dr. Christoph Hanhart and Prof. Jouni Niskanen.

I thank Prof. Jouni Niskanen for the hospitality during my stay at his home institute in Helsinki. In this context, I would also like to acknowledge financial support from the DAAD.

I would like to thank all my colleagues at the IKP for a friendly and supportive environment that made working in Jülich a pleasant experience.

Special thanks go to Felix (for many discussions, not necessarily restricted to physics and for invaluable assistance in computer problems), to Andreas (not only for the cookies...) and to the "Chiral Office", particularly Bastian, Lucas and Matthias for countless chats on physics, work and life in general.

Last but not least I thank my friends and family. They proved to be a vital connection to the "outside world". Without their encouragement and support this thesis would hardly have been possible.

Forschungszentrum Jülich
in der Helmholtz-Gemeinschaft

Jül-4134
Mai 2004
ISSN 0944-2952